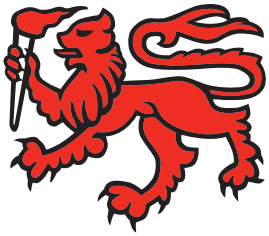

UNIVERSITY *of* TASMANIA

School of Physical Sciences

Water maser follow-up of the Methanol Multibeam survey

Anita Titmarsh

December 2015

Supervisors:
Prof. Simon Ellingsen
Dr. Shari Breen

Submitted in fulfilment of the requirements for the Degree of
Master of Physics

Declaration of Originality

This thesis contains no material which has been accepted for a degree or diploma by the University or any other institution, except by way of background information and duly acknowledged in the thesis, and to the best of my knowledge and belief no material previously published or written by another person except where due acknowledgement is made in the text of the thesis, nor does the thesis contain any material that infringes copyright.

Signed:

Date: 9/12/2015

Authority of Access

Signed:

Date: 9/12/2015

Statement of Co-Authorship

The following people contributed to the publication of work undertaken as part of this thesis:

Candidate	Titmarsh, A.M.	University of Tasmania, CSIRO Astronomy & Space Science
Co-Author 1	Ellingsen, S.P.	University of Tasmania
Co-Author 2	Breen, S.L.	CSIRO Astronomy & Space Science
Co-Author 3	Caswell, J.L.	CSIRO Astronomy & Space Science
Co-Author 4	Voronkov, M.A.	CSIRO Astronomy & Space Science

Paper 1: *A search for water masers associated with class II methanol masers - I. Longitude range 6° to 20°*, 2014, Monthly Notices of the Royal Astronomical Society, 443, 2923.
Paper 2: *A search for water masers associated with class II methanol masers - II. Longitude range 341° to 6°*, 2015, Monthly Notices of the Royal Astronomical Society, submitted.

This thesis combines the work in these two publications in Chapters 3 - 5. The candidate was the primary author and co-authors 1, 2 and 3 contributed to the idea and formalisation. Writing and data analysis was done primarily by the candidate, with some paragraphs provided by co-author 1 and ideas and input for the analysis provided by all co-authors. The observations for the data presented in Chapter 3 were collected by the candidate, with co-authors 2, 3 and 4 providing instruction on how to operate the telescope, design the survey and assisting with the observations. Feedback and editing for the purposes of publication was provided by all co-authors.

Signed:____

Date: 9/12/15

Prof. Simon Ellingsen, Primary Supervisor
School of Physical Sciences, University of Tasmania

Abstract

The Australia Telescope Compact Array has been used to search for 22-GHz water masers towards the 323 6.7-GHz methanol masers detected in the Methanol Multibeam survey between Galactic longitudes 341° to 20°, through the Galactic centre, and we find water masers associated with 156 (∼48 %). Methanol masers with associated water masers have a higher mean integrated luminosity than those without. In sources where both maser species are observed, the luminosities of the methanol and water masers are weakly correlated even after accounting for the partial correlation due to distance. We have inspected the GLIMPSE three colour images of the regions surrounding the masers and cross-matched the maser positions with existing catalogues of Extended Green Objects and Infrared Dark Clouds. We find more Extended Green Objects at sites where both methanol and water masers are present than at sites with only methanol masers, but no significant difference in the fraction embedded within Infrared Dark Clouds. Studying the mid-infrared colours from GLIMPSE, we found no differences between the colours of those sources associated with both methanol and water masers and those associated with just methanol. Analysis of the 1.1-mm thermal dust emission shows dust clumps associated with masers have greater 1.1-mm flux densities and higher column densities than those without. Dust clumps associated with both water and 6.7-GHz methanol masers are generally the most compact clumps followed by those associated with only methanol then the clumps without associated maser emission. Comparing the column density and dust mass calculated from the thermal dust emission at 870 μm, we found no differences between those sources associated with both water and methanol masers and those with methanol only. At 870 μm we found dust clumps at the very highest column densities (above $\sim 10^{25}$ cm^{-2}) almost all had an associated methanol maser. We conclude that there is some evidence that protostars with both methanol and water masers are often older than those with only methanol, however, we suggest that the evolutionary phase traced by water masers is not as well defined as for 6.7-GHz methanol masers. Since water masers are collisionally pumped and often show emission further away from their accompanying YSO than the radiatively pumped 6.7-GHz methanol masers, it is likely that water maser properties are not as tightly correlated to the evolution of the parent YSO.

Acknowledgements

Firstly, I would like to thank my supervisors Simon Ellingsen and Shari Breen for being amazing supervisors and sticking with me throughout this whole process. You both have been wonderful and I could not have asked for better supervisors.

I am also very grateful to the late James Caswell for being the most kind, patient and knowledgeable grand-supervisor ever.

Thanks to Maxim Voronkov for assistance in the observations and publications that make up this thesis.

The University of Tasmania and the CSIRO Astronomy and Space Science, Australia Telescope National Facility for their financial support.

To Robin Wark, Jamie Stevens and the other technical staff at the Australia Telescope Compact Array: thanks for all the observing help and being available at sometimes crazy hours to fix things. Thanks to the other observatory staff there, in particular the lovely Marg always looking out for me.

Thanks to everyone in Maths and Physics at the University of Tasmania. Especially Karen for always having my back and my fellow students Jay, Chris, Courtney and Vaasant for your scripting help and discussions.

Lastly, thanks to my parents for all your support through all these years at university.

Contents

List of Figures

List of Tables

Chapter 1

Introduction

How high-mass (M > $\sim$8M$_\odot$) stars are formed is important in many different areas of astrophysics. They have an enormous influence on the structure and evolution of the galaxies in which they reside, because they are a major contributor to turbulence and mixing in the interstellar medium, and also the primary source of heavy elements and UV radiation in the Universe. Still, we are yet to reach a unified theory of star formation and the mechanisms through which high-mass stars are formed remains hotly debated.

To help answer the questions surrounding the formation of high-mass stars, signposts are needed to identify the evolutionary stages of their formation while they are still embedded in their natal molecular clouds. Masers have a unique role to play here, as some transitions have been proposed to trace an evolutionary sequence of high-mass star formation (e.g. Ellingsen et al. 2007; Breen et al. 2010b). They have other advantages too, being bright and arising at radio frequencies, they are not obscured by the dust at star forming sites. Masers are also point sources, and with high resolution observations, allow us to pin-point the precise young stellar object they are associated with.

However, it is still not well understood how some maser transitions fit within this evolutionary timeline of high-mass star formation. One such transition is the 22-GHz water maser and that is the topic of this thesis - particularly the overlap of 22-GHz water masers and 6.7-GHz methanol masers. How the 6.7-GHz methanol maser transition fits into the evolutionary timeline of high-mass star formation has been quantified in Breen et al. (2010b). In this thesis I have used a statistically complete sample of 6.7-GHz methanol masers from the Methanol Multibeam (MMB) survey and made interferometric observations towards them for 22-GHz water masers. The aim is to ascertain how water masers fit in this evolutionary sequence compared to 6.7-GHz methanol masers using the maser properties, infrared tracers of outflows and star formation and submillimeter dust emission.

In the following sections I give an introduction to telescope used for the observations, data reduction and visualisation packages and summary of each chapter.

1.1 The Methanol Multibeam survey

The MMB was conducted to make an unbiased survey of the Galactic plane for 6.7-GHz methanol masers. The MMB covered the entire Galactic Plane observable with the Parkes

64-m dish in Australia (longitudes 186°, through 0°, to 60°) with latitude coverage of $|b| \leq 2°$. 972 sources were detected in the survey. For sources where interferometric positions were not already available, the detections were followed-up with interferometric observations with the Australia Telescope Compact Array (ATCA) and the Multi-Element Radio Linked Interferometer Network (MERLIN) to obtain precise positions. Catalogues covering the entire MMB region have now been published (Green et al. 2009; Caswell et al. 2010; Green et al. 2010; Caswell et al. 2011; Green et al. 2012; Breen et al. 2015).

1.2 The Australia Telescope Compact Array

All of the water maser data presented in this thesis was observed using the Australia Telescope Compact Array (ATCA). The ATCA is owned and operated by Commonwealth Science and Industrial Research Organisation (CSIRO), Astronomy and Space Science along with their other radio telescopes Parkes, Mopra and the Australian Square Kilometre Array Pathfinder. The ATCA is an array of six 22-m antennas located 500-km northwest of Sydney, in the Paul Wild Observatory. Five of these antennas can move along a 3-km long east-west track or a 214-m north spur. The sixth antenna is fixed, being located out 6-km along the east-west track.

As it is located at a latitude of 30° South, the ATCA can track sources for 12 hours giving excellent *uv*-coverage for sources with declination south of –24°, although the array can still be used to observe sources up to +48°. Imaging of equatorial sources requires the use of the north spur as the synthesised beam becomes very elongated on the east-west baselines.

The ATCA operates between 1.1 - 105 GHz and in the last few years the correlator has been upgraded with the Compact Array Broadband Backend (CABB; Wilson et al. 2011). For the water maser observations presented in this thesis CABB has delivered excellent velocity resolution (0.50 km s^{-1}) and velocity coverage of $>$ 800 km s^{-1}. Water masers are known for their high velocity emission and the large velocity coverage of CABB enabled us to discover the highest ever velocity feature of a water maser in a high-mass star formation source (See *10.472+0.027* in Chapter 3).

The ATCA accepts applications for observing time twice a year and is highly oversubscribed. This is particularly so during the winter semester when conditions are best for millimetre and Galactic Plane observations as the Milky Way is observable during the cold nights. Hence, the application process is very competitive with the applications being prioritised by a Time Allocation Committee.

1.3 Data reduction software

All of the water maser data presented in this thesis was reduced using MIRIAD, the standard radio interferometry data reduction package for the ATCA (Sault et al. 1995). MIRIAD was used for everything from loading in the data files, to imaging and extracting positions and spectra. These images where then inspected using kvis from the Karma package of astronomy visualisation tools.

Kvis is able to display images, movies of the data cubes and show line profiles which

we used to help determine maser positions. We were also able to examine the infrared environments of the maser sources in kvis by loading in the *Spitzer* Galactic Legacy Infrared Midplane Survey Extraordinaire (Benjamin et al. 2003, GLIMPSE) data, make three colour images with it and overlay annotations of the maser positions.

1.4 Thesis summary

This thesis starts with a review of relevant literature in Chapter 2.

In Chapter 3 I give the details of the water maser observations with the ATCA, the data reduction and the masers detected associated with their MMB targets. The spectra of the water masers are shown in Figure 3.3, the maser parameters in Table 3.1 and sources of special note are remarked on in Section 3.2.1.

Chapter 4 contains discussion of the detection rate, luminosities and velocities of the water masers observed in this survey and their methanol maser targets. I also compare these results to those in similar surveys such as Beuther et al. (2002); Szymczak et al. (2005); Xu et al. (2008); Breen et al. (2010a). Some of the water masers detected in this work have been previously observed in Breen et al. (2010a) and Walsh et al. (2014) allowing us to study their variability.

In Chapter 5 I study the infrared environments of the young stellar objects hosting the masers, particularly Extended Green Objects which are indicators outflows and shock activity and Infrared Dark Clouds which are found at the earliest stages of star formation. Sub-millimetre thermal dust emission from the clumps the masers are embedded in is also discussed using the 1.1-mm emission and the 870-μm emission.

Chapter 6 I finish with come concluding remarks and suggestions for future work.

In most of this thesis I have used “we” instead of “I”. This is for stylistic reasons and this thesis is all my own work except where acknowledged in the Statement of Co-Authorship.

Chapter 2

Literature Review

In this chapter a review of astrophysical masers and other relevant Galactic surveys is presented. A brief background about high-mass star formation is also given.

2.1 High-mass star formation

Understanding high-mass stars is necessary for understanding galactic structure and evolution as they are the main source of heavy elements and UV radiation in the Universe. They have a major influence on the galaxies in which they reside through their powerful winds, outflows, HII regions and supernova mixing and creating turbulence in the interstellar medium (ISM). Despite this, many questions still remain about their formation.

The formation of low-mass stars by accretion is well understood (Shu et al. 1987). However, for high-mass stars (OB stars with enough mass to produce a type II supernova $M_* > 8M_\odot$) the Kelvin-Helmholtz time for the core to start converting gravitational potential energy into heat is smaller than the free-fall time (the collapse time). This causes nuclear fusion to start before gravitational collapse has finished and the resulting radiation pressure is enough to halt spherical accretion.

It is now accepted that high-mass stars can continue to accrete material via an accretion disk after nuclear fusion has commenced. The two main competing theories attempting to explain high-mass star formation are monolithic collapse (Krumholz et al. 2009) and competitive accretion (Bonnell & Bate 2006). The main difference between these two theories is that in monolithic collapse objects only accrete material from nearby in the molecular cloud they are embedded in and the only competition for material is between close stars. The asymmetries produced by the disks and jets are how radiation pressure is overcome and accretion can continue after fusion has begun. In competitive accretion however, the material that makes up any star can originate from a large volume of the cloud they are born in, depending on the specific details of the gravitational potential and other forces acting on the gas, with protostars in the centre of the cloud benefiting most from being at the bottom of the gravitational potential well of the cloud. In competitive accretion the location of the core in the molecular cloud is the critical factor in determining the final size of the star however in monolithic collapse it is the initial size of the core when collapse begins that is more important.

High-mass stars are embedded in the clouds of gas and dust for about 15 % of their

lifetime before they become optically visible main-sequence stars (Churchwell 2002). This embedded phase presents many challenges to observers as these gas and dust clouds have high extinction, making optical observations difficult or impossible and they always form alongside many other companions deep in the potential wells of these clouds. High-mass stars are also rare, at large distances and their evolution is very fast compared to that of low-mass stars. Hence, understanding the formation of high-mass star is much more difficult than that of lower mass stars.

Figure 2.1 is a cartoon of the evolution of a high-mass star formation region. A group of stars will start their life in a clumpy molecular cloud. From this cloud, compressed pockets of gas will form from the molecular cores and filaments that are experiencing turbulence. Some of these stay gravitationally bound setting the stage for the cloud to collapse and star formation to begin (Mac Low & Klessen 2004; Padoan & Nordlund 2002; Klessen et al. 2005). These cold cores are very cold and dense (gas temperatures between 10 - 20 K and molecular hydrogen densities $\sim 10^5$ cm^{-3}) showing little to no emission in the infrared (see the first panel of Figure 2.2). They are often associated with Infrared Dark clouds (IRDCs Perault et al. 1996) (see Section 2.6) and show emission from molecules that trace cold dense gas such as CO, CO_2 and CS.

In low-mass stars accretion ends before hydrogen burning commences, however, in high-mass stars, they continue to accrete matter and evolve even once hydrogen burning has started becoming hotter and more luminous (Kudritzki 2002). As they warm up the surrounding dust they begin to become visible in the far-infrared such as the 24 μm emission from *Spitzer* (see second panel in Figure 2.2). The complex organic molecules are both evaporated off the dust grains and formed through gas-phase reactions. At this stage they also begin to show maser emission. Since accretion is occurring in the warm-core phase, to conserve angular momentum they produce outflows from their poles which become visible in molecular tracers like SiO and in the mid-infrared as Extended Green Objects (see Section 2.6).

Once hydrogen burning has commenced, expanding pockets of ionised gas called hyper- and ultra-compact HII regions are formed due to the winds, pressure gradients and ionising photons produced by star. Gradually, the gas of the whole region of star-forming objects is ionised or dispersed, often by several sources. The molecular cloud in which they were embedded is disrupted leaving HII regions and OB associations visible in the optical and near-IR.

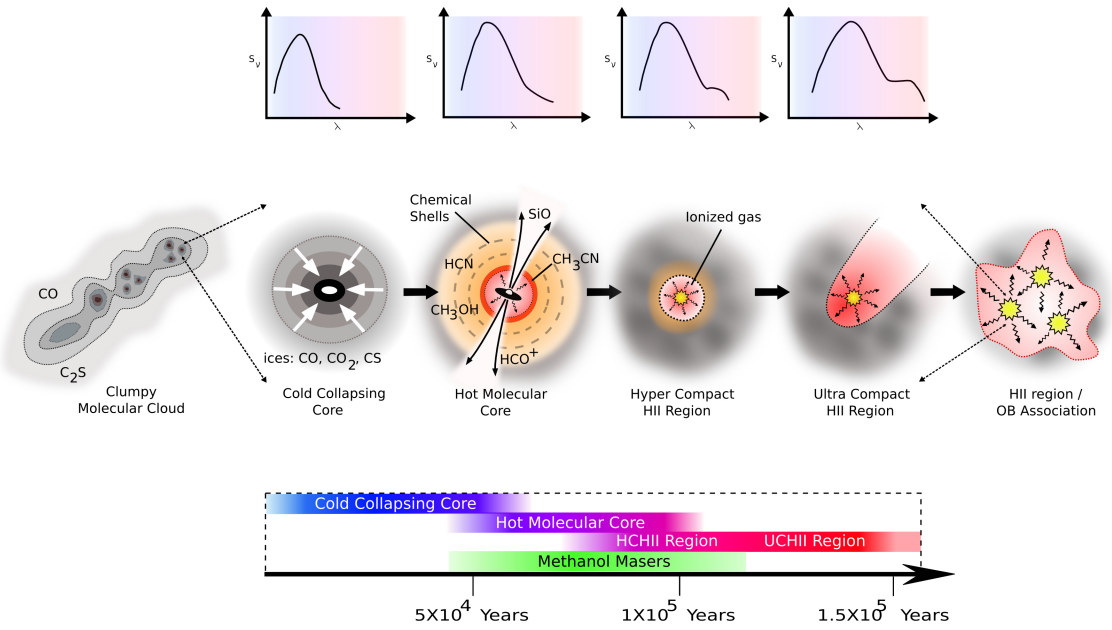

Figure 2.1: Cartoon by Cormac Purcell showing the formation of a cluster of high-mass stars starting with a molecular cloud and finishing with an optically visible HII region.

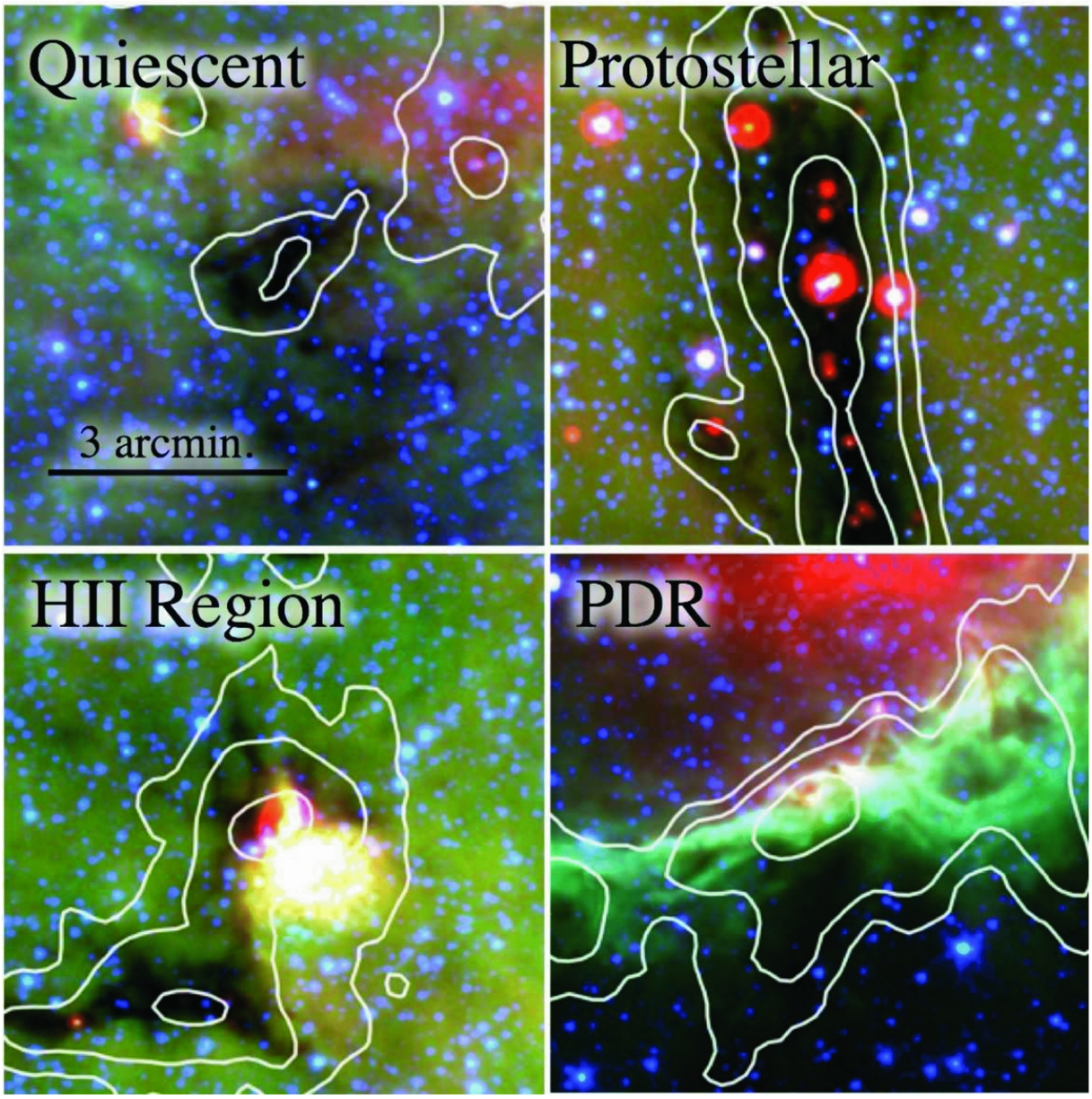

Figure 2.2: Figure from Jackson et al. (2013) of the *Spitzer* GLIMPSE and MIPSGAL images of different phases of star formation. The blue, green and red colours correspond to the 3.6 μm, 8.0 μm and 24 μm respectively. The white contours are the 870-μm emission from the ATLASGAL survey (Schuller et al. 2009).

2.2 Early maser discoveries

Some of the best signposts of high-mass star formation are interstellar masers. They are common, intense and, being observable at radio frequencies, they do not suffer the high extinction that affects other frequency bands. The most common maser species are water, methanol and hydroxyl, and along with maser pumping models, they provide us with valuable information about the physical conditions at sites of star formation.

The theoretical work describing masers in the laboratory was first presented at the conference *All-Union Conference on Radio-Spectroscopy* in 1952 by the Russian scientists Nikolay Basov and Alexander Prokhorov and in 1953 Charles Townes, James Gordon and Herbert Zeiger built the first maser using ammonia and producing 24-GHz microwaves.

The first discovery of astrophysical masers came by accident while looking for absorption of OH against bright background radio sources. Strong, narrow emission lines were seen in the spectrum and hence Weaver et al. (1965) announced discovery of mysterium. Afterwards it was recognised that this source was an OH maser (Weinreb et al. 1965).

Interferometric observations by Cudaback et al. (1966) discovered that these sources were extremely compact, implying brightness temperatures of $\sim 10^6$ K which is impossible from purely thermal processes. Confirmation of the non-thermal nature of the emission came from Very Long Baseline Interferometry (VLBI) observations by Moran et al. (1968) who found these sources to be a maximum of a few arcseconds in size and further VLBI observations of water masers by Burke et al. (1970) found them to be less than a few milliarcseconds in size.

2.3 Maser species

2.3.1 Hydroxyl Masers

Hydroxyl masers were the first maser species to be discovered (Weaver et al. 1965) and their maser emission comes from the hyperfine splitting of the $^2\Pi_{3/2}$ and $^2\Pi_{1/2}$ rotational ladders. They are pumped by infrared radiation from warm dust and they favour conditions of cooler gas (<100 K) and moderately high densities (10^5 - 10^8 cm^{-3}, although higher temperatures and/or lower densities can also produce masers; Cragg et al. 2002).

OH masers are found in Active Galactic Nuclei (e.g. Baan et al. 1982), supernova remnants (e.g. Wardle & Yusef-Zadeh 2002), evolved stars (e.g. Sevenster et al. 1997) and high-mass star forming regions (e.g. Caswell 1997, 1998). Their strongest and most common lines in star formation regions are the main-line transitions at 1665 and 1667 MHz. In unbiased observations of the OH 1665- and 1667-MHz transitions in the Galactic Plane which detected more than 100 OH maser sources, Caswell & Haynes (1987) found the 1665-MHz transition to be the most common and generally the strongest, typically by a factor of three. They observed the 1667-MHz transition towards 90 % of the 1665-MHz sources and interferometric observations confirmed that they were from the same young stellar object as the two maser transitions were coincident to within an arcsecond. Other excited and satellite-line transitions can also be found at sites of star formation, including the 1612-, 1720-, 6030-, 6035-, 13442- and 4765-MHz transitions.

Polarisation is common in OH masers and many sources are 100 % circularly polarised.

They make ideal tracers of magnetic fields as they have a large Zeeman splitting factor with the 1665-MHz transition having the largest known (Heiles et al. 1993). Magnetic fields of a few mG are commonly observed in star formation regions (Caswell & Reynolds 2001; Fish et al. 2003) and can be up to ∼40 mG (Fish & Reid 2007).

OH masers have a median total velocity ranges of ∼9 km s^{-1} (Caswell 1998). This emission is generally close to the systemic velocity of the molecular clouds they are embedded in and they are not usually associated with outflows. However, there are rare case where weak OH maser emission is associated with outflows, for example Argon et al. (2003) who found OH towards a bipolar outflow traced by water masers.

The intensity of their emission can remain stable on ∼20 year timescales, while others show intensity changes of more than a factor of two (Caswell 1998).

2.3.2 Water Masers

Water masers were first discovered by Cheung et al. (1969) towards Sgr B2, Orion A and W49 and are now known to be the most widespread of the maser species known (e.g. Walsh et al. 2011). According to the model by Elitzur et al. (1989) they need dissociative shocks in dense gas with temperatures up to ∼400 K and preshock densities ∼ 10^7 cm^{-3} - 10^9 cm^{-3} to form. The 22-GHz $6_{1,6} \rightarrow 5_{2,3}$ rotational transition is the brightest spectral line at radio frequencies, and other transitions of water have also been observed, especially the higher frequency vibrational transitions towards evolved stars (Menten & Batrla 1989).

Water maser spots are often found in clusters, these groups of spots are not generally distributed over more than ∼1 arcsecond (Forster & Caswell 1989). Although there are some extreme cases where water maser spots with angular separations extensive as 4 arcseconds are observed (Reid et al. 1988). VLBI is needed to resolve maser spots as their physical sizes are tens of AU or less (e.g. Richards et al. 2011).

Water masers are commonly associated with high-mass star formation. VLBI observations of water masers have shown that they are found towards high-mass young stellar objects in the disks surrounding them (Torrelles et al. 1998), in their high velocity bipolar outflows (Genzel et al. 1981; Hofner & Churchwell 1996, e.g.) and in the bow shocks from outflows and expanding shells (Hofner & Churchwell 1996).

In addition, water masers are found associated with low-mass star formation (e.g. Furuya et al. 2003), late M-type stars (e.g. Dickinson 1976), planetary nebulae (e.g. Miranda et al. 2001), Mira variables (e.g. Hinkle & Barnes 1979) and asymptotic giant branch stars (e.g. Barlow et al. 1996). They are also found in extra-galactic sources like the circumnuclear regions around active galactic nuclei (e.g. Claussen et al. 1984).

To investigate the proportions of water masers associated with different phenomena, Walsh et al. (2011) conducted unbiased survey of the southern Milky Way. They found that 69 % of the water masers they detected are associated with star formation, 19 % with evolved stars and 12 % unknown. They also found water masers associated with evolved stars typically have more maser spots and are distributed over smaller angular scales than those associated with star formation.

Because water masers often have many maser spots within small areas, their spectra are generally more complex than other maser species. Sources with higher far-infrared luminos-

ity tend to excite more emission components over a wider velocity range, and the brightest features are typically closer to the velocity of the molecular cloud it is embedded in (Brand et al. 2003). Water masers are well known for exhibiting weaker features red- or blue-shifted 100 km s^{-1} or more from the systemic velocity, indicating outflow activity at the associated YSO. However, there are a small number of sources where these high velocity features dominate their spectrum. Caswell & Phillips (2008) reported a distinct class of water masers with dominant blue-shifted outflows. These masers have strong blue-shifted emission offset a long way (50 km s^{-1} in the case of 353.273+0.641) from their weak emission at the systemic velocity of the region.

It is common for water masers to show variability in their flux densities over time; much greater than those of other species. Variability in water masers was first discovered by Knowles et al. (1969) who observed eight sources and saw that the spectra varied greatly on a time scale of less than three weeks.

Sullivan (1971) suggested that water maser variability could be caused by changes in any of the following:

- intensity of the input radiation to be amplified
- difference between the water molecules in the $6_{1,6}$ and $5_{2,3}$ rotational states
- maser path length
- supply of the "pump" energy available in the masing region to maintain the population inversion

One of the longest studies of water maser variability is the Arcetri project (Brand et al. 2003; Felli et al. 2007). It covered a wide range of timescales and luminosities of the powering YSO. The Arcetri project performed single dish monitoring of a sample of water masers that continued for several decades, but with a fairly small sample size (43 in Felli et al. (2007), and a subset of 14, with more detailed analysis, in Brand et al. (2003)). They found that variability can occur over a large range of timescales from hours-days to months-years and that these changes in flux density can be gradual or burst-like (Felli et al. 2007). In addition, individual spectral features can drift in velocity by up to a few km s^{-1} per year (Brand et al. 2003). Figure 2.3 shows the variability of the W75-N spectra from the Arcetri project. As is seen in many water masers, the features in W75-N closest to the systemic velocity are most persistent and the further from the systemic velocity the more variable features become. Figure 2.4 overlays VLA observations of water masers associated with this source on the continuum emission from Carrasco-González et al. (2015). The water masers trace out a shell structure with many more features in 2014 than in 1996.

The objects powering water masers have a large influence on how variable they are. Brand et al. (2003) found higher luminosity YSOs are generally associated with brighter more stable water masers and Claussen et al. (1996) found water masers emission to be weaker and more variable from low-mass stars compared to high-mass stars. With large sample size (hundreds of masers), but with only a few epochs of observations, Breen et al. (2010a) and Walsh et al. (2014) both found that weaker water masers with simpler spectra are more likely to disappear.

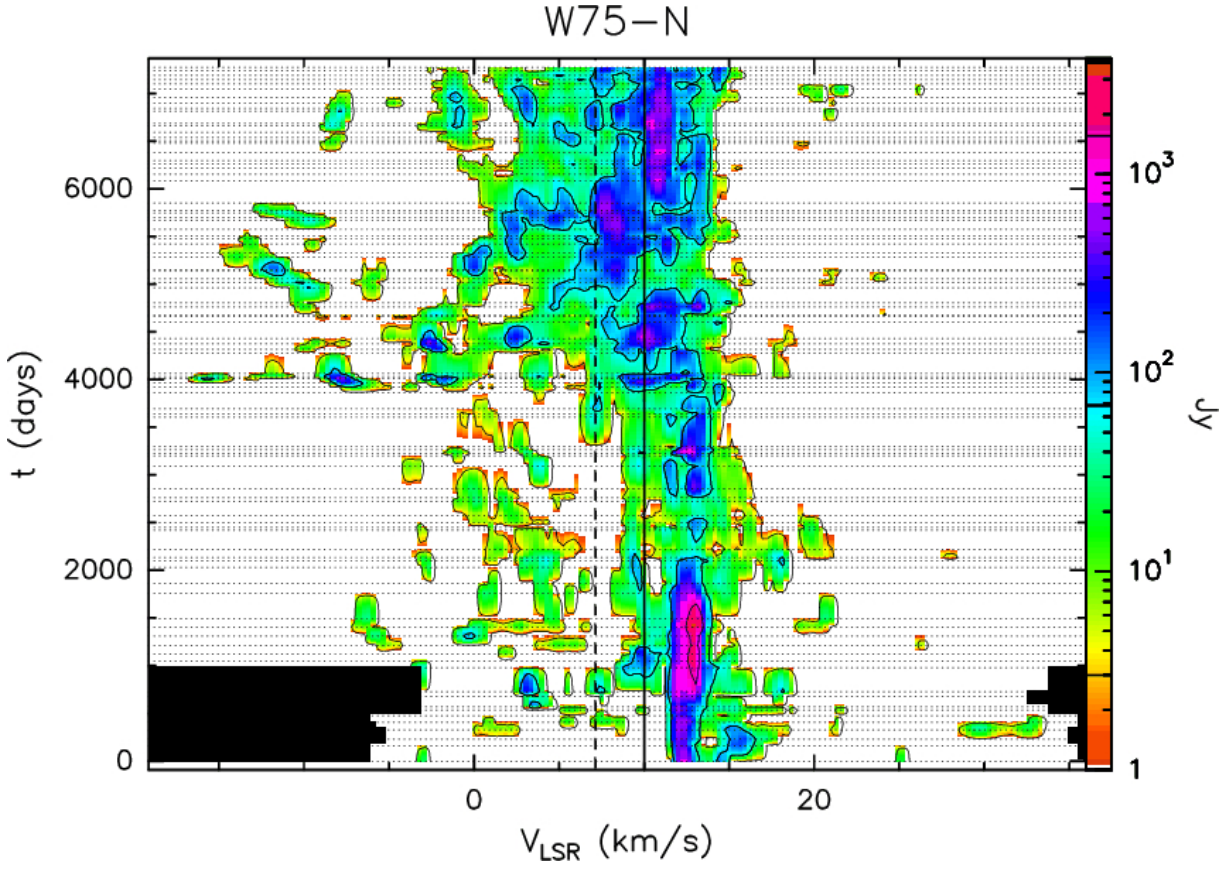

Figure 2.3: Velocity features vs. time for the W75-N water maser from Felli et al. (2007). The flux density of the features is shown on the colour scale, the solid vertical line is the velocity of the associated molecular cloud and the vertical dashed line is the mean velocity of this maser. The area in black are velocities that were not observed.

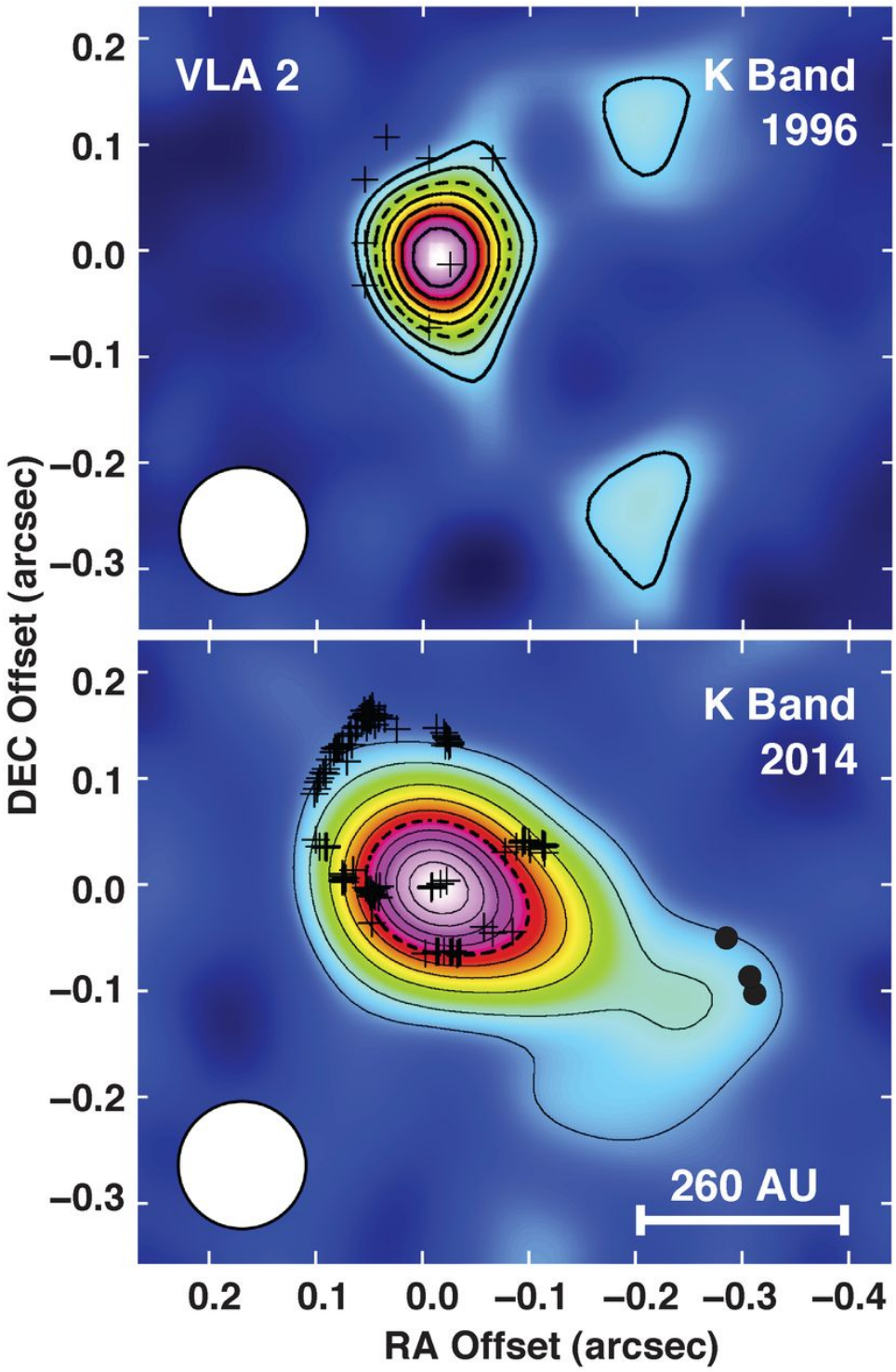

Figure 2.4: Water masers associated with W75N(B) in 1996 and 2014 with the VLA (indicated with + symbols). The background image and contours are the K band continuum observed with the VLA. The black dots are the methanol masers (Carrasco-González et al. 2015).

2.3.3 Methanol Masers

The first discovery of an interstellar methanol maser was by Barrett et al. (1971) who observed the transition at 25.0-GHz towards Orion-KL. It was over a decade before the next methanol maser transition was discovered by Wilson et al. (1984, 1985) who first observed the 19.9- and 23.1-GHz transitions towards W3(OH). The discovery of the common transitions of 12.2-GHz (Batrla et al. 1987) and 6.7-GHz (Menten 1991) where soon to follow. Now more than 50 methanol maser transitions have been discovered (e.g. Müller et al. 2004).

Methanol masers have been empirically divided into class I and class II types. Class I methanol masers appear spread around a star forming region, distributed over linear scales of up to 1 pc (e.g. Kurtz et al. 2004; Voronkov et al. 2006; Cyganowski et al. 2009; Voronkov et al. 2014; Jordan et al. 2015), whereas, class II methanol masers reside close to their parent YSO (e.g. Caswell 1997). Modelling of maser pumping mechanisms has shown that class I methanol masers are pumped by collisions with molecular hydrogen, whereas the class II methanol masers are pumped by infrared radiation (e.g. Cragg et al. 1992, 2002; Voronkov et al. 2005).

Currently there have been more than twenty class I methanol maser transitions detected (Müller et al. 2004) and the most common Class I transitions are at 36 and 44 GHz. Class I methanol masers are often associated with UCHII regions, outflows, infrared dark clouds, shocks traced by 4.5-μm emission and 8.0-μm filaments (Cyganowski et al. 2009; Voronkov et al. 2014). They are typically distributed on scales of a few to 10s of arcseconds within a star formation region (Voronkov et al. 2006, 2014) and can have features offset up to 30 km s^{-1} from the peak of the emission (Voronkov et al. 2010).

Voronkov et al. (2014) performed a high resolution survey of the 36 and 44-GHz methanol maser transitions with the ATCA. They found the class I masers to generally be more spread out compared to the 6.7-GHz methanol masers which were typically centrally located with an accompanying infrared source (see Figure 2.5). The number of class I masers detected fell exponentially with the projected linear distance from the associated class II 6.7-GHz methanol maser. For both transitions, this distribution had a scale of 263 $\pm$ 15 mpc. The class I sources associated with OH masers were generally more spread out in both space and velocity, which is consistent with other evidence that these sources are more evolved.

Class I methanol masers have been found to be associated with low and intermediate mass star formation (Kalenskii et al. 2010) but they are more commonly found at sites of high-mass star formation. Jordan et al. (2015) performed a blind survey of 5 squares degrees of the Galactic Plane observing 12 different molecular transitions (including both maser and thermal cases) at 45 GHz with the ATCA. They found many class I methanol masers without other associated masers and they suggest that these may be associated with young regions of high-mass star formation or low-mass star-forming regions. The majority of class I masers, however, are associated with other high-mass star-forming masers or dense gas as traced by CS clumps.

Class II methanol masers (such as the $5_1 - 6_0$ A$^+$ transition at 6.7-GHz) are pumped by far-infrared radiation (Sobolev & Deguchi 1994; Cragg et al. 2005) and are observed exclusively at sites of high-mass star formation (Minier et al. 2003; Xu et al. 2008; Bartkiewicz et al. 2011; Breen et al. 2013). This is because methanol is produced in high abundance in

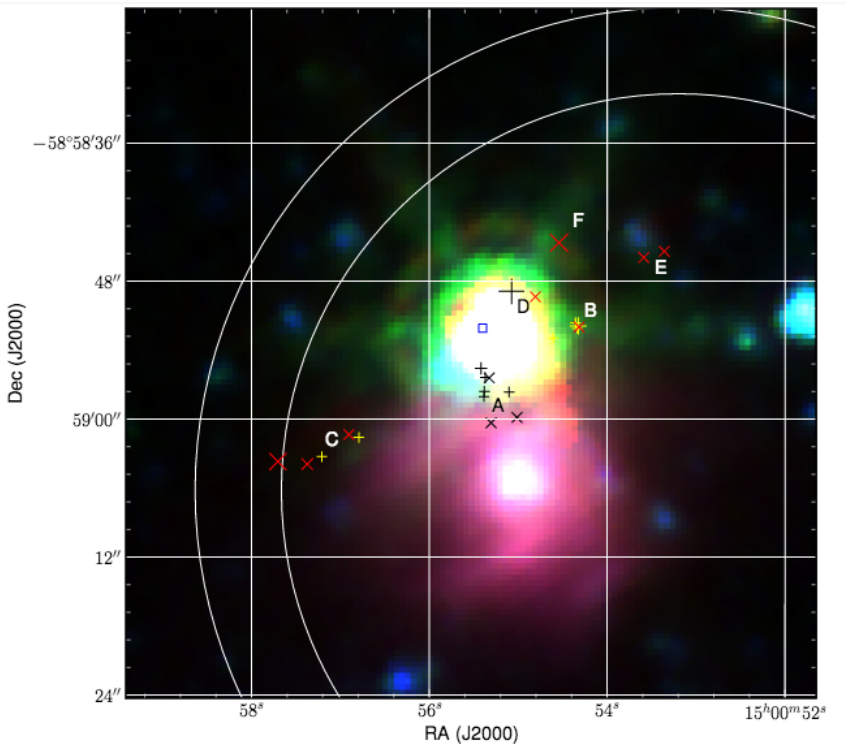

Figure 2.5: Voronkov et al. (2014) observations of the class I methanol masers at 36 GHz (crosses) and 44 GHz (pluses). The class II 6.7-GHz methanol maser is shown by a square. The background is a *Spitzer* three colour image with 8.0, 4.5 and 3.6-μm IRAC bands shown as red, green and blue, respectively. The concentric circles are the full width half maximum for the primary beam of the 36 and 44-GHz observations.

relatively restricted circumstances. It forms on the mantles of dust grains at temperatures < 10 K during the cold-core phase of high-mass star formation (Taquet et al. 2013), is released into the gas phase as the temperature rises, but then is rapidly depleted through gas phase reactions. Methanol masers can form at similar densities to water masers (10^7 cm^{-3} - 10^9 cm^{-3}) but they are favoured by lower temperatures (100 K - 150 K; Cragg et al. 2002, 2005). To date there have been more than twenty class II methanol maser transitions detected (Müller et al. 2004).

The 6.7-GHz methanol maser transition traces the systemic velocity of the star-forming regions they are found in. They typically have narrow spectral features (total velocity ranges less than 16 km s^{-1}; Caswell 2009) and central velocities within $\pm$ 3 km s^{-1} of the systemic velocity of the region (Szymczak et al. 2007; Caswell 2009; Pandian et al. 2009) making them ideal for kinematic distance estimates. They are found exclusively at sites of high-mass star formation and so are restricted to spiral arms they make ideal tools for studying Galactic structure also. Measurements of VLBI parallax distances to the methanol masers in the Galactic Plane are currently underway to map its spiral structure (Reid et al. 2009; Krishnan et al. 2015). They found that the kinematic distance estimates are often too large, sometimes by more than a factor of two.

Class II methanol masers are not very variable. Caswell et al. (1995) studied a sample of 48 masers found that the majority of them vary less than about 20 % on month to year timescales. However, there are some 6.7-GHz methanol masers that have been shown to flare periodically (e.g. Szymczak et al. 2015; Goedhart et al. 2009).

Another strong and common class II transition occurs at 12.2 GHz. This transition is generally found to be co-spatial within a few milliarcseconds of the 6.7-GHz transition (e.g. Moscadelli et al. 2002) and so observing both is useful to probe the physical conditions of the maser environments (e.g. Cragg et al. 2001; Sutton et al. 2001). Modelling suggests that the conditions for the 6.7- and 12.2-GHz transitions overlap, but are not identical (Cragg et al. 2005). Since there are many 6.7-GHz methanol masers without and 12.2-GHz counterparts, the conditions in these environments must be near the point where the 12.2-GHz transition switches on or off (e.g. Caswell et al. 1995; Breen et al. 2010b). The 12.2-GHz emission is rarely stronger than its companion 6.7-GHz maser and there have been no serendipitous detections of 12.2-GHz masers without an associated 6.7-GHz maser.

2.4 Masers tracing an evolutionary sequence in high-mass star formation

It has been known for several decades that different masers species can trace different stages of star formation. For example, Forster & Caswell (1989) found that OH masers are more evolved than water masers. Masers can be found throughout the formation-stage of high-mass stars, from the earliest stages embedded within infra-red dark clouds (Ellingsen 2006), to the later stages with ultra-compact HII regions (Phillips et al. 1998; Walsh et al. 1998).

More recently, work has been done to quantify the presence and/or absence of various maser transitions tracing different evolutionary stages in high-mass star formation (see Figure 2.6; Ellingsen et al. 2013; Breen et al. 2010b; Ellingsen et al. 2007). Breen et al. (2010b)

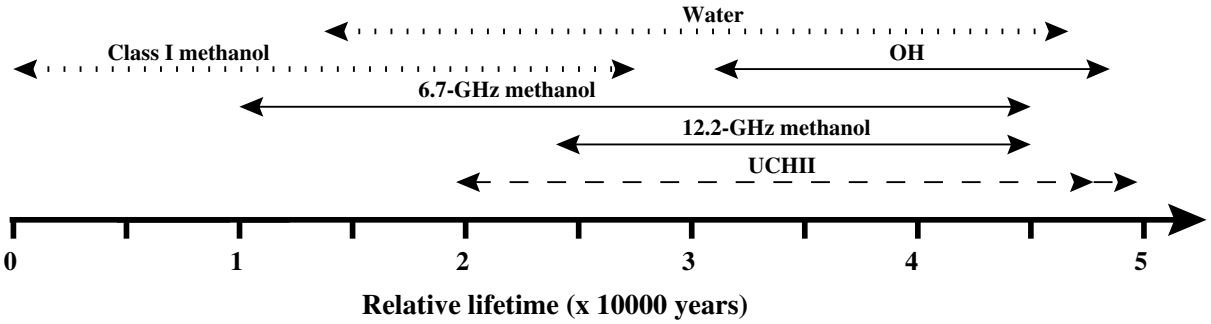

Figure 2.6: The Breen et al. (2010b) evolutionary sequence of masers associated with high-mass star formation regions. Class I and water masers (represented with dotted lines) are estimates from the literature and unpublished data.

show, through statistical analysis of maser presence/absence and multi-wavelength continuum observations, that the presence of 12.2-GHz methanol and OH masers signpost star forming regions that are more evolved than those showing just 6.7-GHz methanol masers. The largest uncertainties remaining in the evolutionary sequence relate to water masers and class I methanol masers. There have been a number of previous studies encompassing both methanol and water masers (e.g. Beuther et al. 2002; Szymczak et al. 2005; Xu et al. 2008), but due to poor spatial resolution and biases in the target sources, how they fit within this evolutionary timeline is not well understood. Hence, high-resolution, unbiased surveys are needed to make progress on these questions.

2.5 Maser surveys

High-resolution observations of 22-GHz water masers towards the statistically complete sample of 6.7-GHz methanol masers from the MMB are presented in this thesis. A number of previous studies comparing water and methanol masers based on various sample selection criteria are outline briefly here (Beuther et al. 2002; Xu et al. 2008; Szymczak et al. 2005; Breen et al. 2010a). Further discussion of these surveys in comparison with the work undertaken in this thesis has been left to Chapter 4.

Beuther et al. (2002) targeted 24 star formation regions, selected based on infrared colours, for water and 6.7-GHz methanol masers with arcsecond resolution. They found ∼60 % of the sources with a methanol maser had an associated water maser (within 1.5 arcseconds) and ∼65 % of the sources with a water maser had an associated methanol maser. Xu et al. (2008) targeted water masers thought to be associated with star formation regions, from the Arcetri catalogue (Comoretto et al. 1990; Brand et al. 1994) for methanol masers with arcminute resolution. 161 of their targets were thought to be high-mass star formation regions, of which 35 % had an accompanying methanol maser.

The studies already undertaken which have the greatest similarity to the study presented in this thesis are those by Breen et al. (2010a) and Szymczak et al. (2005). Szymczak et al. (2005) searched a statistically complete, but flux-limited to a peak intensity above 1.6 Jy, for water masers using the Effelsberg 100m telescope. They targeted 79 sources and found water towards 52 %. Breen et al. (2010a) made a water maser search towards a large sample

of 270 methanol at high-resolution with the ATCA. These methanol masers were primarily those with associated OH maser emission, or those without OH maser emission which had an accurate position determined by Caswell (2009). The Caswell (2009) sample in particular is biased towards sources with a higher 6.7-GHz peak flux density. Their detection rate for water masers towards 6.7-GHz methanol masers was 73 % over two epochs.

The search for water masers presented in this thesis has a great advantage over previous studies because the MMB data is now available. The MMB (as outlined in Chapter 1) performed a sensitive, unbiased search of the Milky Way for 6.7-GHz methanol masers between longitudes 186°, through 0°, to 60° with latitude coverage of $|b| \leq 2°$. They detected 972 sources and all the high-resolution maser positions have now been published (Green et al. 2009; Caswell et al. 2010; Green et al. 2010; Caswell et al. 2011; Green et al. 2012; Breen et al. 2015).

Many other follow-ups of the MMB have been/are being performed. For example, the 12.2-GHz methanol maser follow-up is being performed with Parkes in the longitudes 186°, through 0°, to 20° (Breen et al. 2012b,a, 2014, Breen et al. 2015 in prep). They found 45 % of the 707 MMB targets they surveyed to have associated 12.2-GHz methanol maser emission. They also compared the 6.7-GHz methanol to OH maser flux density ratio to the luminosity of the associated 12.2-GHz methanol maser and found some evidence that the 12.2-GHz methanol maser luminosity starts to decrease about the time an OH maser becomes detectable. There is also a class I methanol maser follow-up currently being undertaken with the ATCA (led by Maxim Voronkov).

The MMB OH follow-up is called Mapping the Galactic Magnetic field through OH masers (MAGMO; Green et al. 2012) is observing the MMB masers with the ATCA for all four ground-state OH maser transitions. So far the pilot region of the Carina-Sagittarius spiral arm tangent (longitudes 280° to 295°) has been surveyed. They detected ground state OH maser emission at 11 of the 23 MMB maser sites in the region. The OH masers detected in this follow-up will also provide information about magnetic fields at sites of high-mass star formation. Zeeman splitting of the OH masers provides both strengths and the orientation of the magnetic fields along the line of sight (towards us or away from us).

A large-scale, unbiased survey for water masers is the H_2O southern Galactic Plane Survey (HOPS; Walsh et al. 2011, 2014). HOPS surveyed 100 deg^2 of our Galaxy for water masers and many other molecular lines with the Mopra Radio Telescope and the water maser detections were subsequently followed-up with the ATCA. HOPS is ideal for studying water masers in all the different environments that they form, however, for comparison with the MMB it lacks sensitivity (HOPS is estimated to be 98 % complete down to 8.4 Jy compared to the the MMB which is estimated to be approaching 100 % completeness at 1 Jy).

A recent unbiased, high-resolution for class I methanol masers was Millimetre Astronomer's Legacy Team-45 GHz (MALT-45; Jordan et al. 2015). The 44-GHz class I methanol masers were observed, along with several other spectral lines in the 42 - 44 and 48 - 49 GHz bands, in the region $l = 330° - 335°$ and $|b| < 0.5°$ with the ATCA. As this is an unbiased survey, it is ideal to study the overlap between the 44-GHz and the 6.7-GHz methanol masers found in the MMB. They found 60 % of the class II masers in the MMB to have associated 44-GHz class I masers and $\sim$ 36 % of 44-GHz class I masers to have an associated class II maser.

2.6 Mid-infrared sources associated with masers

Data from the *Spitzer Space Telescope* has greatly advanced our knowledge of the mid-infrared environments associated with masers. *Spitzer* launched in 2003 and undertook a range of investigator-led and legacy science programs until the supply of liquid helium used to cool the telescope ran out in 2009. Two of the instruments on board are the Infrared Array Camera (IRAC) and the Multiband Imaging Photometer for Spitzer (MIPS). IRAC operated at 3.6, 4.5, 5.8 and 8 μm. The 3.6 and 4.5 μm bands have been able to continue operating after 2009 as part of the *Spitzer Warm Mission*. A major survey to come from *Spitzer* is the Galactic Legacy Infrared Midplane Survey Extraordinaire (GLIMPSE; Benjamin et al. 2003) which surveyed the Galactic Plane in four infrared bands: 3.6, 4.5, 5.8 and 8.0 μm using IRAC. GLIMPSE produced images as well as point source catalogues in all four wavelengths.

Ellingsen (2006) used point sources identified by GLIMPSE to compare the colours of the mid-infrared objects associated with 6.7-GHz methanol masers to the general population of point sources. They used 56 methanol masers, most of which came from a blind single dish survey for methanol masers in $l = 325^\circ - 335^\circ$ (Ellingsen et al. 1996). They found that the mid-IR point sources associated with masers tended to exhibit redder colours than sources without masers, which is consistent with them coming from low-mass Class 0 YSOs (see Figure 2.7). Ellingsen (2006) also compared the colours of 6.7-GHz methanol masers with and without associated OH masers and found colours consistent with sources harbouring an OH maser to be more evolved than those without.

Breen et al. (2010b) compared the GLIMPSE point source colours of a sample of 113 6.7-GHz methanol masers with and without associated 12.2-GHz methanol masers. They found no difference in the colours of the two groups and they proposed that the masers themselves are more sensitive than the mid-infrared data to evolutionary changes in the YSO.

A similar study by Gallaway et al. (2013) examined the mid-infrared colours of the mid-IR sources hosting the MMB masers. Since many of the mid-IR sources associated with methanol masers were more extended than the GLIMPSE point spread function, they used Adaptive Non-Circluar Aperture Photometry (ANCAP) to measure the extended flux densities in all four GLIMPSE bands. Not all of the maser counterparts were included as they were outside the GLIMPSE survey range, fluxes were not available in all four bands or there was more than one possible counterpart (the full MMB catalogue was not available at the time). They found the maser associated sources to be very similar to those of Ellingsen (2006).

Masers are also associated with more extended objects in the GLIMPSE images. For example, shock tracers such as extended emission in the 4.5 μm band, often referred to as either Extended Green Objects (EGOs; Cyganowski et al. 2008), or "green fuzzies" (Chambers et al. 2009) as the 4.5 μm emission is usually coloured green in GLIMPSE three colour images. The 4.5 μm band covers the wavelength range of a number of H_2 and CO spectral lines which are excited by shocks. The presence of strong, extended emission in this band is thought to be a good tracer of outflows from protostellar objects. De Buizer & Vacca (2010) made direct spectroscopic measurements of two EGOs with high surface brightness from Cyganowski et al. (2008) however, and found at one source there was 4.5 μm emission from H_2 spectral lines within the outflow, and at the other source no emission lines were detected in this band, only

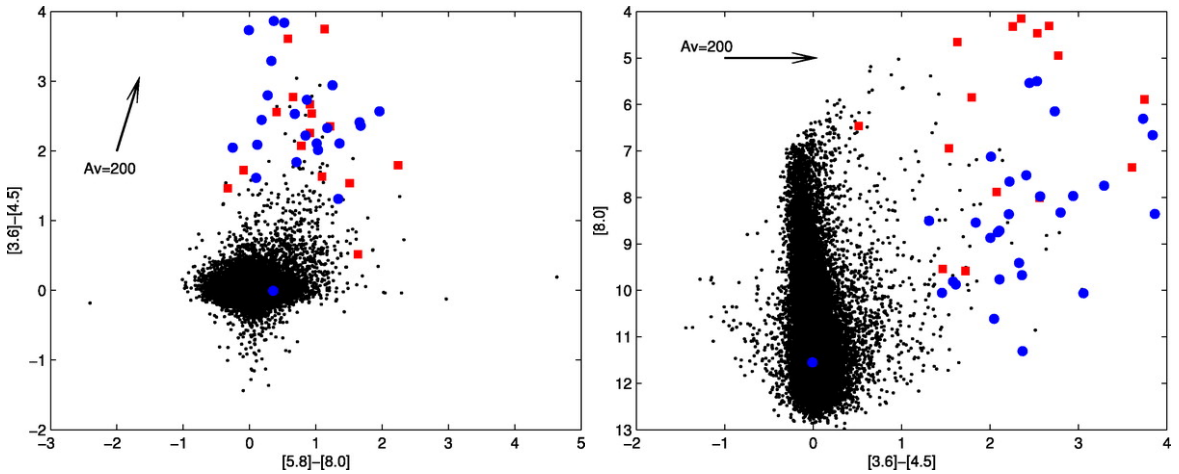

Figure 2.7: Ellingsen (2006) colour-colour and colour-magnitude diagrams made from GLIMPSE point source catalogue data. The methanol masers in the region $l = 325° - 335°$ are red squares and other methanol masers for which ATCA positions were available are blue circles. The black dots are all the sources in the GLIMPSE point source catalogue within 30' of $l = 326.5°$, $b = 0°$.

bright continuum emission - no evidence for any outflow. Hence, EGOs may not be tracing only one evolutionary state of their YSOs.

Also, the exact association between EGOs and masers has been difficult to quantify, as the identification of these objects is somewhat subjective. Cyganowski et al. (2008) complied a catalogue of more than 300 EGOs from the GLIMPSE I survey region which they compared with 6.7-GHz methanol maser surveys of Ellingsen (2006), Walsh et al. (1998) and Caswell (1996). Of the EGOs that fell within these survey areas, they found 73 % of the "likely" EGO candidates and 27 % of the "possible" EGO candidates to have an associated methanol maser. Gallaway et al. (2013) took the statistically complete sample of 6.7-GHz methanol masers from the MMB and compared it with the Cyganowski et al. (2008) catalogue of EGOs. They found ∼18 % of the masers to be associated with EGOs. Conversely, they find 52 % of the "likely" and 25 % of the "possible" EGO candidates to have associated methanol masers.

Cyganowski et al. (2009) observed 20 EGOs for class I 44-GHz and class II 6.7-GHz methanol masers with the VLA. In this smaller sample size, they detected 6.7-GHz methanol masers towards ∼64 % of the EGOs, and of these they found 44-GHz masers associated with ∼89 %. They also compared the spatial distributions of the different maser classes and found that the collisionally pumped class I masers were widely distributed tracing the diffuse 4.5 μm features. However, the radiatively pumped class II masers were more centrally concentrated close to the 24 μm emission (see Figure 2.8).

Chen et al. (2011) observed a subset of the the Cyganowski et al. (2008) EGOs for class I 95-GHz methanol masers with the Mopra 22-m telescope and found a 55 % detection rate. Later they compiled a catalogue of the 98 EGOs in the GLIMPSE II survey region on which they performed a similar search, finding a detection rate of ∼70 %.

Cyganowski et al. (2013) surveyed the 94 EGOs from their Cyganowski et al. (2008) catalogue visible with the Nobeyama 45 m telescope for water maser emission. The beam size of Nobeyama at 22-GHz is 73 arcseconds and the median noise was ∼0.11 Jy. They

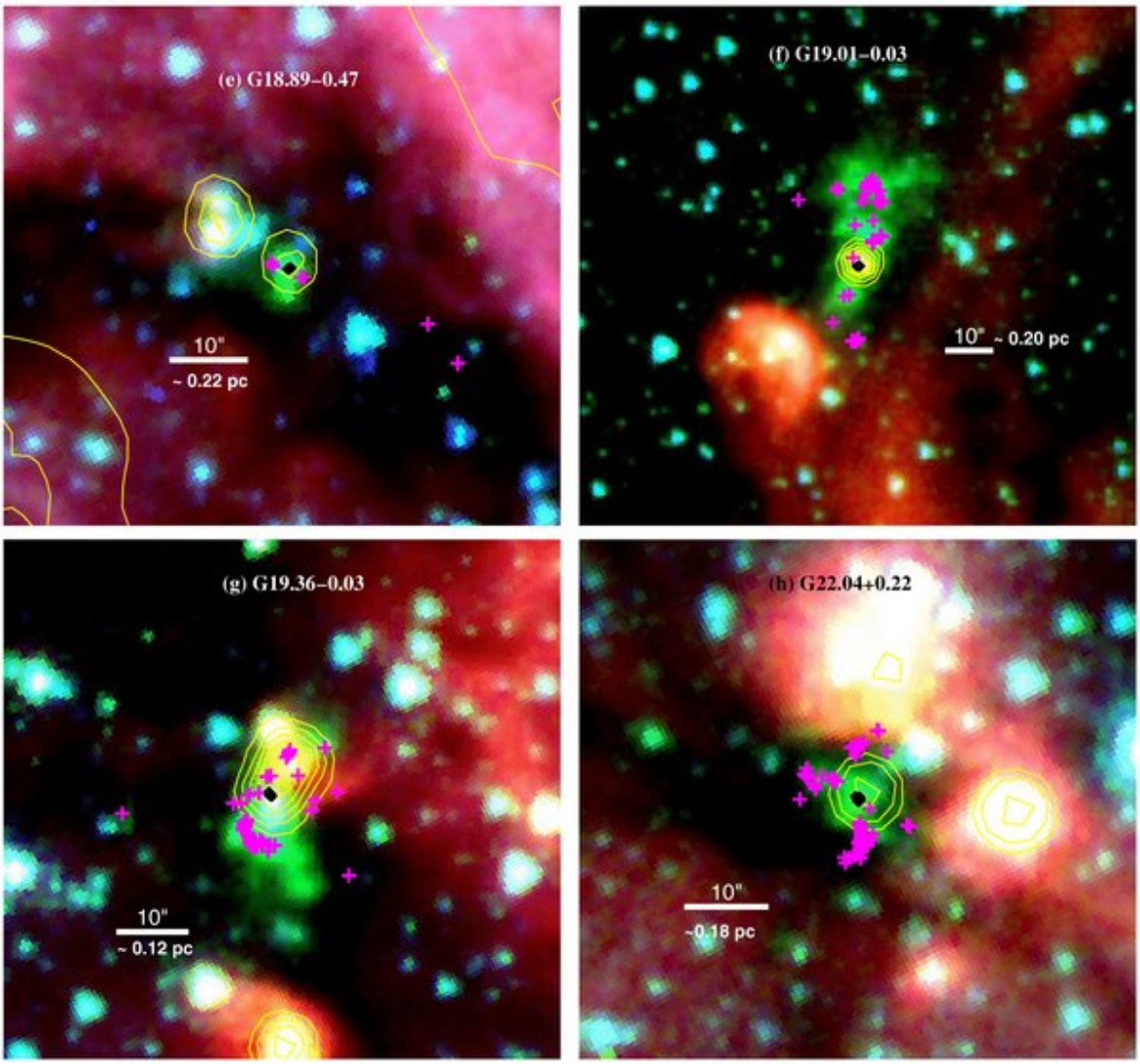

Figure 2.8: Four three colour GLIMPSE images of EGOs from Cyganowski et al. (2009) with 24 μm contours from MIPSGAL plotted in yellow, positions of 44-GHz class I methanol masers in magenta crosses and 6.7-GHz class II methanol masers with diamonds.

detected water maser towards 68 % of the EGOs in their sample and in 81 % of the EGOs with both class I and class II methanol masers present.

Infrared dark clouds are cold ($T < 20$ K), dense ($n > 10^5$ cm^{-3}) cores first discovered in Perault et al. (1996) in a 15 μm survey of the Galactic Plane by *Infrared Space Observatory*. Egan et al. (1998) studied these objects with *Midcourse Space Experiment* and *IRAS* and found they were dark from 7 to 100 μm.

Ellingsen (2006) took a subjective look at the GLIMPSE images and suggested $\sim$ 10 - 20 % of IRDCs have associated methanol masers, implying that in many IRDCs high-mass star formation has already commenced. They suggest that IRDCs where no masers are present may be the sites where an even earlier stage of high-mass star formation is occurring.

Gallaway et al. (2013) did a systematic survey of the MMB masers for IRDCs. They identified two categories of masers within IRDCs: (i) masers embedded within an IRDC with no IRAC counterpart and (ii) masers that are located in or on the perimeter of an IRDC but have an IRAC counterpart (see Figure 2.9). In categories (i) and (ii) they found 5 % and 21

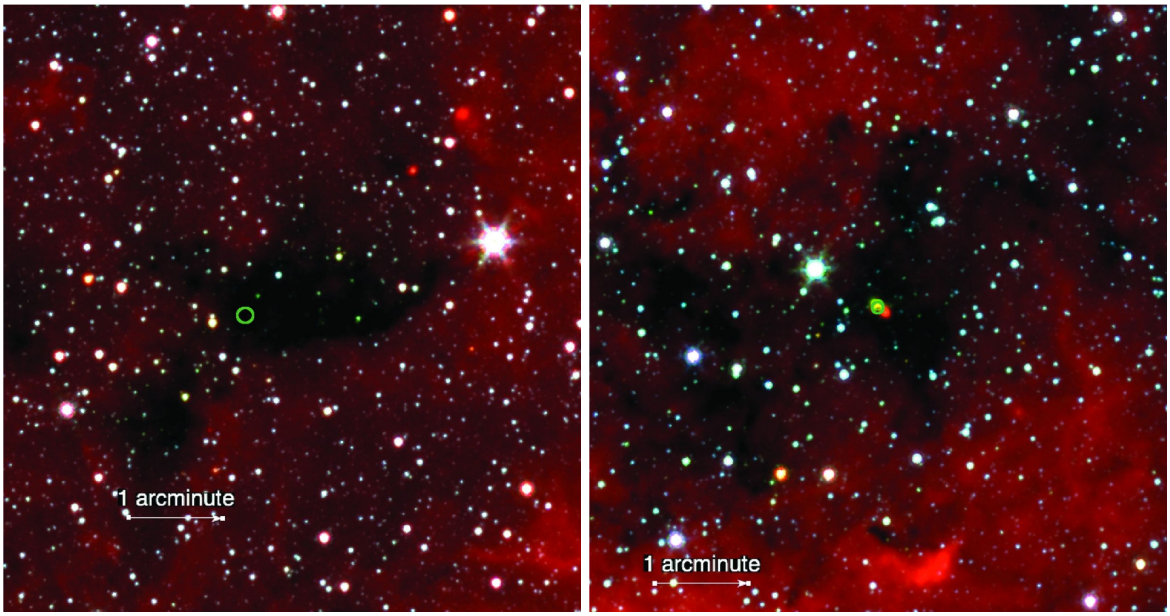

Figure 2.9: Gallaway et al. (2013) GLIMPSE three colour image of an IRDC with the 6.7-GHz methanol maser position marked with a green circle. The maser in the left panel is located within an IRDC but has no IRAC counterpart and the one on the right is located within an IRDC but is associated with an IRAC counterpart.

% of the MMB masers respectively to be located.

2.7 Submillimetre emission associated with masers

Since masers are found within the dusty envelopes of high-mass star formation regions, is it useful to compare maser data to the thermal dust emission. Dust emission is optically thin at submillimetre wavelengths and is useful for tracing column densities and clump masses. Submillimetre emission allows us to study the coldest, densest regions where stars are forming.

Recently, there have been two large, unbiased surveys of the Galactic Plane in the submillimetre regime. The Bolocam Galactic Plane Survey (BGPS; Rosolowsky et al. 2010) and APEX Telescope Large Area Survey of the GALaxy (ATLASGAL; Schuller et al. 2009; Contreras et al. 2013; Csengeri et al. 2014). Both the BGPS and ATLASGAL have resolutions much coarser than the size of a star forming core associated with a maser which means that their flux densities will potentially include emission from many other surrounding sources from the clustered environments where high-mass stars are formed.

The BGPS used the Bolocam instrument on the Caltech Submillimeter Observatory to undertake a continuum survey of the Milky Way at 1.1-mm. The BGPS had an effective resolution of 33 arcseconds and the catalogue is 98 % complete from 0.4 Jy to 60 Jy.

Chen et al. (2012) surveyed 214 BGPS targets for class I 95-GHz methanol masers that satisfied the *Spitzer* GLIMPSE mid-infrared criteria of [3.6] - [4.5] $>$ 1.3, [3.6] - [5.8] $>$ 2.5, [3.6] - [8.0] $>$ 2.5 and 8.0 μm mag less than 10 from Ellingsen (2006) that also had an associated 1.1-mm dust clump from the BGPS. They detected class I methanol masers in 29 % of their targets. They found the that intensity of the masers was not correlated with the mid-infrared colours of the target sources, however, they were correlated with the mass

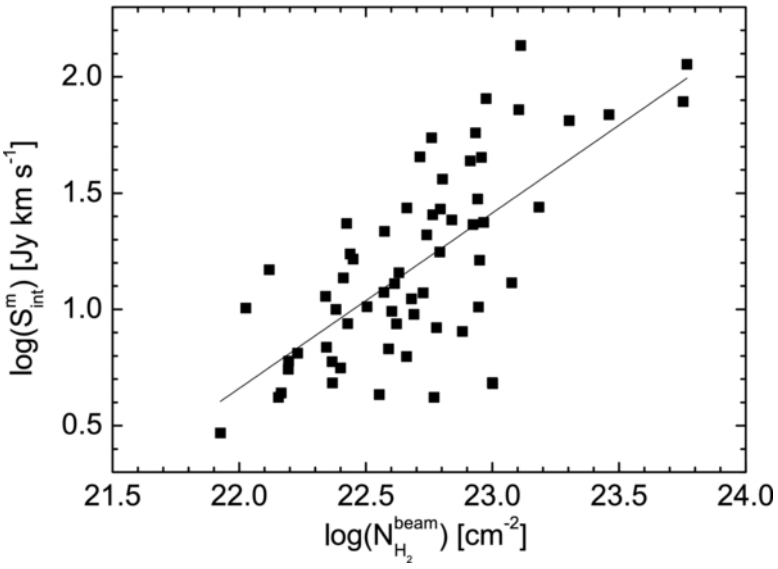

Figure 2.10: Correlation between class I 95-GHz methanol maser integrated flux densities and the beam-averaged column densities of their associated BGPS clumps (Chen et al. 2012).

and beam-averaged column density of the associated BGPS sources. Figure 2.10 shows the correlation between the maser intensity and the beam-averaged column density they found. Comparing BGPS sources with and without class I methanol masers, they found sources with an associated maser had higher column densities and flux densities than those without (Figure 2.11). For the BGPS sources associated with a class I maser, those also associated with a class II maser had higher column densities and flux densities (see Figure 2.12).

Cyganowski et al. (2013) compared their sample of 94 water masers found towards EGOs with the associated BGPS dust clumps. They found no correlation between the water maser luminosity and the clump number density, however, they did find that the water maser luminosity to be weakly correlated with the clump mass.

ATLASGAL surveyed the Galactic Plane at 870 μm with the APEX telescope in Chilie. ATLASGAL had a spatial resolution of 19.2 arcseconds and a 5 σ sensitivity of 0.25 Jy beam^{-1}. Urquhart et al. (2013) studied the ATLASGAL sources associated with the statistically complete sample of the 6.7-GHz methanol masers from the MMB and found masers to be preferentially associated with higher mass clumps.

In this thesis we have used the BGPS and ATLASGAL data to calculate the gas masses and beam averaged column densities of the clumps that the masers are embedded in. The gas mass was calculated for both the BGPS and ATLASGAL using the equation

$$M_{gas} = \frac{S_{int} D^2}{\kappa_d B_\nu(T_{dust}) R_d} \tag{2.1}$$

where S_{int} is the integrated flux density of the source at 1.1 mm for the BGPS data and 870 μm for the ATLASGAL data. D is the distance to the source, for clumps without masers we were not able to calculate the masses as we did not have distance measurements for them. κ_d is the mass absorption coefficient per unit mass of dust, we used $\kappa_d = 1.14$ cm^2 g^{-1} for 1.1 mm Ossenkopf & Henning (1994) and 1.85 cm^2 g^{-1} for 870 μm (from Schuller et al. (2009) who calculated this value by interpolating to 870 μm using Ossenkopf & Henning (1994)).

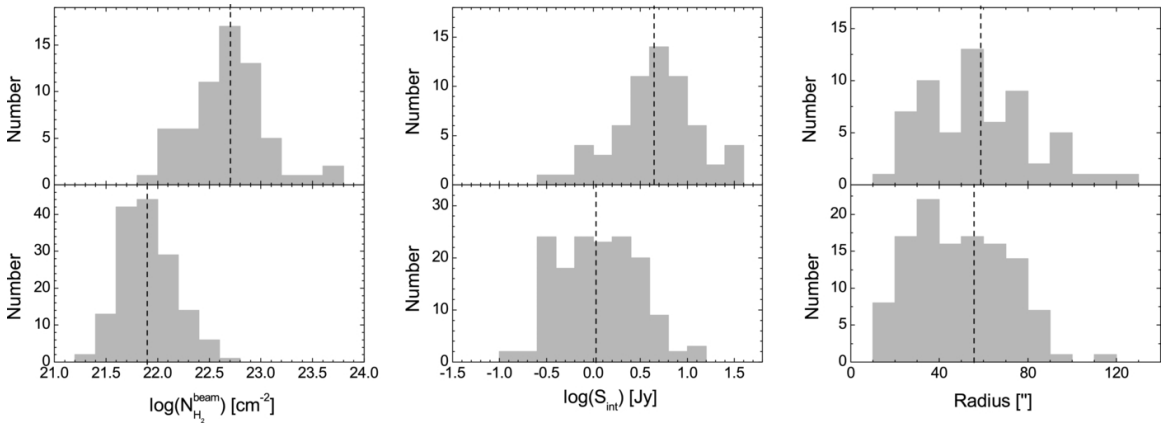

Figure 2.11: Number of BGPS clumps as functions beam-averaged column density, BGPS integrated flux density and BGPS source radius. The top panels are the clumps associated with class I methanol masers and the bottom those without. The mean of each distribution is marked with a dashed line (Chen et al. 2012).

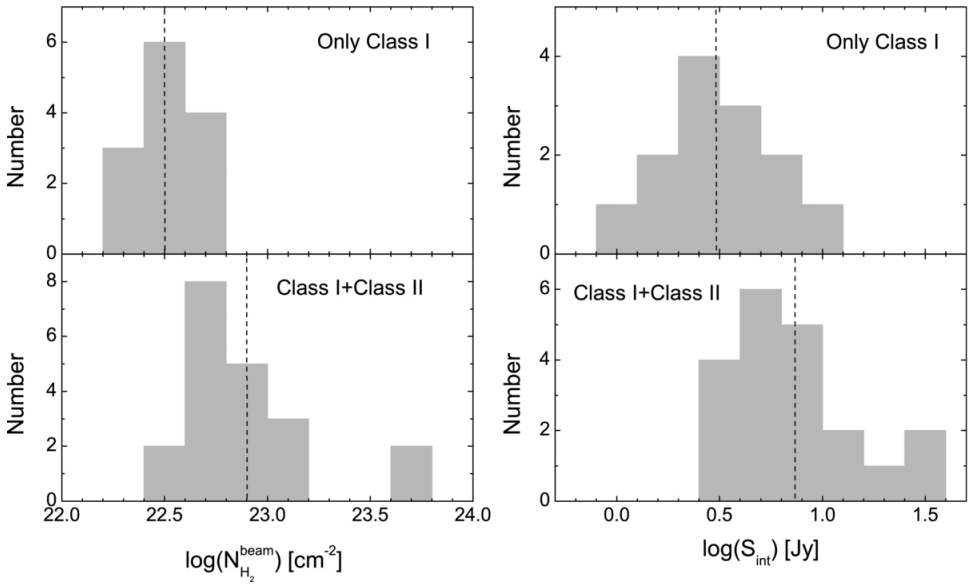

Figure 2.12: Comparison of the beam-averaged column densities and BGPS integrated flux densities of BGPS clumps with associated class I and class II masers and those with only class I (Chen et al. 2012).

$B_\nu(T_{dust})$ is the Planck function at temperature T_{dust} which we assumed to be 20 K and R_d is the dust-to-gas ratio assumed to be 1:100. The mass equation is from Hildebrand (1983) and assumes that the submillimetre continuum emission is optically thin.

The column density is the molecular hydrogen column inferred from the observed dust emission, an assumed dust-to-gas ratio and assuming that the dust emission is optically thin. For comparisons with previous work by Chen et al. (2012) and Urquhart et al. (2013), we have calculated the beam averaged column density for the BGPS data and for ATLASGAL.

The BGPS beam averaged column density was calculated using

$$N_{H_2}^{beam} = \frac{S_{40"}}{\Omega_{beam}\mu\kappa_d B_\nu(T_{dust})R_d} \tag{2.2}$$

$S_{40"}$ is the 1.1 mm flux density within an aperture with a diameter of 40 arcseconds, Ω_{beam} is the solid angle of the beam, μ is the mean mass per particle (we used $\mu = 2.3\ m_H$ for consistency with Chen et al. (2012)) and the other values are as defined for Equation 2.1. For the BGPS $S_{40"}$ we applied a 1.5 correction factor to the Rosolowsky et al. (2010) flux densities as suggested by Dunham et al. (2010) and also an aperture correction of 1.46 to for the power outside the 40 arcsecond aperture due to the sidelobes of the beam (Aguirre et al. 2011).

The ATLASGAL column density was calculated using

$$N_{H_2} = \frac{S_\nu}{\Omega_{beam}\mu\kappa_d B_\nu(T_{dust})R_d} \tag{2.3}$$

where S_ν is the peak flux density of the clumps and the other values are as defined for Equation 2.2.

In this thesis, we have used these masses and column densities calculated from dust emission data, along with other YSO age indicators such as their associated 6.7-GHz methanol maser properties and mid-infrared emission to investigate how water masers fit within an evolutionary timeline of high-mass star formation.

Chapter 3

Water maser observations and results

Here we present the survey method and results of the water maser observations towards Methanol Multibeam (MMB) targets between $l = 341^\circ$ to 20° (through the Galactic Centre).

3.1 Survey Observation Method and Data Reduction

The water maser observations were carried out using the Australia Telescope Compact Array (ATCA) in the H214 and H168 array configurations. These hybrid array configurations have both East - West and North - South baselines and so provide better *uv* coverage for equatorial sources.

Although the observations were made with a relatively compact array, configurations having longer baselines would not necessarily equate to greater astrometric accuracy. The absolute astrometric accuracy of the ATCA is about 0.4 arcseconds (set by the astrometric accuracy of the phase calibrators and the degree to which they are point sources for the array configuration, the frequency of the observation and the accuracy to which we know the locations of the telescopes; Caswell 1997). The astrometric accuracy for these observations is estimated to range from 0.4 - 2.0 arcseconds (as some of the observations were made in poor weather). Weather is a major consideration when observing water masers because of absorption and emission in the 6_{16} - 5_{23} transition by the water vapour in the Earth's atmosphere.

The primary beam for the ATCA at 22 GHz is 2.1 arcminutes and the synthesised beams of the H214 and H168 configurations are ~ 9.6 and ~ 12.4 arcseconds respectively. Some of our sources were observed by Breen et al. (2010a) with the ATCA and our positions agreed with the positions they obtained to within ~ 2 arcseconds. Uncertainty is also introduced as water maser clusters are typically spread over linear scales of around 30 mpc (1 arcsecond angular scale at 6 kpc; see Forster & Caswell 1989); although in some regions the linear scales are as much as 5 times greater (4 arcsecond angular scale at 8 kpc; see Reid et al. 1988).

The observations were conducted 2010 November 2-3 (taken with the H214 array configuration), 2011 June 3-5 (H214), 2011 August 8 (H168) and 2011 August 10 (H168). Our targets consisted of all 6.7-GHz methanol masers in the $l = 341^\circ - 20^\circ$ through Galactic Cen-

tre region, including those which had previously been observed. 323 targets in total. This is because water masers are known to have extremely variable flux densities (e.g. Breen et al. 2010a) and we wish to have a statistically complete sample of masers at one epoch.

We observed groups of six 6.7-GHz methanol maser targets which were close together on the sky for 1.5 minutes each before observing a phase calibrator for 1.5 minutes. Each methanol maser position was observed at least four times, over an hour angle range of at least six hours, to ensure sufficient *uv* coverage for imaging giving a total on-source time of at least six minutes. Observations of PKS B1934-638 were taken for primary flux density calibration (expected to be accurate to ~ 20 %) and PKS B1253-055 was used for bandpass calibration. The phase calibrators were PKS B1646-50 (for the $l = 341^\circ - 348^\circ$ targets), PKS B1714-336 ($l = 348^\circ - 5^\circ$), PKS B1730-30 ($l = 6^\circ - 15^\circ$) and PKS B1829-106 ($l = 15^\circ - 20^\circ$).

The Compact Array Broadband Backend (CABB; Wilson et al. 2011) was configured with two bands to observe the 22.235-GHz water maser transition in the first band and the ammonia (1,1) and (2,2) transitions in the second band centred between the two transitions at 23.708 GHz. Each band had 64 MHz bandwidth with 2048 spectral channels corresponding to a velocity width of 0.42 km s^{-1} and 0.39 km s^{-1} for the water and ammonia transitions respectively and velocity resolutions for uniform weighting of the spectral channels of 0.50 km s^{-1} and 0.47 km s^{-1} and velocity coverages of > 800 km s^{-1}. The 5 σ detection limit for these observations ranged from $\sim$40 mJy to $\sim$250 mJy depending on weather conditions and total time on-source. In addition 2 x 2 GHz continuum bands with 32 x 64 MHz channels were available for the 2011 August observations.

The water maser data were reduced in MIRIAD (Sault et al. 1995) using standard techniques for ATCA spectral line data. We determined the positions for the masers by fitting a gaussian, with the width of the point spread function of the image, to the emission in the peak channel. The spectra were produced from these image cubes by integrating the emission at each maser site. We inspected the image cubes within an small radius of each methanol maser to find the associated water masers. We did not inspect the whole cubes throughly since the focus of this study was the evolutionary state of water maser with respect to 6.7-GHz methanol masers.

3.2 Results

In this thesis the 22-GHz water masers detected towards 6.7-GHz methanol masers from the MMB in Galactic Longitudes 341° to 20° (through the Galactic Centre) are reported.

Figure 3.1 shows a histogram of the offsets between the target methanol masers and the water masers detected around them. We have used an offset of ≤ 3.0 arcseconds from the 6.7-GHz methanol maser to establish association with the exception of 5.885–0.393, 6.795–0.257 and 10.342–0.142 (for details see Section 3.2.1). Note: 3 arcseconds is not the positional uncertainty of our maser sites, rather the angular separation we deem reasonable to determine if masers are associated with the same YSO. For the most distant sources in our sample 3 arcseconds corresponds to a linear scale of $\sim$200 mpc. We have used a 3 arcsecond criteria as it will include all the real associations and is consistent with what has been used in other large, high resolution surveys of water masers with the ATCA such as Breen et al. (2010a)

and Caswell et al. (2010).

We found 156 of the 323 MMB sources in this range to have associated water maser emission ($\sim$ 48 %). The spectra of the associated water masers taken with the ATCA are presented in Figure 3.3 and comments on individual sources of interest are given in Section 3.2.1. We have only determined maser associations based on their angular separation. We did not use their velocities as water masers are well known for showing emission a long way from the systemic velocity of the region often spanning many tens to hundreds of km s^{-1}.

We have looked at the distributions of the physical separations in the plane of the sky as we have good distance estimates to these masers. The distances were taken from Green & McClure-Griffiths (2011) or Motogi et al. (2011) where available, of which a few are astrometric distances but the majority are the kinematic distances with the near-far ambiguity resolved using HI self-absorption. For the remaining sources we used the 6.7-GHz methanol peak velocities and the Reid et al. (2009) rotation curve to estimate their distances. For 15 sources the Reid et al. (2009) rotation curve produced very unrealistic distance estimates, particularly near the Galactic centre where non-circular motions are large. For these sources we used estimates which utilise a Baysian approach which takes into account a range of distance estimations including any trigonometric parallax distances of nearby sources, CO and kinematic distances (Mark Reid, private communication).

The distribution of projected distances between the methanol and water masers is given in Figure 3.2. Given the varying distances to the masers, determining association based on linear separations is desirable, however for ease of comparison with previous work, we have used the 3 arcsecond angular separation criteria. This will make little difference to our results as most of the water masers we have classified as associated are within 0.05 pc of their methanol maser and all are within 0.2 pc. There are a small number of masers that we have classified as not associated within 0.05 pc. A couple are separated by less than 3 arcseconds, however, these were both close pairs of methanol masers with only one water maser detected (within 3 arcseconds of both of them) and the water masers have been assigned to the closest methanol maser. The rest have separations greater than 3 arcseconds.

The results of the search are summarised in Table 3.1: column 1 gives the source name (Galactic Longitude and Latitude) of the target 6.7-GHz methanol maser; columns 2 and 3 give the position of the water maser in Right Ascension and Declination (J2000); column 4 the peak velocity; columns 5 and 6 the minimum and maximum velocities of the emission; column 7 the peak flux densities; column 8 the integrated flux densities; columns 9, 10 and 11 the peak, minimum and maximum velocities of the associated 6.7-GHz methanol masers; column 12 the angular offsets; column 13 the epoch of the water observations and column 14 lists the distances to the MMB sources.

Column 15 of Table 3.1 lists the associations with 12.2-GHz methanol and OH masers from Breen et al. (2012b), Breen et al. (2014), Caswell (1998) and Caswell et al. (2013). Note that the 12.2-GHz associations are complete, coming from targeted observations towards the MMB sources. The OH observations are not complete towards all the MMB sources. Caswell (1998) surveyed the Galactic Plane between $l = 312^\circ - 356^\circ$ and $|b| < 0.6^\circ$ and will have detected most of the masers above $\sim$3 Jy. We have indicated MMB sources that lie within the area of this survey, but no OH emission was detected. Also indicated in this column,

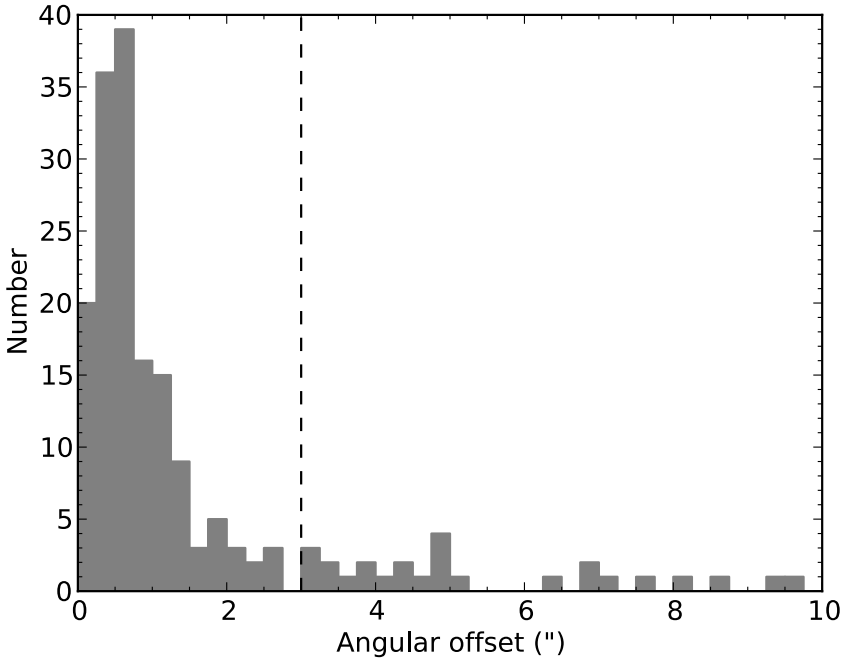

Figure 3.1: Separations between methanol maser targets and our detected water masers. Some water masers further than 10 arcseconds from their targets were also detected. We have zoomed in on this axis for clarity.

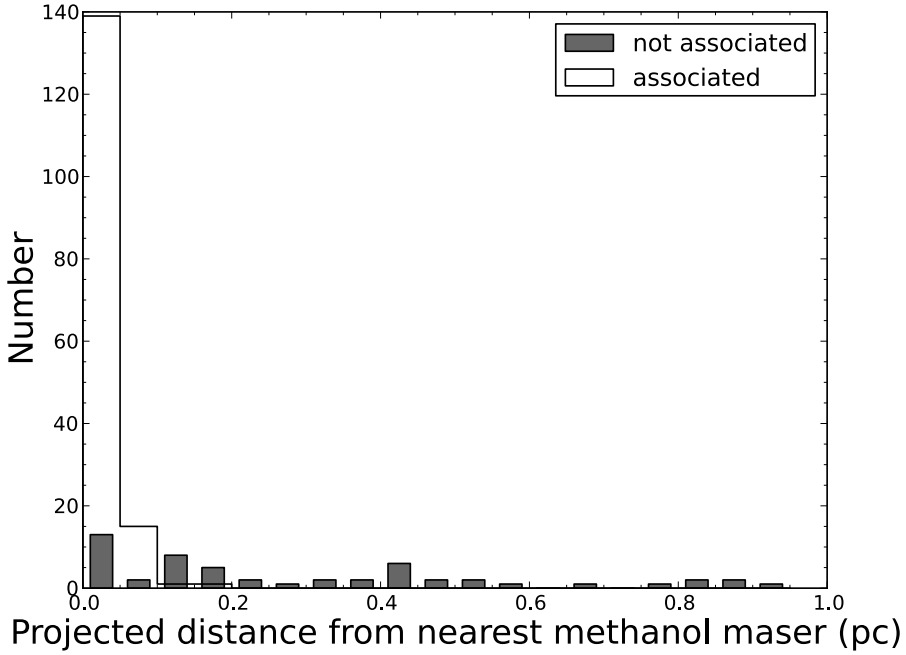

Figure 3.2: Linear separations between methanol maser targets and our detected water masers. We only show up to 1 pc for clarity.

are sources that were observed for water maser emission in Breen et al. (2010a). In addition to the maser associations for the sources between $l = 6^\circ - 20^\circ$, associations with Extended Green Objects and Infrared Dark Clouds are listed.

The methanol maser sites observed for which we found no associated water emission are listed in Table 3.2 along with the 5σ detection limits for each source. Note that 23 of the sites in these tables have shown water emission at other epochs (Breen et al. 2010a; Pillai et al. 2006b), as identified in the 4th column (associations) and are discussed in Sections 3.2.1 and 4.3.

Table 3.1: Positions and parameters of the water masers between $l = 341° - 6°$ (through 0°) associated with 6.7-GHz methanol masers. RA and DEC are in J2000 coordinates. Epochs are coded 1, 2, 3, 4, 5, 6, 7 and 8 for 2011 June 3, 2011 June 4, 2011 June 5, 2011 August 8, 2010 November 2, 2010 November 3, 2011 August 9 and 2011 August 10 respectively. Associations with 12.2-GHz methanol masers (Breen et al., 2012; Breen et al., 2014) are indicated with an 'm', associations with the 1665 MHz transition of OH masers (Caswell, 1998; Caswell et al. 2013) are indicated with an 'o' and sources marked with a '*' are within the survey region for OH by Caswell (1998) and no emission was detected. Sources observed for water masers in 2003 and/or 2004 by Breen et al. (2010a) are indicated with a 'w'. From inspection of the GLIMPSE infrared images, masers associated with an Infrared Dark Cloud or Extended Green Object are indicated with an 'i' or 'e' respectively. Sources outside of the GLIMPSE survey range are indicated with an '+'. GLIMPSE images were only inspected for sources between $l = 6° - 20°$. Distances estimates are from Green et al. (2011) or Motogi et al. (2011) where available, others are the near kinematic distances (these are in italics) and the remainder are from Mark Reid (private communication) (these are in square brackets).

MMB Target	Equatorial Coordinates						S_{int}	6.7-GHz methanol			Off-			
Name	RA	DEC	V_{pk}	V_l	V_h	S_{pk}	(Jy km	V_{pk}	V_l	V_h	sets	Ep.	Dist.	Assoc.
(l, b)	(h m s)	(° ' ")		(km s^{-1})		(Jy)	s^{-1})		(km s^{-1})		(")		(kpc)	
341.218−0.212	16 52 17.88	−44 26 52.8	−39.5	−51.1	−34.8	106.	505.	−37.9	−50.0	−35.0	0.6	1	3.1	mow
341.276+0.062	16 51 19.38	−44 13 44.9	−74.9	−77.1	−70.8	1.6	6.9	−70.5	−77.5	−65.5	0.5	1	11.5	mow
341.973+0.233	16 53 02.96	−43 34 55.1	−13.9	−17.1	−8.7	1.2	6.1	−11.5	−12.5	−10.5	0.4	1	1.0	*
342.446−0.072	16 55 59.91	−43 24 23.1	−20.2	−28.2	−18.6	1.0	4.3	−30.0	−32.5	−14.0	0.7	1	2.0	m*
342.484+0.183	16 55 02.30	−43 13 00.1	−49.4	−53.2	−31.5	14.9	108.	−41.9	−44.5	−38.5	0.3	1	12.9	m*w
342.954−0.019	16 57 30.63	−42 58 34.6	−6.1	−15.8	2.7	3.3	20.9	−4.1	−14.0	−2.0	0.3	1	0.7	*
343.502−0.472	17 01 18.46	−42 49 37.3	−48.6	−50.7	−25.5	3.6	26.0	−42.0	−43.0	−32.0	0.9	1	3.0	m*
343.756−0.163	17 00 49.88	−42 26 08.8	−38.8	−45.0	−5.3	34.8	268.	−30.8	−32.5	−24.0	0.7	1	2.5	*
344.227−0.569	17 04 07.90	−42 18 39.3	−1.4	−52.1	10.1	11.0	230.	−19.8	−33.0	−10.5	1.4	1	2.1	mow
344.581−0.024	17 02 57.71	−41 41 53.9	−3.4	−35.3	19.1	366.	2840	1.6	−5.0	2.5	0.2	1	16.2	ow
345.003−0.223	17 05 10.92	−41 29 06.6	−83.6	−86.8	21.8	11.3	62.3	−23.1	−25.0	−20.1	0.6	1	2.2	mow
345.012+1.797	16 56 46.88	−40 14 08.2	−11.3	−31.2	9.6	88.7	534.	−12.2	−16.0	−10.0	0.9	1	1.3	mw
345.131−0.174	17 05 23.23	−41 21 10.6	−27.1	−32.3	−20.9	4.9	40.8	−28.9	−31.0	−28.0	0.2	1	2.7	*
345.407−0.952	17 09 35.43	−41 35 56.3	−16.2	−25.4	−11.8	0.4	3.3	−14.3	−15.5	−14.0	0.8	1	1.5	ow
345.424−0.951	17 09 38.55	−41 35 04.6	−14.1	−26.3	−9.0	0.9	7.7	−13.2	−21.0	−5.0	0.1	1	1.4	w
345.441+0.205	17 04 46.87	−40 52 38.1	−20.3	−37.5	3.6	2.7	42.4	0.9	−13.0	2.0	0.1	1	10.8	*
345.487+0.314	17 04 28.37	−40 46 29.8	5.7	−58.4	7.6	1.7	12.9	−22.6	−24.0	−21.5	1.9	1	2.3	*w
345.505+0.348	17 04 22.95	−40 44 24.6	−22.4	−26.2	−9.6	4.8	45.4	−17.8	−23.1	−10.5	3.0	1	10.8	mow
345.807−0.044	17 06 59.84	−40 44 08.2	2.7	−3.8	3.6	1.0	4.1	−2.0	−3.0	−0.5	0.0	1	10.8	m*
345.824+0.044	17 06 40.70	−40 40 09.8	−20.4	−24.1	−1.2	8.1	44.5	−10.3	−12.0	−9.0	0.1	1	10.9	*
345.949−0.268	17 08 23.61	−40 45 21.3	−8.1	−11.8	−3.8	1.2	7.8	−21.9	−22.5	−21.4	0.3	1	14.1	*
345.985−0.020	17 07 27.57	−40 34 43.4	−77.6	−90.5	−69.9	11.3	77.7	−84.1	−85.5	−81.7	0.2	1	11.0	*
346.036+0.048	17 07 20.01	−40 29 48.9	−12.3	−20.5	−7.6	5.0	19.7	−6.4	−14.5	−3.9	0.1	1	10.9	*
346.231+0.119	17 07 39.05	−40 17 52.6	−91.9	−109.4	−90.2	3.1	10.0	−95.0	−96.6	−92.6	0.6	1	10.7	*
346.517+0.117	17 08 33.07	−40 04 14.7	2.2	−4.3	3.5	0.6	3.8	−1.7	−3.0	1.0	1.4	1	10.9	*
346.522+0.085	17 08 42.21	−40 05 08.4	8.1	−5.9	10.2	2.3	16.8	5.7	4.7	6.1	1.1	1	10.9	*w
347.230+0.016	17 11 11.14	−39 33 27.2	−74.8	−78.8	−68.8	9.6	33.1	−68.9	−69.9	−68.0	0.4	1	11.5	*
347.583+0.213	17 11 26.74	−39 09 22.4	−100.4	−104.5	−93.1	0.5	6.0	−102.5	−103.8	−96.0	0.3	1	5.3	m*
347.628+0.149	17 11 50.97	−39 09 29.8	−92.3	−95.0	−90.4	6.7	20.3	−96.5	−98.9	−95.0	0.9	1	5.3	ow
347.631+0.211	17 11 36.13	−39 07 06.9	−89.8	−97.1	−85.4	24.5	97.3	−91.9	−94.0	−89.0	1.0	1	5.7	*w
348.550−0.979	17 19 20.30	−39 03 51.8	−24.1	−25.4	−15.4	0.8	4.1	−10.6	−19.0	−7.0	1.3	1	1.7	mo
348.579−0.920	17 19 10.61	−39 00 24.5	−10.6	−16.9	−8.5	8.0	30.4	−15.0	−16.0	−14.0	0.4	1	1.9	o
348.617−1.162	17 20 18.64	−39 06 50.7	−9.3	−23.5	−4.2	1.5	8.0	−11.4	−21.5	−8.5	0.1	1	1.9	m
348.654+0.244	17 14 32.41	−38 16 16.7	18.1	13.3	20.9	17.0	63.3	16.9	16.5	17.5	0.5	1	11.2	*
348.884+0.096	17 15 50.08	−38 10 12.7	−78.5	−90.3	−73.1	5.3	46.5	−74.5	−79.0	−73.0	0.6	2	11.1	mow
348.892−0.180	17 17 00.17	−38 19 28.2	7.1	−18.3	13.3	1.5	14.0	1.5	1.0	2.0	0.9	2	11.2	ow
349.067−0.017	17 16 50.70	−38 05 14.3	13.0	−9.0	16.9	0.9	3.8	11.6	6.0	16.0	0.4	2	11.3	ow
349.092+0.106	17 16 24.54	−37 59 45.8	−80.5	−87.3	−54.6	15.8	115.	−81.5	−83.0	−78.0	0.6	2	*5.6*	mow
349.151+0.021	17 16 55.86	−37 59 47.7	15.2	12.5	22.9	0.8	6.2	14.6	14.1	25.0	0.3	2	11.3	*
349.799+0.108	17 18 27.70	−37 25 03.5	−60.7	−73.5	−55.0	4.1	18.2	−62.4	−65.5	−57.4	0.5	2	*5.1*	m*
350.015+0.433	17 17 45.36	−37 03 11.5	−25.3	−41.6	−8.5	1.8	17.7	−30.4	−37.0	−29.0	1.0	2	12.9	ow
350.104+0.084	17 19 26.64	−37 10 53.0	−74.0	−83.3	−62.1	15.2	140.	−68.1	−69.0	−67.5	0.4	2	*5.3*	*
350.189+0.003	17 20 01.38	−37 09 30.3	−65.5	−67.6	−61.3	0.6	2.3	−62.4	−65.0	−62.0	0.4	2	*5.1*	*
350.340+0.141	17 19 53.39	−36 57 21.2	−54.9	−90.1	−51.4	0.8	14.2	−58.4	−60.0	−57.5	2.5	2	11.5	m*
350.356−0.068	17 20 47.54	−37 03 41.6	−71.3	−74.4	−63.1	0.4	1.6	−67.6	−68.5	−66.0	0.3	2	11.2	*
350.520−0.350	17 22 25.40	−37 05 13.4	−26.9	−38.4	−9.2	3.3	30.8	−24.6	−25.0	−22.0	1.0	2	3.0	*
350.686−0.491	17 23 28.59	−37 01 48.6	−14.1	−17.1	−11.5	22.0	57.5	−13.8	−15.0	−13.0	0.5	2	2.1	mow
351.161+0.697	17 19 57.44	−35 57 53.2	−3.7	−17.4	2.8	45.1	341.	−5.2	−7.0	−2.0	0.8	2	1.8	ow
351.417+0.645	17 20 53.36	−35 47 00.0	−7.3	−43.4	13.7	156.	2800	−10.4	−12.0	−6.0	1.1	2	*1.7*	mow
351.581−0.353	17 25 25.20	−36 12 44.0	−91.6	−112.8	−58.8	110.	864.	−94.2	−100.0	−88.0	2.3	2	5.1	ow
351.611+0.172	17 23 21.23	−35 53 32.3	−20.1	−88.7	−17.2	1.1	27.2	−43.7	−46.0	−31.5	0.3	2	*4.6*	m*
351.775−0.536	17 26 42.57	−36 09 19.1	−0.4	−28.7	28.1	61.9	769.	1.3	−9.0	3.0	1.6	2	0.4	mo
352.133−0.944	17 29 22.26	−36 05 00.5	−12.4	−13.6	2.6	2.2	12.6	−7.8	−18.8	−5.6	0.7	2	2.1	w
352.517−0.155	17 27 11.29	−35 19 32.0	−48.6	−50.4	−44.3	2.2	10.0	−51.3	−52.0	−49.0	0.7	2	11.5	ow
352.584−0.185	17 27 29.51	−35 17 14.3	−77.2	−79.7	−76.4	1.2	2.6	−85.6	−92.6	−79.7	0.8	2	5.1	*
352.630−1.067	17 31 13.82	−35 44 08.5	10.6	−18.2	18.1	14.1	126.	−3.0	−8.0	−2.0	1.1	2	0.9	ow
352.855−0.201	17 28 17.61	−35 04 12.5	−60.2	−62.7	−5.6	0.8	9.6	−51.4	−54.1	−50.1	0.5	2	11.3	*
353.216−0.249	17 29 27.68	−34 47 48.3	−14.5	−51.4	10.5	4.8	30.6	−23.0	−25.0	−15.0	1.8	2	3.3	*
353.273+0.641	17 26 01.55	−34 15 15.1	−52.2	−117.8	6.3	182.	954.	−4.4	−7.0	−3.0	0.4	2	*0.8*	w
353.537−0.091	17 29 41.25	−34 26 28.6	−60.3	−72.1	−55.6	0.6	3.7	−56.6	−59.0	−54.0	0.2	2	11.0	m*
354.308−0.110	17 31 48.52	−33 48 29.2	9.1	4.0	20.9	6.1	39.7	18.7	11.0	19.5	0.5	2	[11.6]	*
355.344+0.147	17 33 29.02	−32 47 58.8	10.0	5.7	124.0	12.7	38.0	19.9	19.0	21.0	0.4	2	[11.5]	o

Table 3.1: – *continued*

MMB Target	Equatorial Coordinates						S_{int}	6.7-GHz methanol			Off-			
Name	RA	DEC	V_{pk}	V_l	V_h	S_{pk}	(Jy km	V_{pk}	V_l	V_h	sets	Ep.	Dist.	Assoc.
(l, b)	(h m s)	(° ’ “)		(km s^{-1})		(Jy)	s^{-1})		(km s^{-1})		(“)		(kpc)	
355.346+0.149	17 33 28.89	–32 47 49.5	9.2	6.8	21.3	4.9	16.7	9.9	9.0	12.5	0.3	2	[11.5]	*w
355.538−0.105	17 34 59.58	–32 46 23.2	–1.5	–4.7	0.9	2.3	7.1	3.8	–3.5	5.0	0.6	2	17.7	*
355.666+0.374	17 33 24.89	–32 24 21.0	–3.3	–5.6	3.1	0.4	2.0	–3.4	–4.5	0.6	0.3	2	16.4	*
357.558−0.321	17 40 57.15	–31 10 59.6	–4.6	–56.6	38.8	28.7	455.	–3.9	–5.5	0.0	0.6	2	*1.8*	–
357.922−0.337	17 41 55.00	–30 52 54.8	4.0	–14.1	7.9	1.4	8.0	–4.9	–5.5	–4.0	0.8	3	2.5	–
357.965−0.164	17 41 20.10	–30 45 16.7	–5.2	–61.1	37.3	3.3	34.1	–8.8	–9.0	3.0	2.3	3	3.9	w
357.967−0.163	17 41 20.27	–30 45 06.2	0.6	–74.2	103.1	57.8	2220	–4.2	–6.0	0.0	0.6	3	2.2	mow
358.386−0.483	17 43 37.69	–30 33 50.2	–1.9	–6.8	4.2	7.1	28.3	–6.0	–7.0	–5.0	1.9	3	*3.5*	ow
358.460−0.391	17 43 26.72	–30 27 11.8	–4.5	–19.5	–1.8	3.2	28.0	1.2	–0.5	4.0	0.7	3	[3.5]	–
358.931−0.030	17 43 09.96	–29 51 46.0	–21.6	–25.3	–12.5	0.7	7.2	–15.9	–22.0	–14.5	0.7	3	*6.4*	–
358.980+0.084	17 42 50.32	–29 45 41.4	–8.1	–10.3	6.1	0.4	3.0	6.2	5.0	7.0	1.9	3	[3.8]	–
359.138+0.031	17 43 25.62	–29 39 17.3	–1.3	–121.4	49.7	304.	2300	–3.9	–7.0	1.0	0.6	3	*3.7*	ow
359.436−0.104	17 44 40.56	–29 28 15.8	–56.7	–61.1	–38.8	13.4	70.4	–46.7	–53.0	–45.0	0.5	3	*7.9*	mow
359.436−0.102	17 44 40.05	–29 28 12.4	–57.1	–61.2	–54.1	13.2	80.3	–54.0	–58.0	–53.6	2.1	3	*8.0*	w
359.615−0.243	17 45 39.08	–29 23 30.3	23.4	–6.1	65.7	80.2	457.	22.6	14.0	27.0	0.4	3	*7.7*	mow
359.970−0.457	17 47 20.18	–29 11 59.0	4.7	2.7	12.8	1.1	6.1	23.8	20.0	24.1	0.4	3	*8.3*	ow
0.167−0.446	17 47 45.46	–29 01 29.4	14.0	7.6	18.1	2.8	22.5	13.8	9.5	17.0	0.2	3	*8.0*	–
0.315−0.201	17 47 09.10	–28 46 16.0	19.9	13.3	33.8	2.9	18.7	19.4	14.0	27.0	0.5	3	*7.8*	mw
0.376+0.040	17 46 21.38	–28 35 39.9	38.8	–15.6	71.5	119.	483.	37.0	35.0	40.0	0.4	3	*8.0*	ow
0.496+0.188	17 46 03.95	–28 24 51.8	0.9	–9.9	20.8	1.5	12.4	0.8	–12.0	2.0	1.0	3	*3.6*	mow
0.546−0.852	17 50 14.41	–28 54 30.1	17.3	–95.0	123.7	204.	3250	11.8	8.0	20.0	1.3	3	*7.0*	mow
0.836+0.184	17 46 52.80	–28 07 36.0	–52.8	–58.7	16.1	0.9	20.3	3.6	2.0	5.0	1.4	3	*4.6*	m
1.008−0.237	17 48 55.28	–28 11 48.0	0.8	–0.5	3.2	1.7	4.5	1.6	1.0	7.0	0.2	3	*2.9*	–
1.147−0.124	17 48 48.50	–28 01 11.1	–22.2	–25.4	0.8	4.3	51.6	–15.3	–20.5	–14.0	0.3	3	*4.1*	–
2.143+0.009	17 50 36.11	–27 05 47.1	60.0	54.9	79.4	1.7	13.0	62.7	54.0	65.0	0.7	4	*7.3*	ow
2.521−0.220	17 52 21.15	–26 53 20.3	2.4	–0.8	4.1	3.8	18.6	4.2	–7.5	5.0	0.8	4	*2.6*	–
2.536+0.198	17 50 46.49	–26 39 45.1	4.9	–0.9	12.5	0.5	5.4	3.2	2.0	20.5	0.4	4	*2.2*	mw
2.591−0.029	17 51 46.70	–26 43 50.5	–12.2	–15.2	–8.9	2.8	12.4	–8.2	–9.5	–4.0	0.7	4	[4.2]	–
2.615+0.134	17 51 12.28	–26 37 36.7	97.6	95.7	103.2	0.5	3.2	94.5	93.5	104.0	0.5	4	*7.5*	m
3.312−0.399	17 54 50.02	–26 17 48.6	7.4	0.3	10.3	3.4	12.9	0.5	0.0	10.0	3.0	4	*0.6*	–
3.502−0.200	17 54 30.08	–26 02 00.3	47.5	45.3	48.5	0.6	1.5	43.9	43.0	45.5	1.0	4	*6.3*	m
4.434+0.129	17 55 19.73	–25 03 44.6	–6.0	–28.0	53.8	2.0	26.9	–0.9	–1.5	8.0	0.2	4	[4.3]	–
4.676+0.276	17 55 18.32	–24 46 45.3	–0.9	–6.9	1.7	0.2	1.5	4.4	–5.5	6.0	0.2	4	*1.6*	–
5.618−0.082	17 58 44.90	–24 08 38.4	–27.4	–33.0	–15.6	0.3	3.5	–27.0	–28.0	–18.5	2.4	4	5.1	m
5.630−0.294	17 59 34.52	–24 14 23.6	18.0	16.1	20.9	1.8	6.9	10.6	9.0	22.0	1.1	4	3.4	m
5.657+0.416	17 56 56.53	–23 51 41.3	18.8	12.6	21.2	4.6	30.4	20.1	13.0	22.0	0.7	4	13.1	–
5.677−0.027	17 58 39.94	–24 03 56.7	–9.3	–14.4	0.1	1.4	9.8	–11.5	–14.5	–11.0	0.6	4	[4.5]	–
5.885−0.393	18 00 30.44	–24 04 00.8	11.8	–59.7	46.0	46.3	269.	6.7	6.0	7.5	3.8	4	1.28	ow
5.900−0.430	18 00 40.72	–24 04 18.9	12.3	–13.4	30.4	2.2	28.2	10.4	0.0	10.6	2.6	4	1.6	w
6.189−0.358	18 01 02.16	–23 47 10.4	-29.4	-48.3	-24.7	13.1	36.5	-30.2	-37.5	-27.1	0.4	7	5.1	ie
6.588−0.192	18 01 16.07	–23 21 25.7	-1.4	-3.5	-0.1	1.6	3.0	5.0	3.5	7.0	1.5	7	1.4	–
6.610−0.082	18 00 54.03	–23 17 02.8	2.9	-4.2	7.1	3.7	21.8	0.8	-6.6	7.5	0.3	6	*0.3*	mw
6.795−0.257	18 01 57.53	–23 12 33.0	14.7	-3.0	19.3	19.8	122.	16.3	12.1	31.4	3.4	6	3.1	ow
7.166+0.131	18 01 17.47	–22 41 43.7	76.3	71.2	81.7	3.6	9.1	85.7	74.5	91.0	0.2	7	11.6	–
7.601−0.139	18 03 14.40	–22 27 00.7	148.5	145.1	154.0	1.4	9.7	154.7	151.0	156.5	0.3	7	7.4	–
7.632−0.109	18 03 11.59	–22 24 32.0	155.3	143.4	156.5	1.1	3.8	157.0	146.5	158.9	0.6	7	7.4	–
8.139+0.226	18 03 00.83	–21 48 10.7	27.2	10.3	31.8	0.4	4.1	19.9	18.8	21.8	1.5	6	3.2	mw
8.317−0.096	18 04 36.09	–21 48 20.2	47.3	31.6	48.5	0.5	2.3	47.1	44.0	49.2	1.2	7	11.7	i
8.669−0.356	18 06 18.97	–21 37 32.2	34.2	22.7	49.3	14.4	114.	39.0	35.8	39.7	0.2	6	4.4	omw
8.832−0.028	18 05 25.65	–21 19 24.8	-9.8	-26.6	9.9	12.3	93.3	-3.8	-6.0	5.9	0.3	7	5.2	e
9.215−0.202	18 06 52.83	–21 04 27.1	36.3	34.6	39.6	2.7	12.7	45.6	36.0	50.0	0.4	7	*4.6*	i
9.621+0.196	18 06 14.77	–20 31 33.8	-6.0	-14.8	11.7	18.2	222.	1.3	-4.8	8.9	2.1	6	5.2	omw
9.986−0.028	18 07 50.14	–20 18 56.4	52.5	41.1	63.0	12.9	72.8	42.2	40.6	51.8	0.3	6	12.0	mwi
10.287−0.125	18 08 49.33	–20 05 58.9	13.8	2.8	15.0	1.0	7.8	4.5	1.5	6.0	0.4	6	*0.7*	mwie
10.320−0.259	18 09 23.28	–20 08 06.6	43.1	40.5	46.4	5.4	13.2	39.0	35.0	39.6	0.3	7	*3.9*	–
10.342−0.142	18 08 59.96	–20 03 39.1	10.0	-1.8	65.1	10.5	191.	14.8	6.0	18.0	3.2	6	*1.8*	w
10.444−0.018	18 08 44.88	–19 54 38.4	71.5	65.6	81.2	12.6	75.0	73.4	67.6	79.0	0.3	6	11.0	omi
10.472+0.027	18 08 38.54	–19 51 50.1	87.6	18.4	286.8	75.3	1340	75.1	57.5	77.6	0.9	6	8.5	omw
10.724−0.334	18 10 29.99	–19 49 06.1	-21.6	-25.4	-18.2	0.8	2.4	-2.1	-2.5	-1.6	0.9	7	5.2	–
10.822−0.103	18 09 50.45	–19 37 13.9	63.5	61.3	67.6	0.4	1.7	72.1	68.0	74.0	1.0	7	*5.3*	–
10.886+0.123	18 09 07.95	–19 27 24.0	13.8	11.2	26.8	21.1	68.9	17.2	14.0	22.5	2.2	7	2.5	e
10.958+0.022	18 09 39.26	–19 26 27.7	24.4	18.5	27.3	5.9	19.9	24.5	23.0	25.5	0.8	6	13.5	w
11.034+0.062	18 09 39.86	–19 21 20.2	17.7	5.4	22.7	0.5	4.7	20.6	15.2	21.0	0.4	6	2.4	ow
12.199−0.033	18 12 23.42	–18 22 51.2	47.4	44.0	55.3	0.9	3.9	49.3	48.2	57.1	0.6	8	12.0	–
12.209−0.102	18 12 39.76	–18 24 18.0	22.0	-13.4	41.7	41.3	1170	19.8	16.0	22.0	1.4	6	*2.3*	omw
12.265−0.051	18 12 35.37	–18 19 52.1	59.2	56.6	63.4	2.6	11.7	68.3	58.0	70.9	0.5	8	11.5	–
12.681−0.182	18 13 54.75	–18 01 46.5	59.9	45.1	74.2	702.	2490	57.5	50.0	62.0	0.0	6	*4.5*	omw
12.889+0.489	18 11 51.39	–17 31 28.8	29.9	23.9	32.8	12.3	44.8	39.2	28.0	43.0	0.8	6	2.3	omw
12.904−0.031	18 13 48.27	–17 45 39.7	66.2	60.7	69.1	13.5	70.4	59.1	55.8	61.0	0.9	8	*4.5*	e
12.909−0.260	18 14 39.51	–17 52 01.2	37.5	33.3	42.1	4.7	19.2	39.9	34.7	47.0	1.3	6	*3.7*	omwe
13.657−0.599	18 17 24.25	–17 22 12.6	47.7	34.5	55.6	10.1	95.0	51.3	45.0	52.7	0.2	8	12.3	o
14.101+0.087	18 15 45.80	–16 39 09.3	8.5	-1.5	10.6	14.5	43.7	15.4	4.4	16.6	0.1	8	5.4	–
14.604+0.017	18 17 01.14	–16 14 39.1	27.4	16.0	35.3	8.2	86.9	24.7	22.1	35.8	1.2	8	2.8	m
15.094+0.192	18 17 20.84	–15 43 45.7	28.3	-14.6	32.0	13.2	99.9	25.8	22.5	26.5	0.8	8	13.8	–
15.665−0.499	18 20 59.79	–15 33 09.9	-6.8	-9.3	-1.3	11.3	58.9	-2.9	-5.0	-2.0	0.7	5	16.7	e
16.585−0.051	18 21 09.16	–14 31 49.0	64.6	54.0	72.1	26.7	196.	62.1	52.0	69.5	0.7	6	4.3	om
16.831+0.079	18 21 09.52	–14 15 08.8	41.1	38.1	84.5	1.2	13.2	58.7	57.2	69.4	0.3	5	11.8	–
16.864−2.159	18 29 24.37	–15 16 04.5	6.1	-12.4	25.4	6.8	40.3	15.0	14.0	20.0	0.6	5	1.70	om +

Table 3.1: – *continued*

MMB Target Name (l, b)	Equatorial Coordinates RA (h m s)	DEC (° ’ “)	V_{pk}	V_l (km s^{-1})	V_h	S_{pk} (Jy)	S_{int} (Jy km s^{-1})	6.7-GHz methanol V_{pk}	V_l (km s^{-1})	V_h	Off-sets (“)	Ep.	Dist. (kpc)	Assoc.
17.021−2.403	18 30 36.31	–15 14 28.1	21.1	15.2	27.4	5.3	25.3	23.6	17.0	25.0	0.4	5	2.0	–$^{+}$
17.638+0.157	18 22 26.47	–13 30 11.6	19.7	12.9	29.3	7.4	55.5	20.8	20.0	22.0	2.5	6	2.0	ow
18.341+1.768	18 17 58.19	–12 07 25.2	13.4	5.7	16.3	0.9	11.4	28.1	26.0	32.0	1.0	5	*2.2*	–$^{+}$
18.661+0.034	18 24 51.10	–12 39 21.9	78.4	21.0	86.3	1.3	16.7	79.0	76.0	83.0	0.5	5	11.2	–
18.735−0.227	18 25 56.46	–12 42 48.0	33.7	18.9	52.6	54.4	590.	38.2	36.3	38.5	1.4	5	13.0	–
18.999−0.239	18 26 29.32	–12 29 07.8	-11.9	-27.0	4.9	5.6	76.4	69.4	65.0	69.8	1.4	5	4.3	i
19.009−0.029	18 25 44.80	–12 22 45.4	67.4	65.3	68.2	0.5	2.4	55.4	53.0	63.0	0.8	5	12.0	e
19.267+0.349	18 24 52.36	–11 58 28.0	27.2	13.6	31.3	7.5	37.9	16.3	12.5	17.5	0.3	5	14.5	–
19.472+0.170n	18 25 54.69	–11 52 33.9	21.6	-84.9	25.8	9.2	72.3	21.7	17.0	23.0	1.0	5	1.8	oi
19.486+0.151	18 26 00.42	–11 52 22.0	26.0	22.2	29.3	2.7	10.2	20.9	19.0	27.5	0.7	5	2.0	o
19.496+0.115	18 26 09.28	–11 52 51.7	125.0	107.3	128.8	0.9	6.9	121.3	120.0	122.0	1.8	5	9.8	ie
19.609−0.234	18 27 38.06	–11 56 37.2	42.5	20.1	69.8	69.7	1320	40.2	36.0	42.0	1.2	6	*2.9*	om
19.612−0.134	18 27 16.56	–11 53 37.8	56.8	53.8	58.5	1.7	6.0	56.5	49.0	61.0	0.7	5	12.1	om
19.614+0.011	18 26 45.23	–11 49 31.9	35.1	32.1	36.7	2.7	8.6	32.9	30.8	34.8	0.5	5	13.2	–
19.701−0.267	18 27 55.47	–11 52 40.3	42.1	36.2	58.9	1.6	14.1	43.8	41.5	46.5	0.7	5	12.6	i
19.884−0.534	18 29 14.36	–11 50 22.7	44.1	0.7	49.6	21.7	178.	46.8	46.0	48.0	0.2	5	3.3	e

Table 3.2: 6.7-GHz methanol masers with no associated water maser emission. Column 1 is the name of the target methanol maser given in Galactic coordinates; column 2 is the 5 sigma detection limit; column 3 is the epoch of observation coded 1, 2, 3, 4, 5, 6, 7 and 8 for 2011 June 3, 2011 June 4, 2011 June 5, 2011 August 8, 2010 November 2, 2010 November 3, 2011 August 9 and 2011 August 10 respectively. Column 4 gives associations with water masers detected in Pillai et al. (2006b) or the Breen et al. (2010a) 2003 or 2004 observations but not in ours are indicated with a 'w', associations with 12.2-GHz methanol masers (Breen et al., 2012; Breen et al., 2014) are indicated with an 'm', associations with the 1665 MHz transition of OH masers (Caswell, 1998; Caswell et al. 2013) are indicated with an 'o', sources marked with a '*' are within the survey region for OH by Caswell (1998) and no emission was detected and associations with Infrared Dark Clouds or Extended Green Objects indicated with an 'i' or 'e' respectively from inspection of the GLIMPSE infrared images. Sources outside of the GLIMPSE survey range are indicated with an '+'. GLIMPSE images were only inspected for sources between $l = 6° - 20°$. Column 5 is the distance to the methanol maser. Distances estimates are from Green et al. (2011) where available, others are the near kinematic distance (these are in italics) and the remainder are from Mark Reid (private communication) (these are in square brackets).

MMB Target Source Name (l, b)	Det. lim. (mJy)	Ep.	Assoc.	Dist. (kpc)	MMB Target Source Name (l, b)	Det. lim. (mJy)	Ep.	Assoc.	Dist. (kpc)
341.124−0.361	250	1	*	3.0	350.470+0.029	175	2	m*	1.3
341.238−0.270	250	1	m*	3.5	350.776+0.138	175	2	*	11.4
341.367+0.336	250	1	*	11.2	351.242+0.670	175	2	–	1.8
341.990−0.103	250	1	*	3.0	351.251+0.652	175	2	–	1.8
342.251+0.308	250	1	*	9.9	351.382−0.181	175	2	m*	5.4
342.338+0.305	250	1	m*	10.3	351.417+0.646	175	2	wmo	1.8
342.368+0.140	250	1	*	0.6	351.445+0.660	185	2	m	1.17
343.354−0.067	250	1	m*	9.9	351.688+0.171	185	2	m*	12.1
343.929+0.125	250	1	m*	18.6	352.083+0.167	185	2	m*	11.0
344.419+0.044	250	1	*	4.4	352.111+0.176	190	2	wm*	5.3
344.421+0.045	250	1	wm*	4.7	352.525−0.158	200	2	w*	11.2
345.003−0.224	250	1	wm*	2.7	352.604−0.225	200	2	*	5.1
345.010+1.792	250	1	wm	2.0	352.624−1.077	200	2	–	17.8
345.198−0.030	250	1	m*	10.8	353.363−0.166	200	2	*	5.1
345.205+0.317	250	1	*	11.8	353.370−0.091	200	2	m*	*5.2*
345.498+1.467	250	1	–	1.5	353.378+0.438	200	2	*	13.9
345.576−0.225	250	1	*	5.5	353.410−0.360	200	2	mo	*3.4*
346.480+0.221	250	1	m*	14.4	353.429−0.090	200	2	*	11.1
346.481+0.132	250	1	w*	10.9	353.464+0.562	200	2	wo	11.2
347.817+0.018	250	1	*	13.8	354.206−0.038	200	2	*	*5.0*
347.863+0.019	250	1	m*	13.1	354.496+0.083	200	2	m*	11.7
347.902+0.052	250	1	m*	*2.9*	354.615+0.472	200	2	wmo	3.8
348.027+0.106	250	1	*	*6.4*	354.701+0.299	200	2	*	6.1
348.195+0.768	250	1	m	*16.5*	354.724+0.300	200	2	mo	5.8
348.550−0.979n	250	1	m	2.2	355.184−0.419	210	2	*	0.1
348.723−0.078	250	1	m*	11.2	355.343+0.148	215	2	wmo	[1.6]
348.703−1.043	250	1	m	1.3	355.545−0.103	225	2	*	11.7
348.727−1.037	125	2	m	1.2	355.642+0.398	225	2	*	14.5
349.092+0.105	125	2	wm*	11.1	356.054−0.095	225	2	*	[11.4]
349.579−0.679	150	2	–	13.5	356.662−0.263	225	2	o	6.6
349.884+0.231	160	2	*	11.3	357.559−0.321	225	3	m	[4.1]
350.011−1.342	170	2	o	*3.1*	357.924−0.337	210	3	m	16.9
350.105+0.083	175	2	wm*	*5.5*	358.263−2.061	200	3	m	[2.2]
350.116+0.084	175	2	*	11.4	358.371−0.468	200	3	wm	[3.4]
350.116+0.220	175	2	m*	17.8	358.460−0.393	200	3	–	*4.1*
350.299+0.122	175	2	wm*	11.3	358.721−0.126	200	3	m	*0.6*
350.344+0.116	175	2	m*	11.4	358.809−0.085	200	3	m	*7.7*

Table 3.2: – *continued*

MMB Target Source Name (l, b)	Det. lim. (mJy)	Ep.	Assoc.	Dist. (kpc)	MMB Target Source Name (l, b)	Det. lim. (mJy)	Ep.	Assoc.	Dist. (kpc)
358.841−0.737	180	3	m	*6.7*	11.936−0.616	150	8	m	3.7
358.906+0.106	175	3	m	*6.6*	11.992−0.272	150	8	–	11.7
359.938+0.170	170	3	–	[7.2]	12.025−0.031	125	8	mo	11.1
0.092+0.663	150	3	m	*8.27*	12.112−0.126	150	8	m	4.1
0.212−0.001	160	3	wm	*8.2*	12.181−0.123	150	8	–	*3.1*
0.316−0.201	200	3	w	*7.9*	12.202−0.120	55	6	i	3.2
0.409−0.504	225	3	–	*7.8*	12.203−0.107	55	6	w	*2.9*
0.475−0.010	225	3	–	*7.8*	12.526+0.016	150	8	m	12.6
0.645−0.042	250	3	–	*7.9*	12.625−0.017	100	8	m	2.7
0.647−0.055	250	3	–	*7.9*	12.776+0.128	150	8	–	13.2
0.651−0.049	250	3	m	*7.9*	13.179+0.061	150	8	i	4.1
0.657−0.041	250	3	wo	*7.9*	13.696−0.156	140	8	m	10.9
0.665−0.036	250	3	–	*8.0*	13.713−0.083	100	8	–	4.0
0.666−0.029	250	3	m	*8.0*	14.230−0.509	120	8	–	*2.6*
0.667−0.034	250	3	m	*8.0*	14.390−0.020	100	8	m	13.6
0.672−0.031	250	3	–	*8.0*	14.457−0.143	110	8	–	3.6
0.673−0.029	250	3	–	*8.0*	14.490+0.014	110	8	i	2.3
0.677−0.025	240	3	–	*8.1*	14.521+0.155	115	8	m	5.5
0.695−0.038	230	3	–	*8.0*	14.631−0.577	150	8	ie	13.7
1.329+0.150	225	3	–	*17.0*	14.991−0.121	140	8	–	12.3
1.719−0.088	225	3	m	[4.2]	15.034−0.677	150	8	mo	2.3
2.703+0.040	125	4	m	*7.5*	15.607−0.255	160	8	–	11.7
3.253+0.018	125	4	m	*1.4*	16.112−0.303	60	5	–	3.0
3.442−0.348	125	4	–	*2.0*	16.302−0.196	45	5	m	3.8
3.910+0.001	125	4	o	*4.4*	16.403−0.181	55	5	–	12.9
4.393+0.079	125	4	m	*1.0*	16.662−0.331	70	5	–	12.7
4.569−0.079	135	4	–	*2.8*	16.855+0.641	80	5	–	13.8
4.586+0.028	140	4	–	*4.8*	16.976−0.005	60	5	m	15.3
4.866−0.171	150	4	–	*1.8*	17.029−0.071	65	5	–	10.8
6.368−0.052	40	7	–	7.4	17.862+0.074	50	5	m	10.2
6.539−0.108	50	7	–	13.9	18.073+0.077	70	5	m	*3.6*
6.881+0.093	50	7	–	17.3	18.159+0.094	50	5	–	12.0
8.683−0.368	50	7	moe	4.5	18.262−0.244	75	5	m	4.7
8.872−0.493	45	7	–	3.4	18.440+0.045	70	5	–	11.8
9.619+0.193	50	7	mo	5.2	18.460−0.004	45	5	oi	3.5
10.205−0.345	40	7	–	1.4	18.667+0.025	45	5	me	11.2
10.299−0.146	50	7	–	*2.7*	18.733−0.224	80	5	–	12.5
10.323−0.160	75	6	mw	*1.6*	18.834−0.300	60	5	–	3.1
10.356−0.148	50	7	i	*4.6*	18.874+0.053	60	5	m	12.9
10.480+0.033	75	6	woi	11.4	18.888−0.475	80	5	ie	3.8
10.627−0.384	50	7	m	*0.2*	19.249+0.267	80	5	i	14.3
10.629−0.333	40	7	i	5.2	19.365−0.030	75	5	e	2.3
11.109−0.114	35	7	mw	13.2	19.472+0.170	60	5	i	1.8
11.497−1.485	75	6	mw^+	1.6	19.612−0.120	75	5	–	12.2
11.903−0.102	50	7	mo	12.9	19.667+0.114	50	5	–	14.4
11.904−0.141	75	6	mwo	4.0	19.755−0.128	80	5	–	9.9
11.936−0.150	150	8	–	12.2					

3.2.1 Comments on individual sites of maser emission.

341.218–0.212. This water maser showed strong variation in its flux density, with a peak flux density of 120 Jy in 2003 and 33 Jy in the 2004 observations of Breen et al. (2010a). In our observations in 2011 it had increased again to 106. Jy. Although the intensity varied greatly, the velocities of the emission remained similar over these three epochs.

345.003–0.223 and 345.003–0.224. This pair of methanol masers has been found to show variability in both sites (Caswell et al. 1995). Goedhart et al. (2004) monitored these methanol masers over more than four years and found no periodicities on these timescales. The water maser associated with 345.003–0.223 was also detected by Breen et al. (2010a) in 2003 to have a peak flux density of 3.0 Jy, in 2004 at 3.7 Jy. It had two main features and Breen et al. (2010a) found the peak to be the feature at 15 kms^{-1}, but in our observations in 2011 the other feature at -83.6 kms^{-1} had flared to 11.3 Jy to become the peak.

345.010+1.792 and 345.012+1.797. 345.010+1.792 is associated with an UCHII region (Caswell 1997), and many other class II methanol maser transitions (Ellingsen et al. 2012). Breen et al. (2010a) detected water maser emission in 2003 with a peak flux density of 2.0 Jy, but it was not detected in their 2004 observations (detection limit of 0.2 Jy) nor in our observations. 345.012+1.797 was observed by Breen et al. (2010a) in 2003 and 2004 and in our observations to have peak flux densities of 50, 29 and 88.7 Jy, respectively.

349.092+0.106. This water maser showed strong variation in its flux density, with a peak flux density of 34 Jy in 2003 and 154 Jy in the 2004 observations of Breen et al. (2010a). In our observations in 2011 it had decreased again to 15.8 Jy. Although the intensity varied greatly, the overall shape of the spectra remained similar with the peak velocity at $\sim$80 kms^{-1} in all three epochs.

351.417+0.645. In 2003 this water maser had peak flux density of 1400 Jy (Breen et al. 2010a, note it was not observed by them in 2004). In our observations its peak flux density had decreased to 156 Jy, and the peak was a different component. The spectra at both epochs had many features, but the spectra in 2003 had a larger total velocity range than in 2011 (-58 to 50 kms^{-1} compared to -43.4 to 13.7 kms^{-1}).

351.581–0.353. In 2003 this water maser had peak flux density of 1600 Jy (Breen et al. 2010a) (note it was not observed by them in 2004). In our observations in 2011 the spectra maintained similar velocities although its peak flux density had decreased to 110. Jy.

352.630–1.067. This water maser showed strong variation in its flux density, with a peak flux density of 35 Jy in 2003 and 700 Jy in the 2004 observations of Breen et al. (2010a). The peak feature was in the centre of the spectra at $\sim$0 kms^{-1} in the Breen et al. (2010a) observations and only this feature showed showed strong variation, with the features on either side remaining similar in each epoch. In our observations the peak feature was at 10.6 kms^{-1} (peak flux density of 14.1 Jy) and the central feature at $\sim$0 kms^{-1} had decreased to $\sim$10 Jy.

353.273+0.641. This source was identified by Caswell & Phillips (2008) to be an unusual water maser dominated by a blue-shifted outflow. It was observed by Breen et al. (2010a) in 2004 with peak flux density of 366 Jy, in 2007 by Caswell & Phillips (2008) with a peak of 45 Jy and in our observations in 2011 with a peak flux density of 182 Jy. It remained dominated by the blue-shifted emission at all epochs with the strongest emission coming from the features clustered around $\sim$50 kms^{-1}.

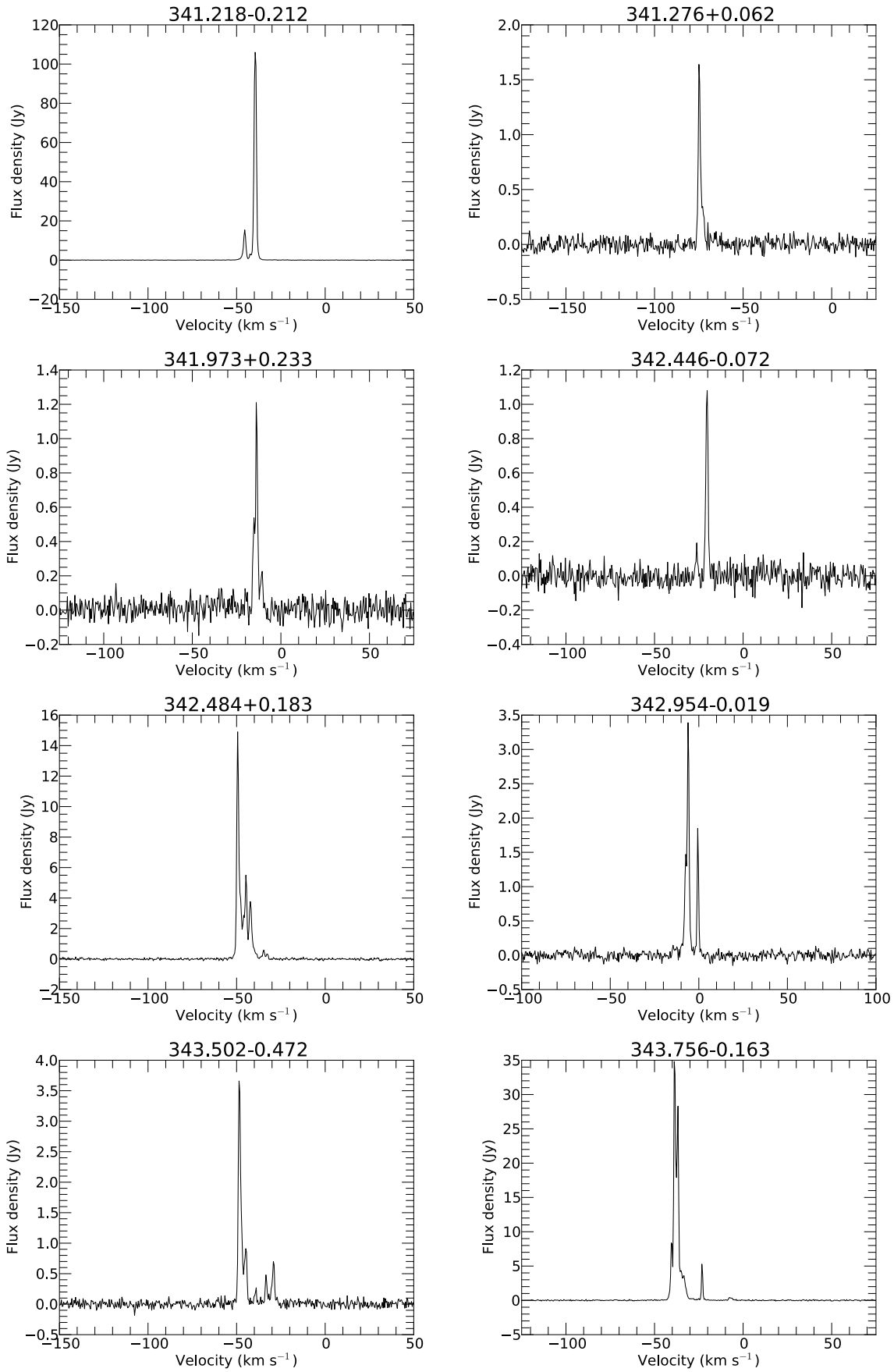

Figure 3.3: Spectra obtained with the ATCA of water masers associated with 6.7-GHz methanol masers.

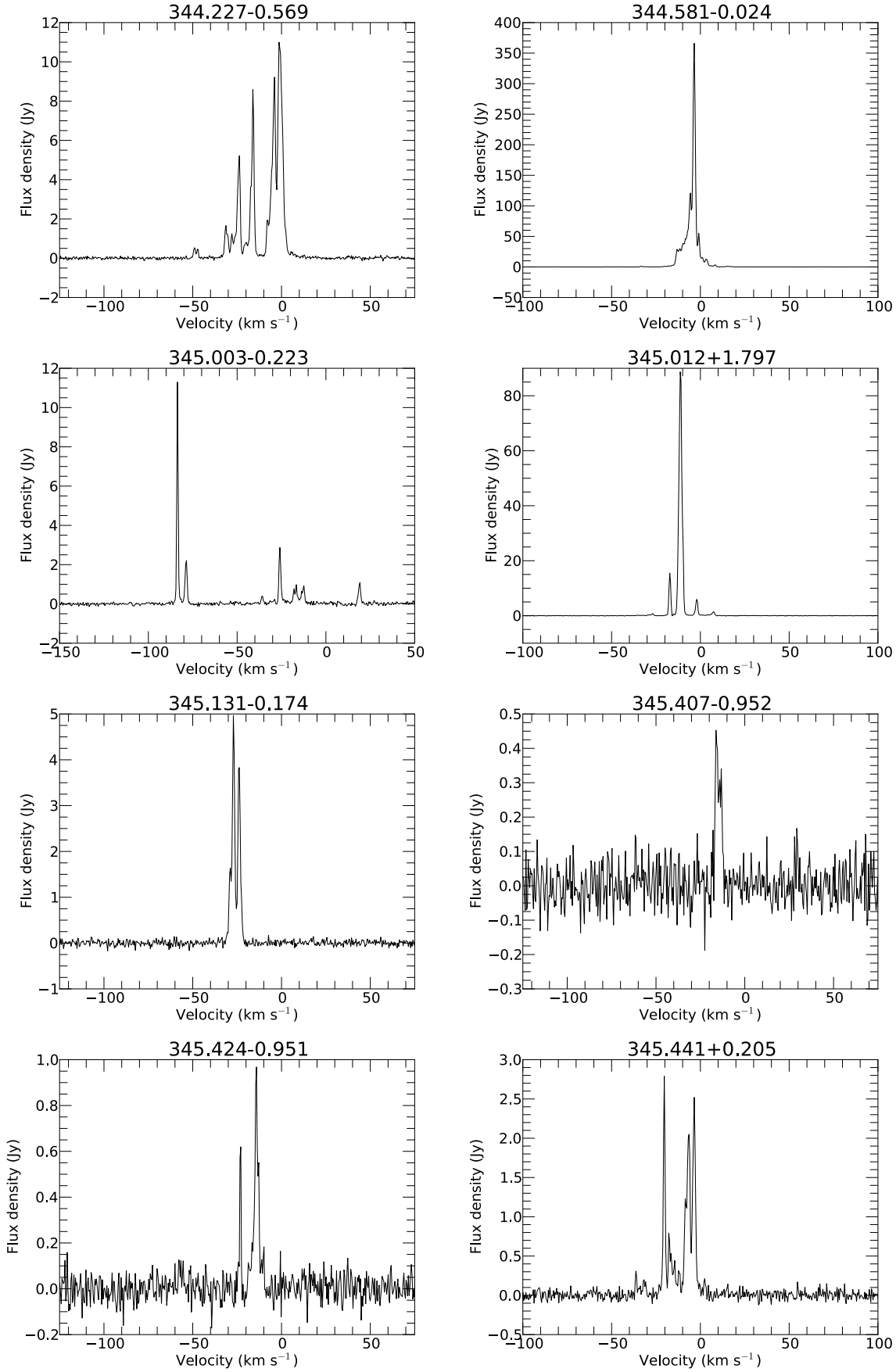

Figure 3.3: – *continued*

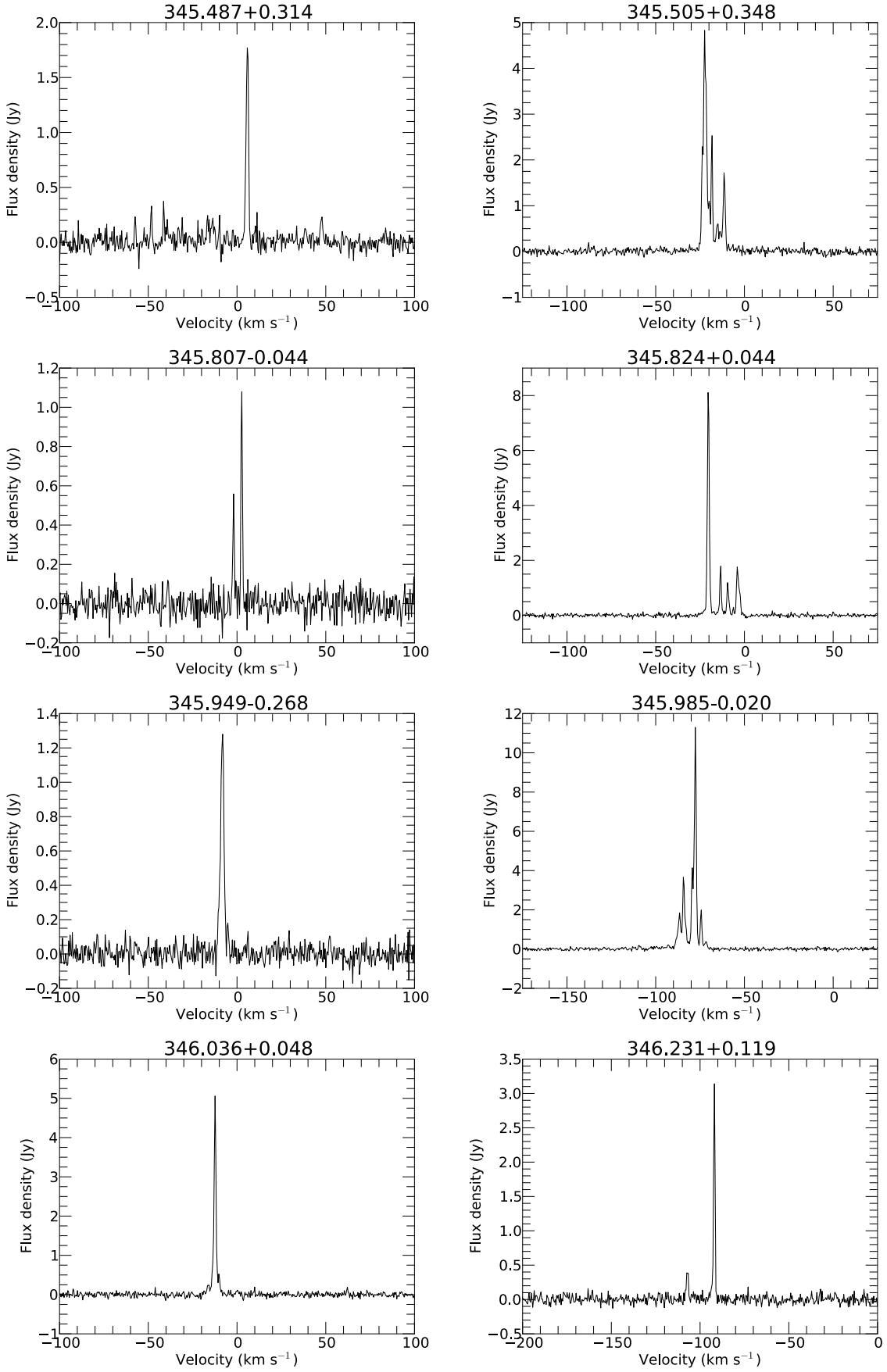

Figure 3.3: – *continued*

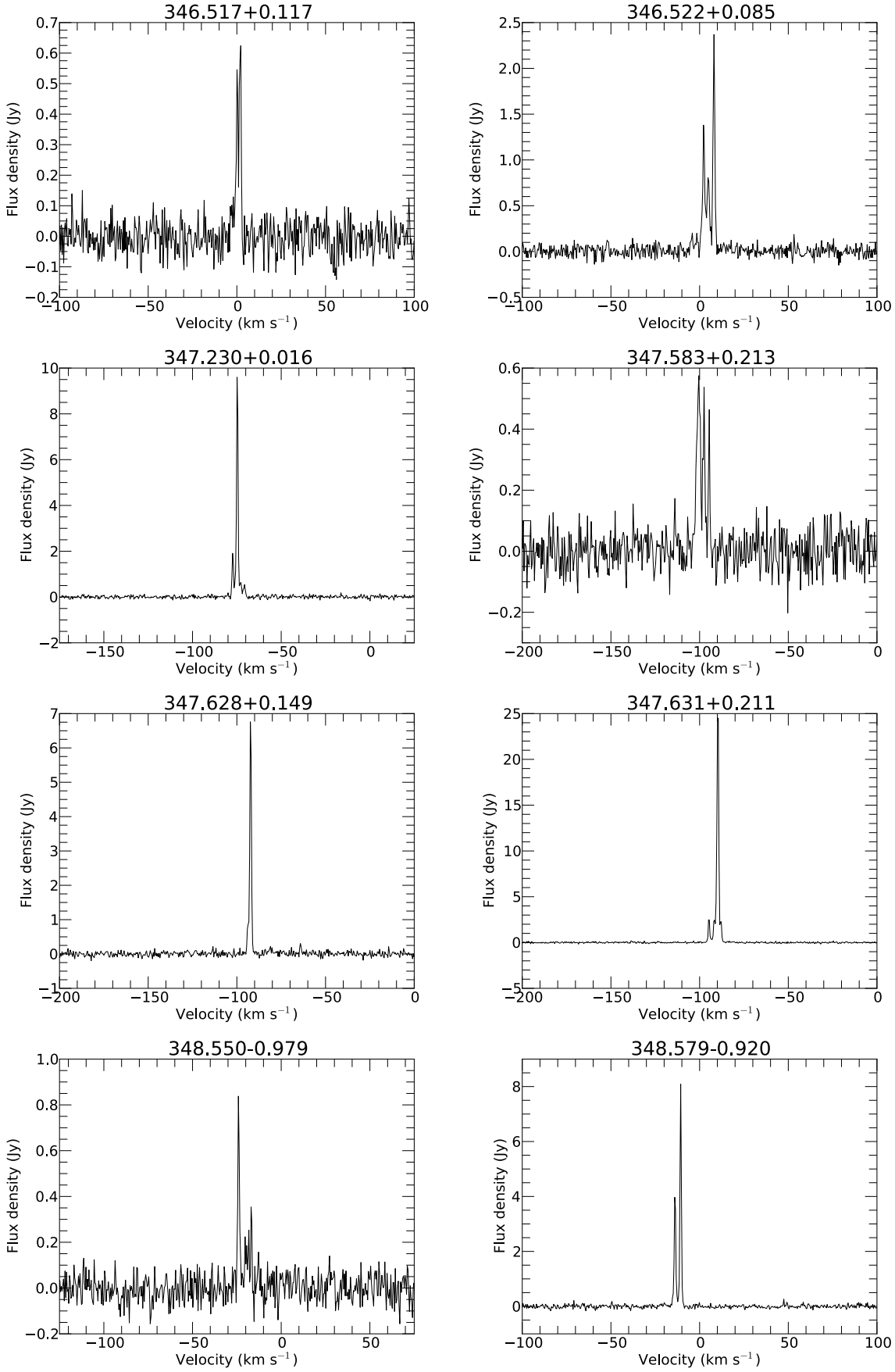

Figure 3.3: – *continued*

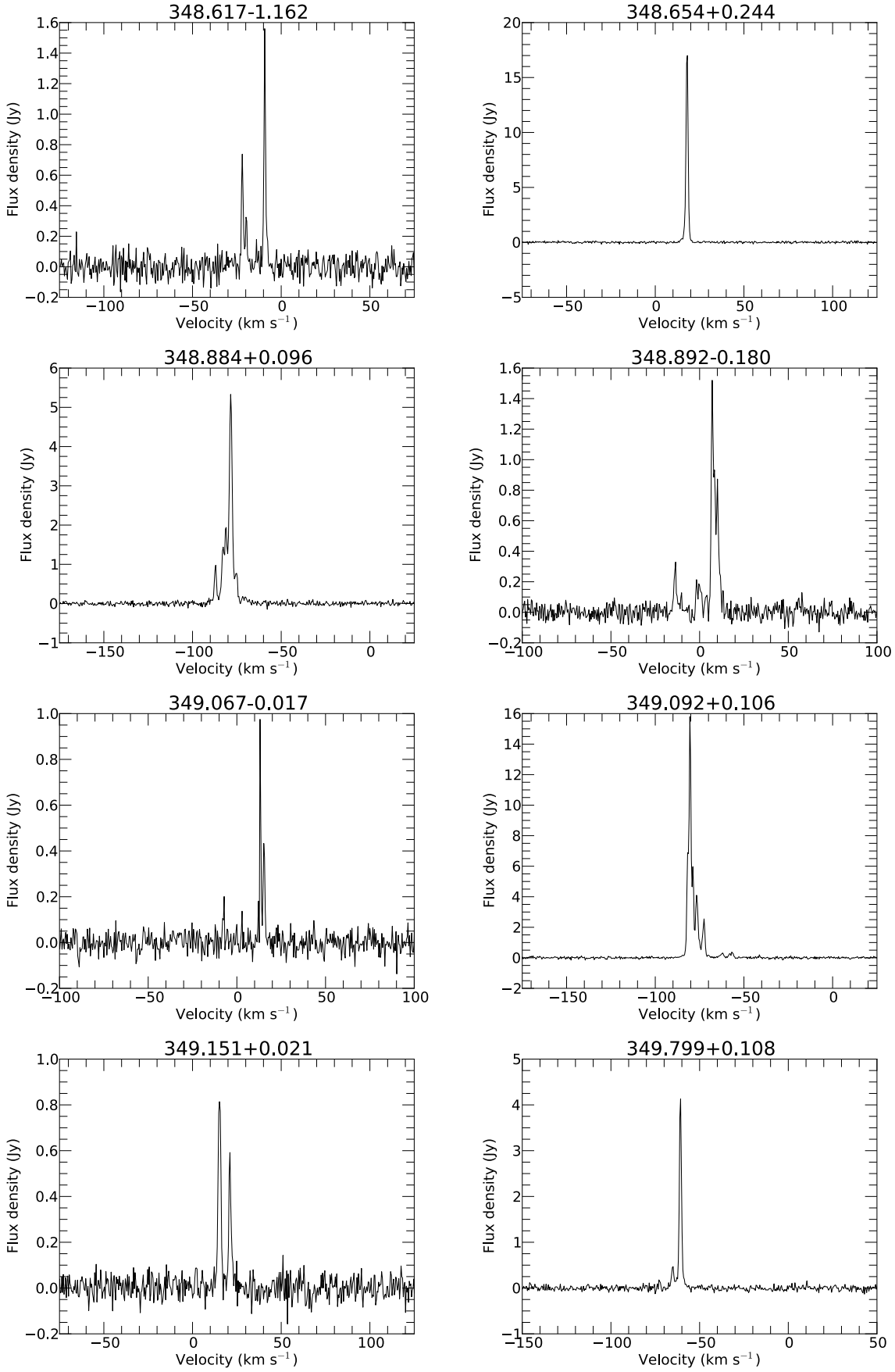

Figure 3.3: – *continued*

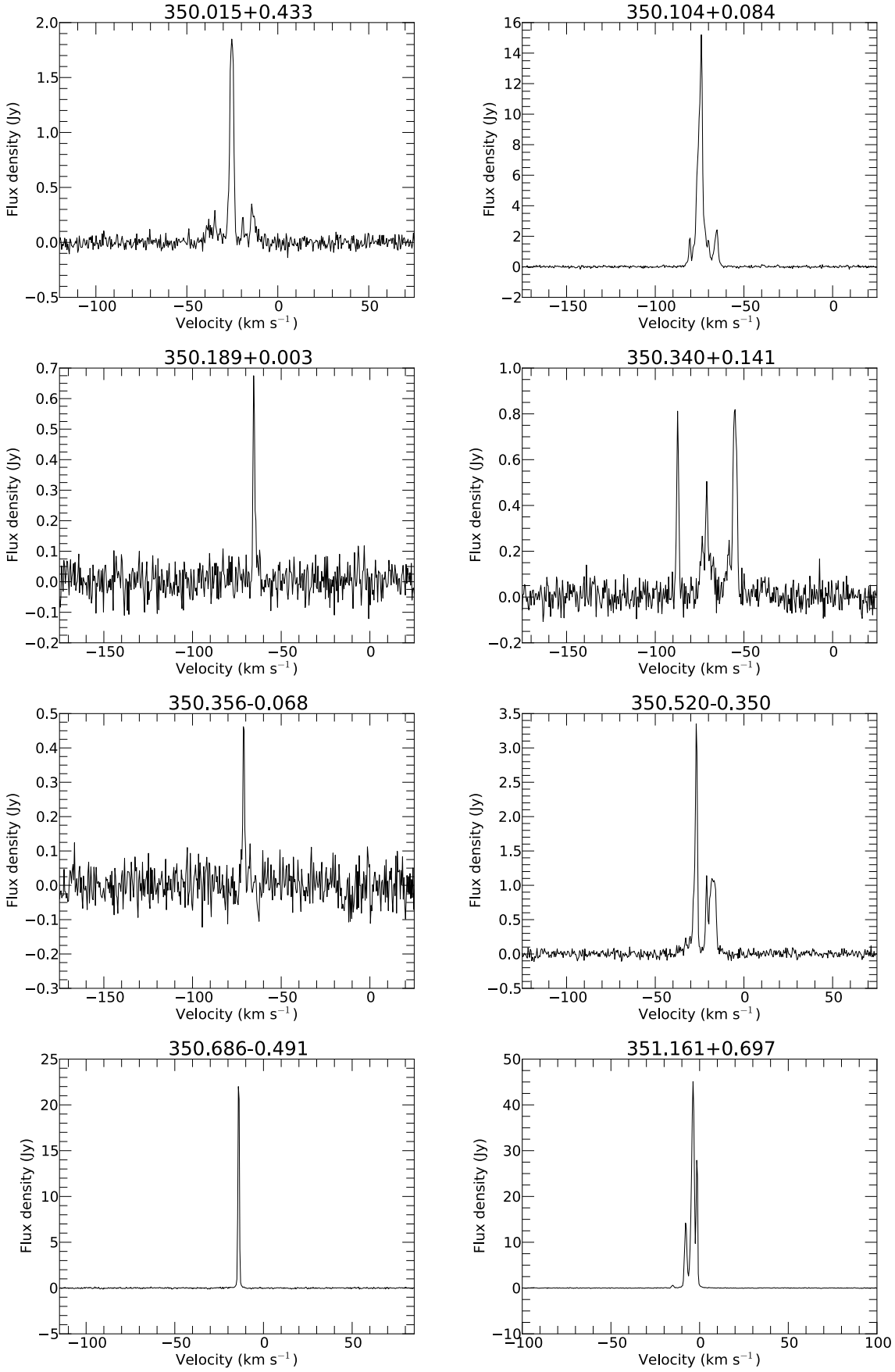

Figure 3.3: – *continued*

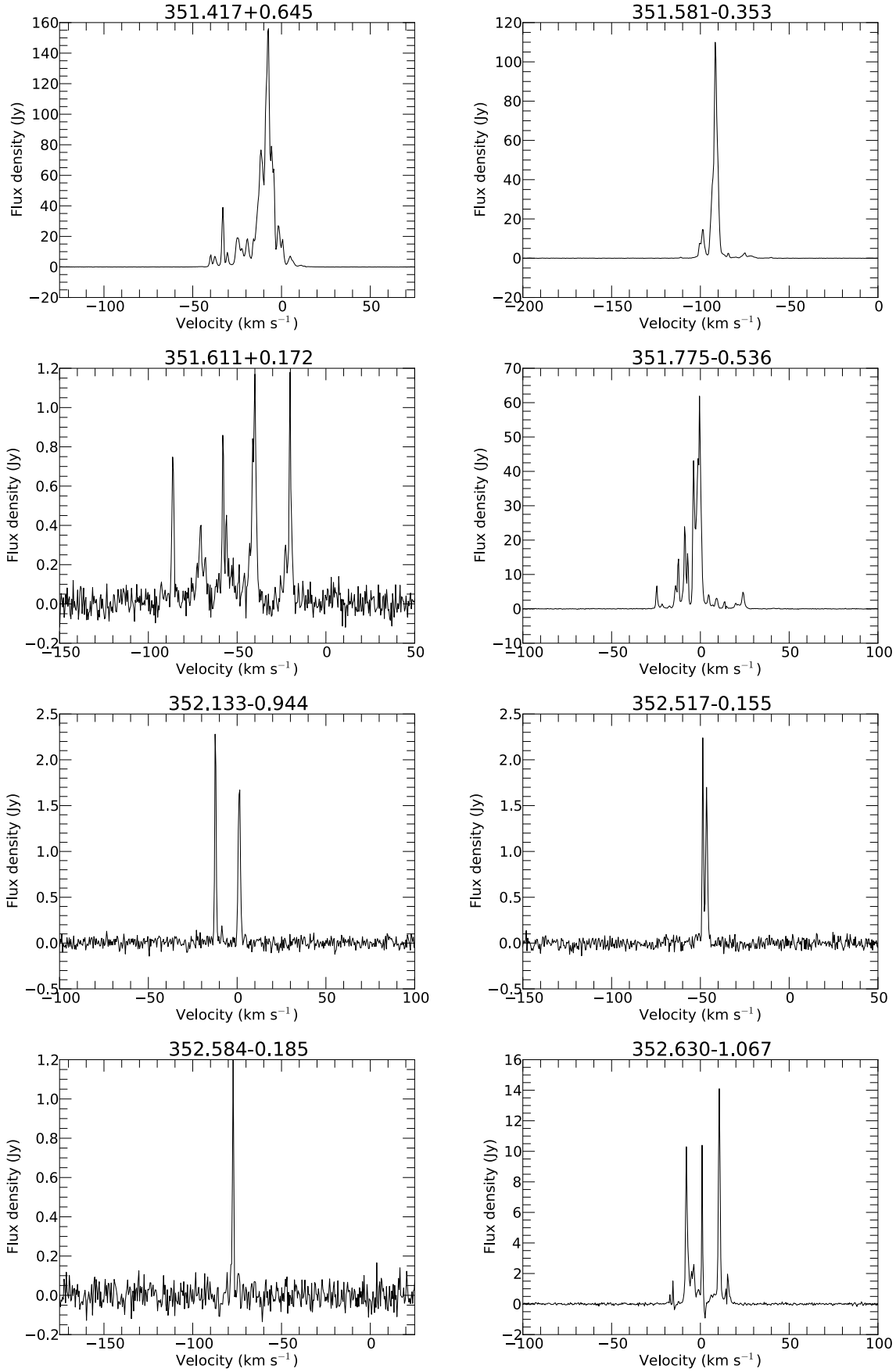

Figure 3.3: – *continued*

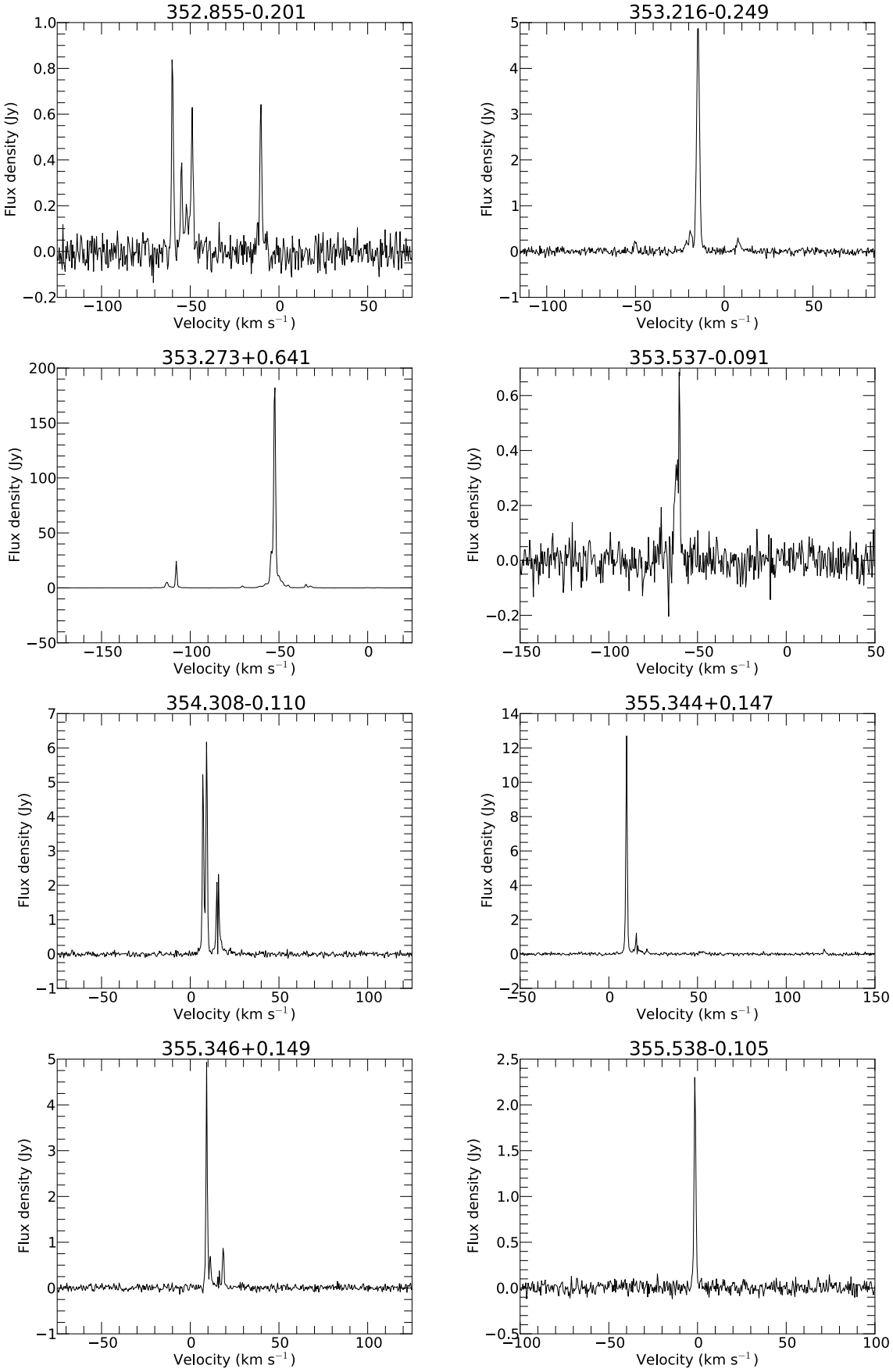

Figure 3.3: – *continued*

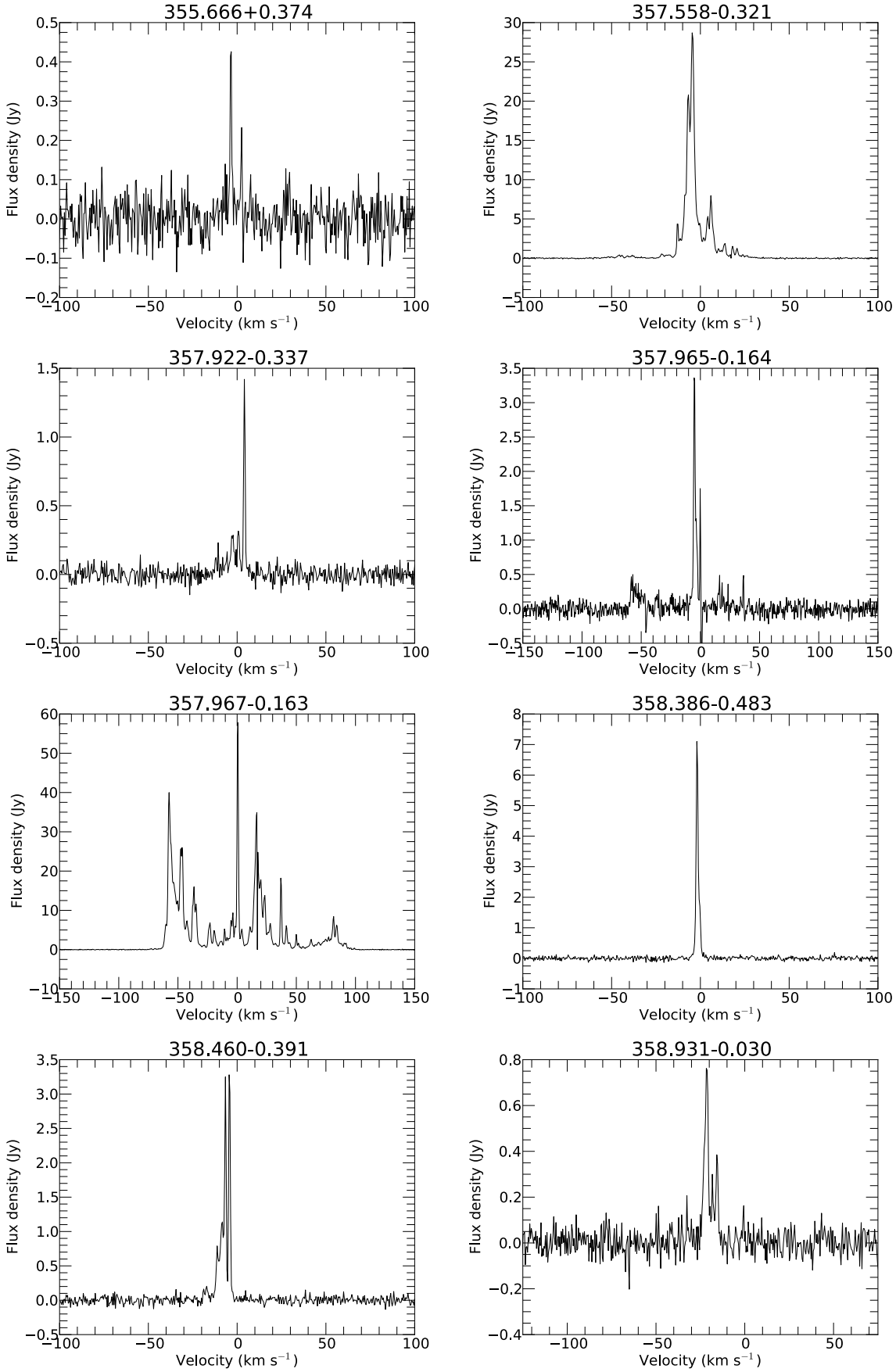

Figure 3.3: – *continued*

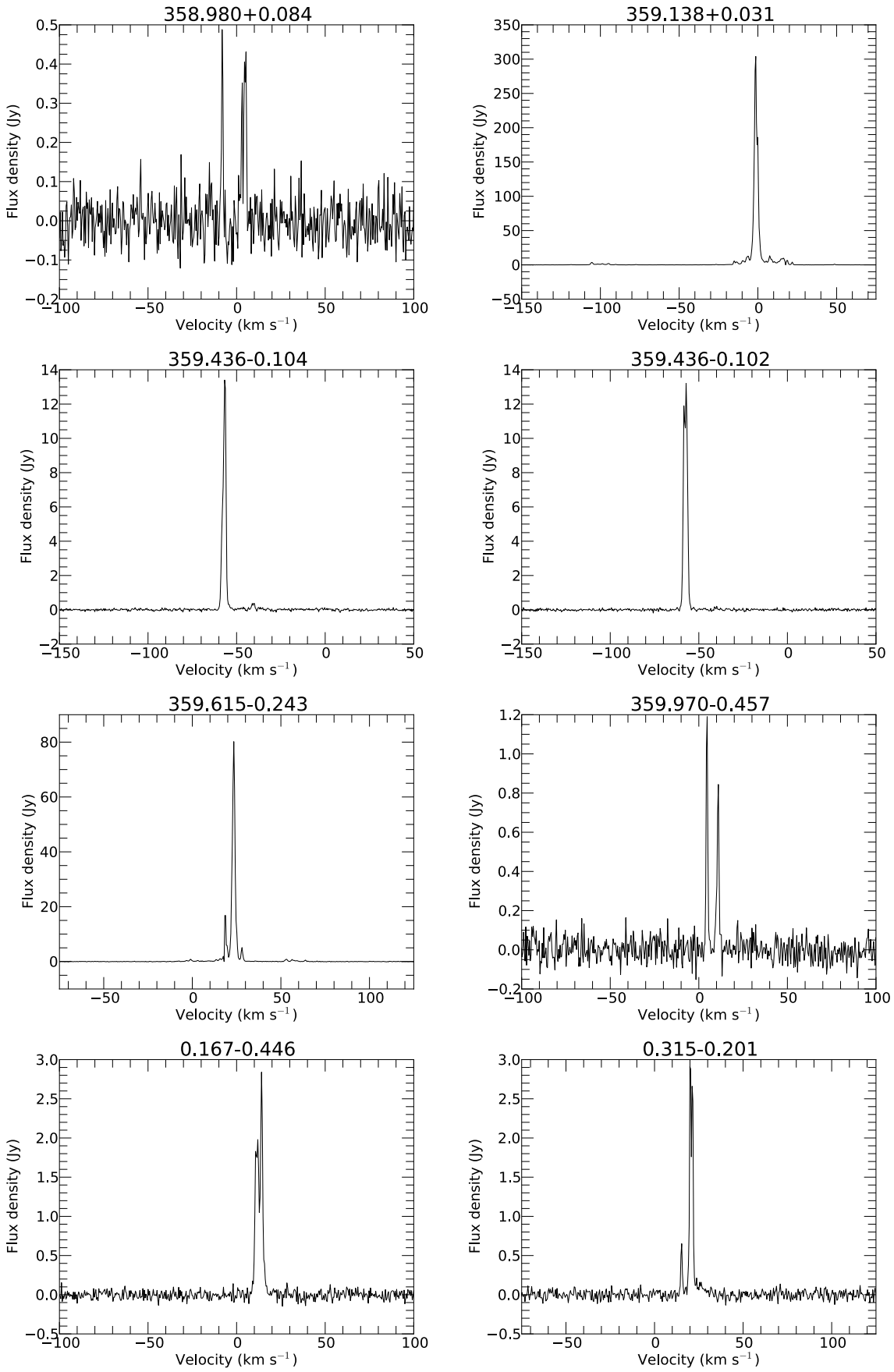

Figure 3.3: – *continued*

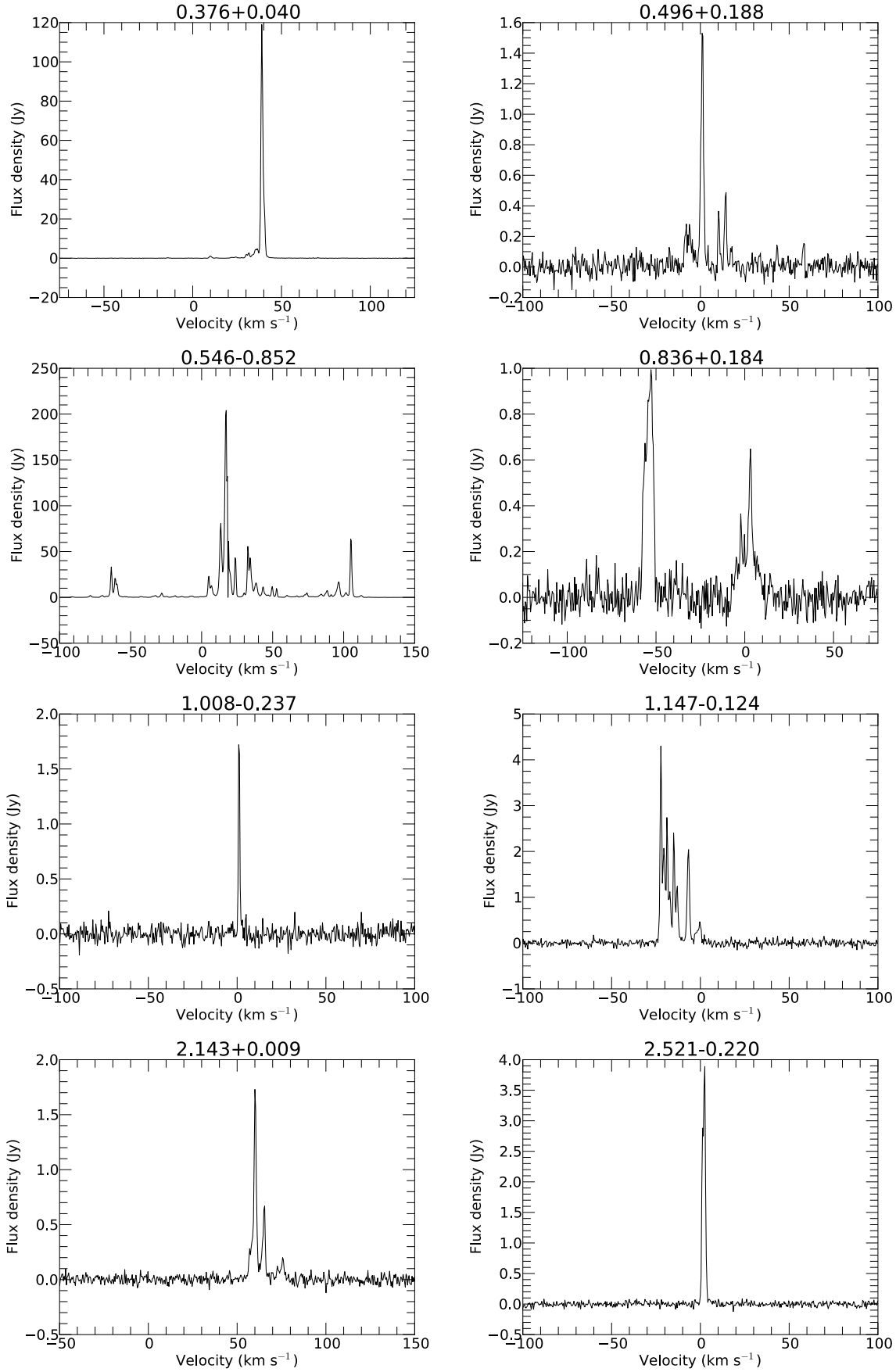

Figure 3.3: – *continued*

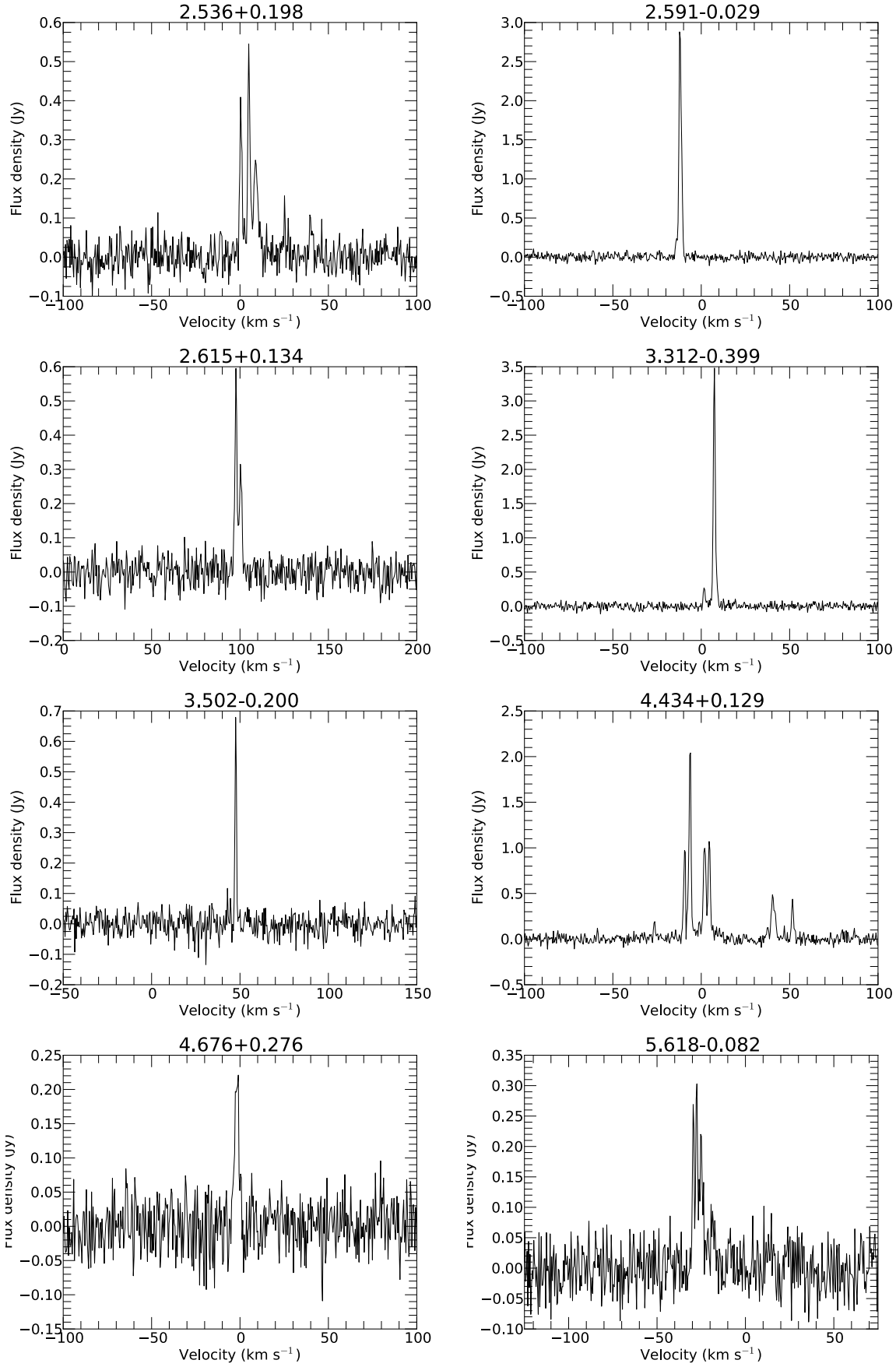

Figure 3.3: – *continued*

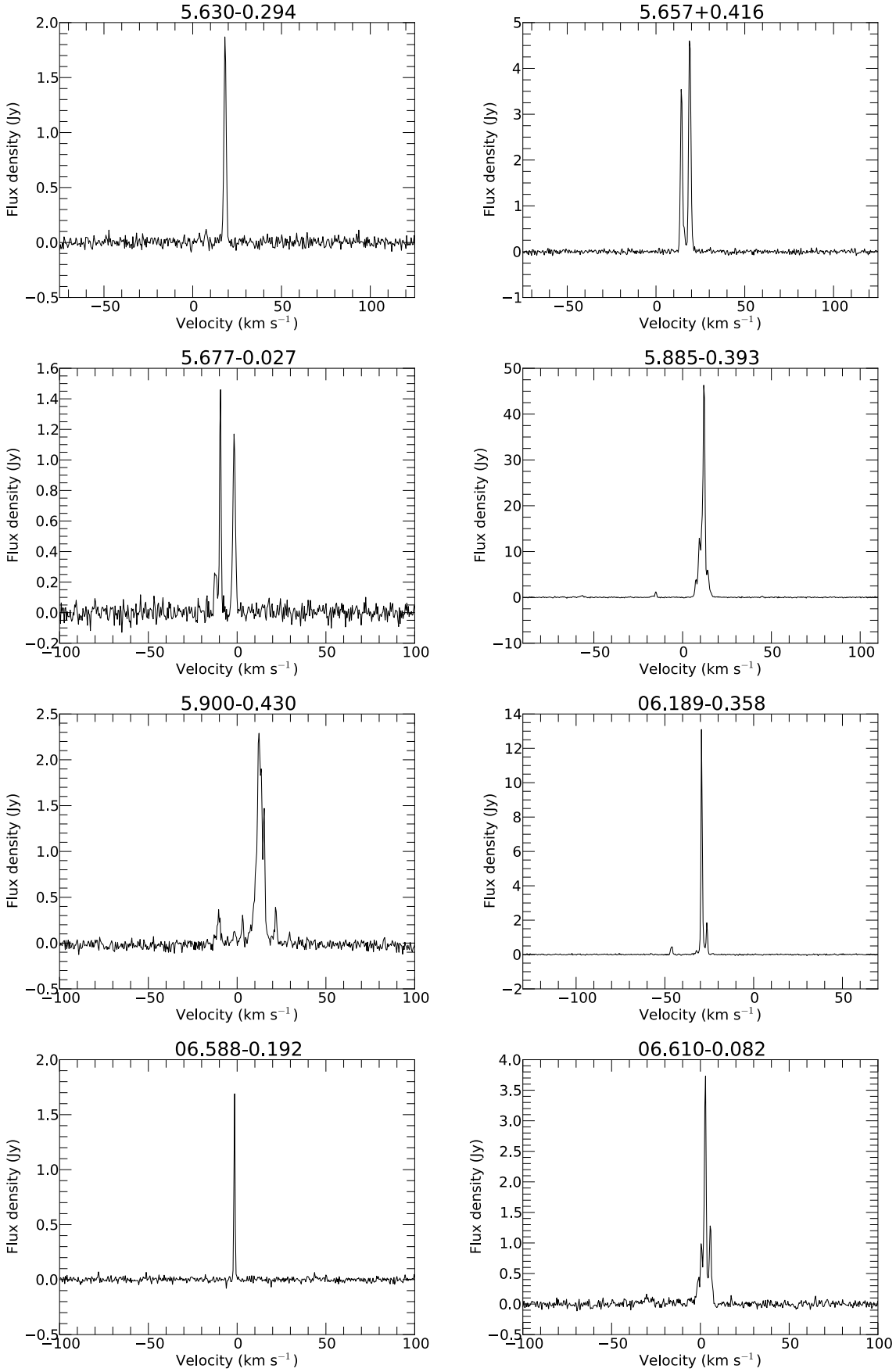

Figure 3.3: – *continued*

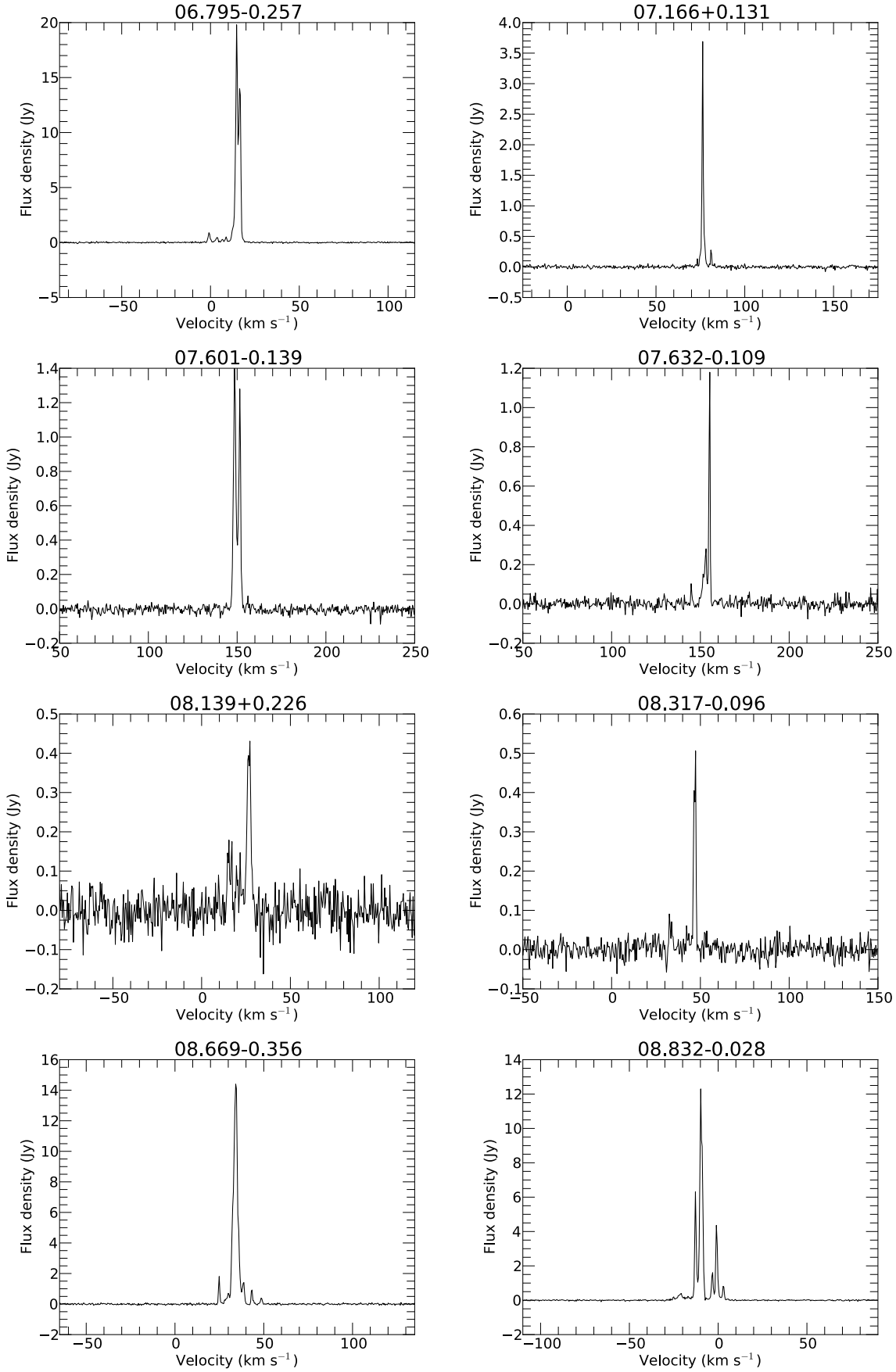

Figure 3.3: – *continued*

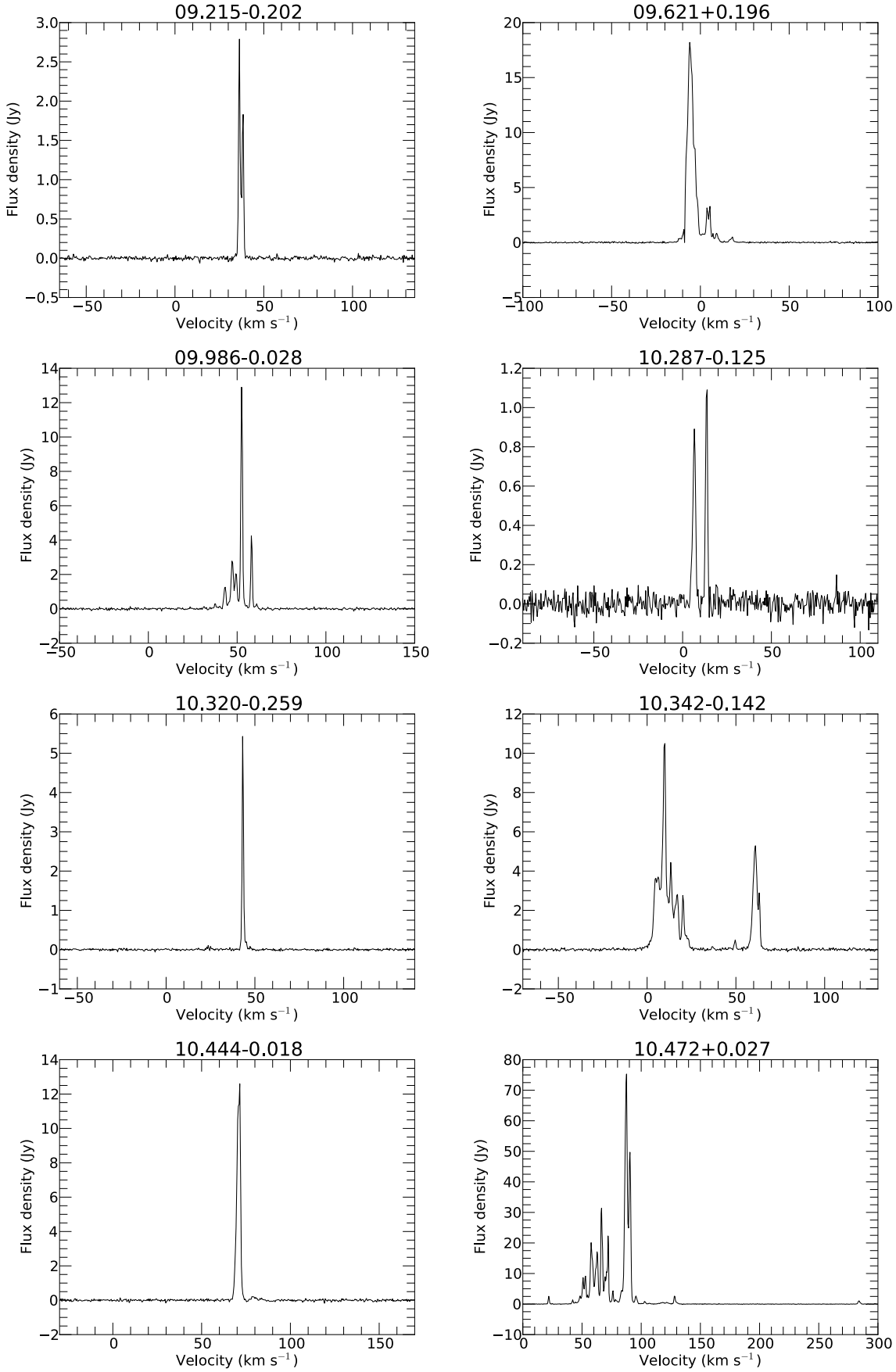

Figure 3.3: – *continued*

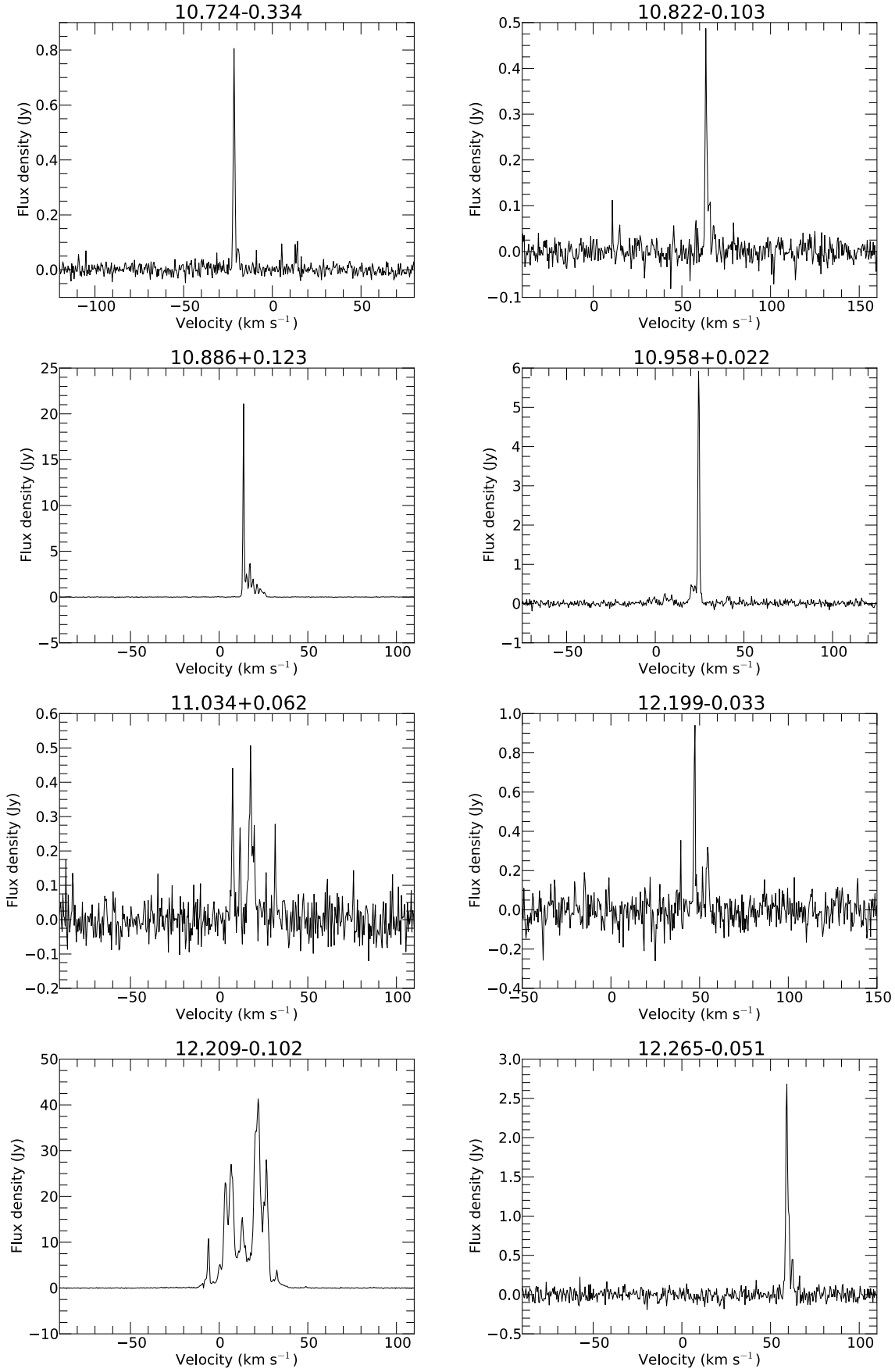

Figure 3.3: – *continued*

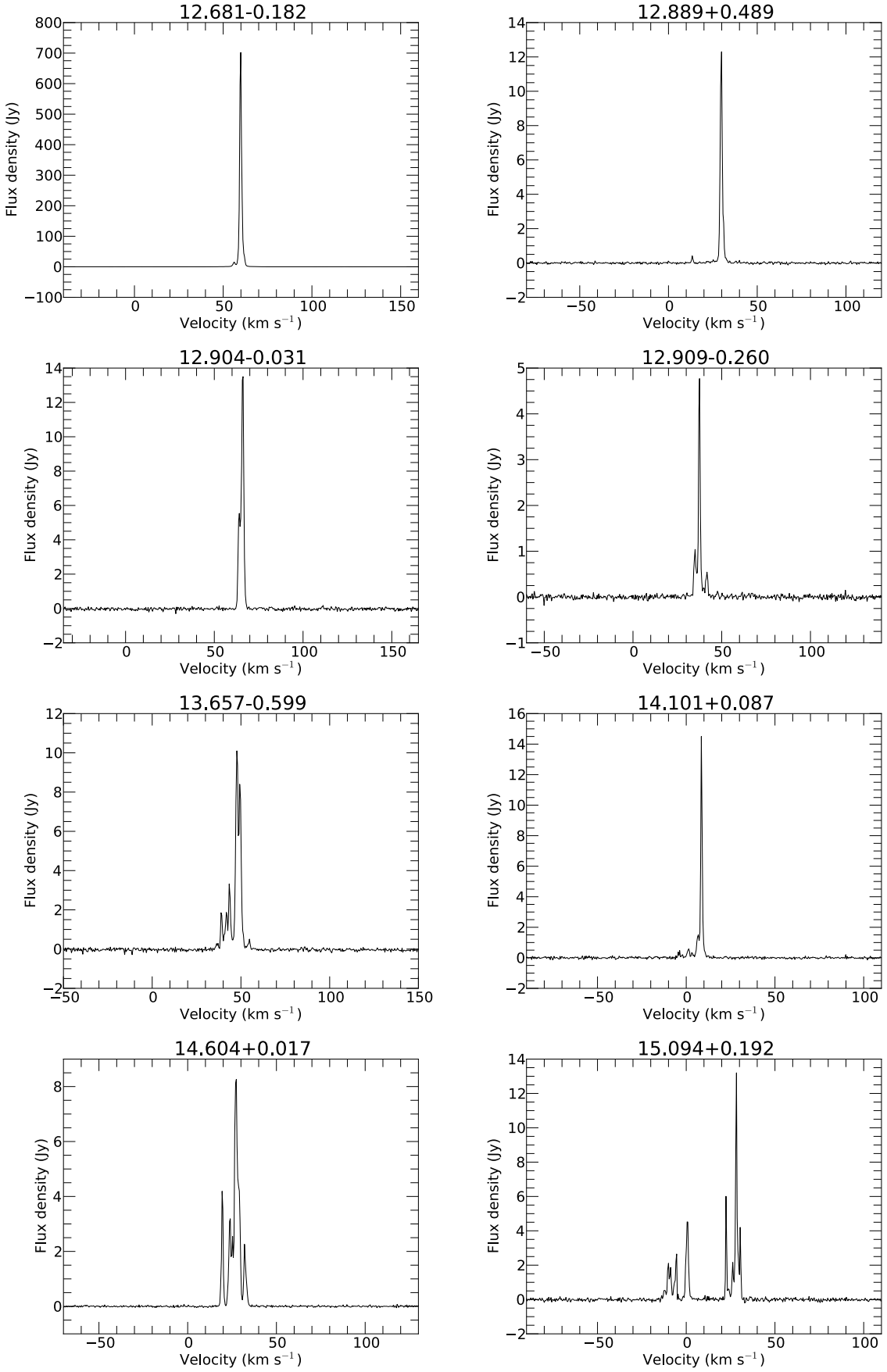

Figure 3.3: – *continued*

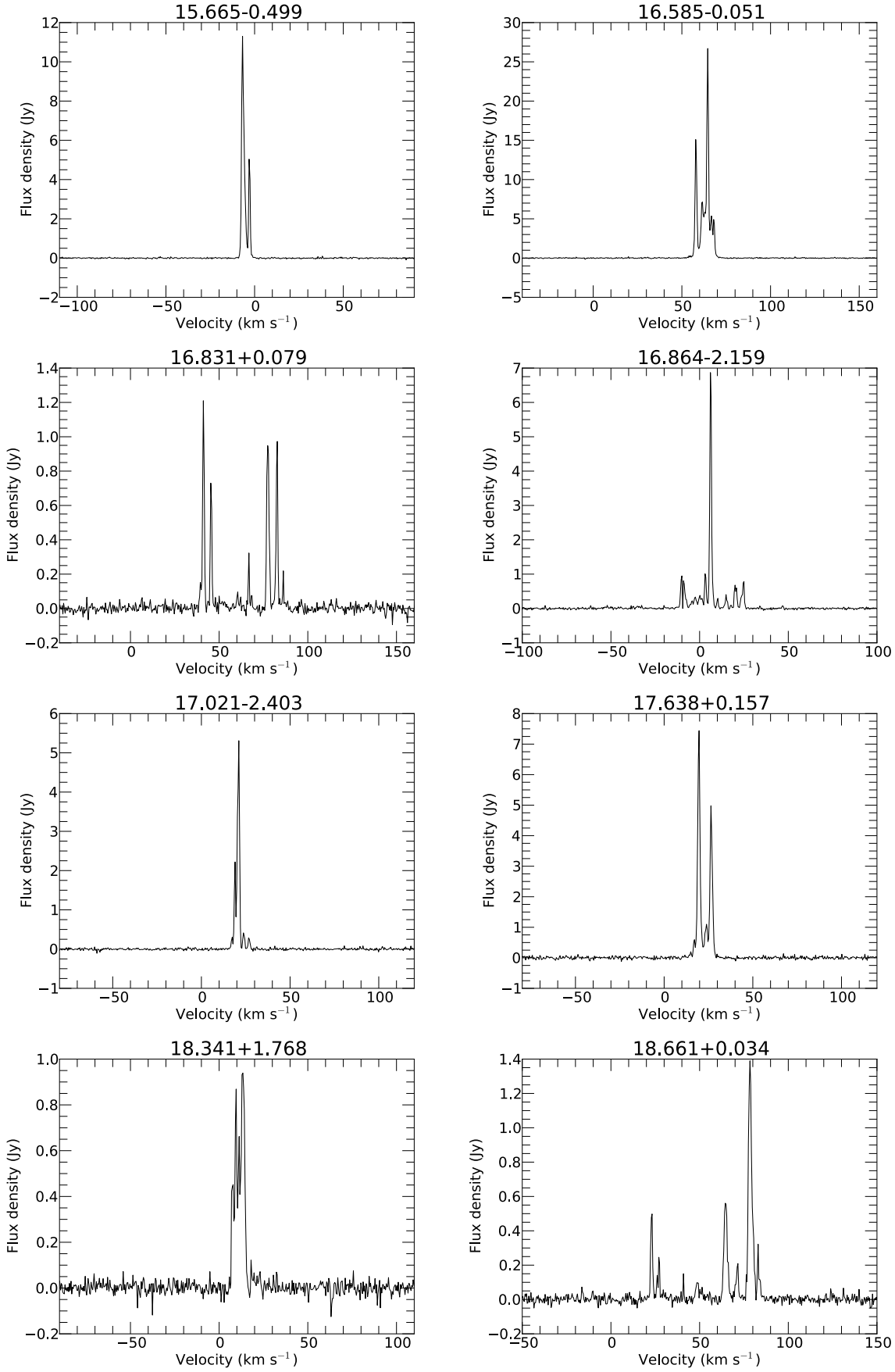

Figure 3.3: – *continued*

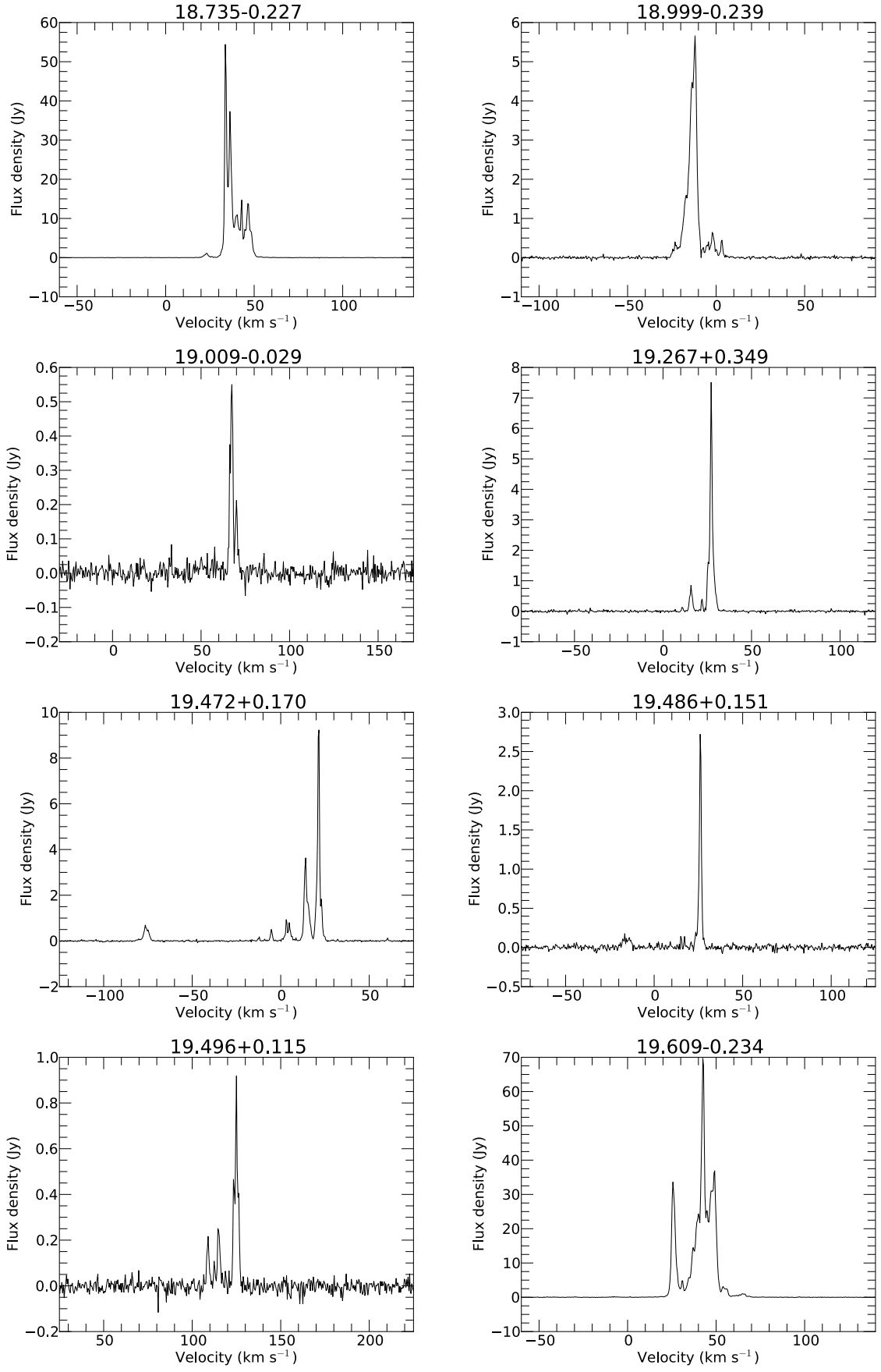

Figure 3.3: – *continued*

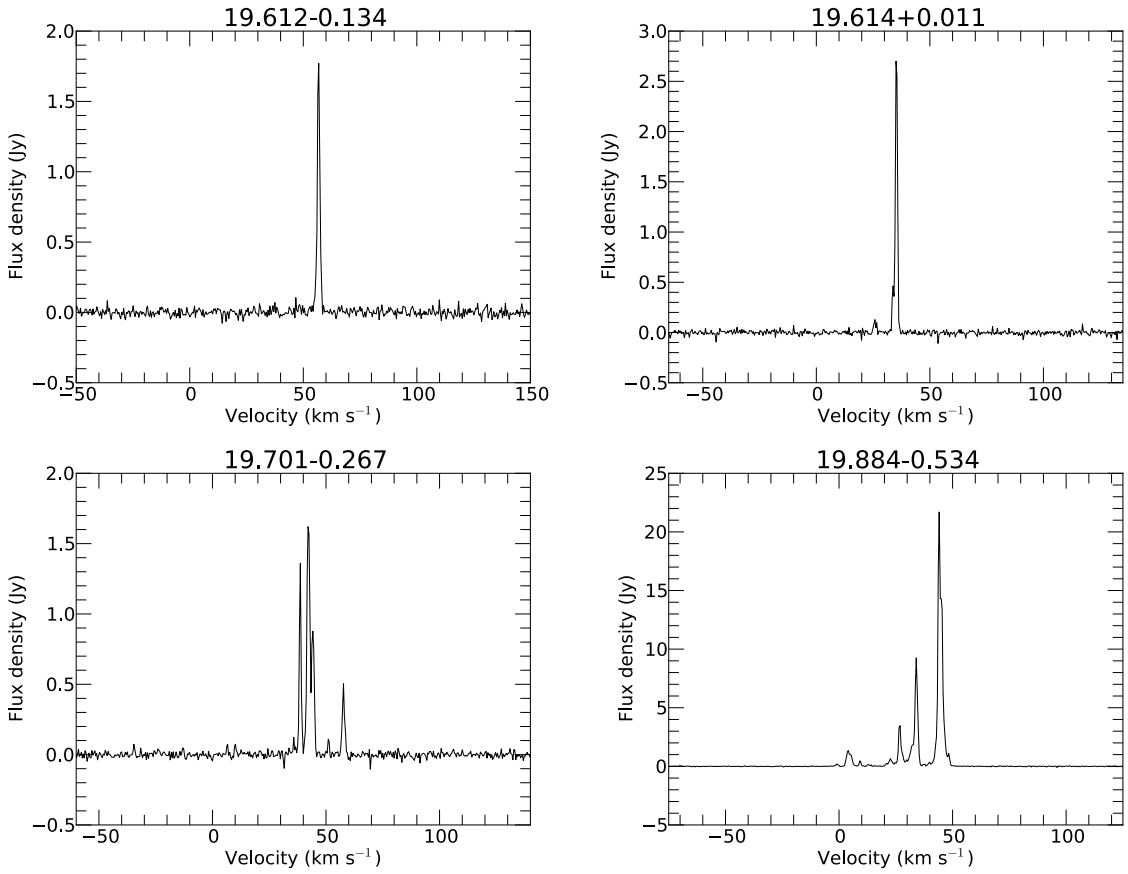

Figure 3.3: – *continued*

357.965–0.164 and 357.967–0.163. These are two distinct methanol maser sites with a small separation (7 arcseconds). We used the near kinematic distances of 3.9 and 2.2 kpc respectively (they are the same within errors) rather than the HI self-absorption distance from Green & McClure-Griffiths (2011) of 15.2 kpc. We have chosen the near distances as 357.965–0.164 is also associated with a rare 23.4-GHz class I methanol maser and very strong 9.9-GHz class I methanol maser whose flux density is more than an order of magnitude stronger than in other known sources (Voronkov et al. 2011) and the Green & McClure-Griffiths (2011) distance was identified as unreliable in their paper. The systemic velocity of the region is $\sim$ –3.0 kms^{-1} as that is the median velocity of the 6.7-GHz methanol maser emission for both sources. *357.967–0.163* has the stronger methanol maser emission and is also accompanied by a 12.2-GHz methanol maser and an OH maser (Breen et al. 2012b; Caswell et al. 2013). It's water maser emission is continuous over 177 kms^{-1}. In our observations it had a velocity range of –74.2 to 103.1 kms^{-1} with a peak velocity of 0.6 kms^{-1} and a peak flux density of 57.8 Jy. Breen et al. (2010a) observed this source in 2003 and found it to have continuous emission over –80 to +100 kms^{-1} with a peak velocity of 0 kms^{-1} and a peak flux density of 40 Jy and in 2004 a velocity range of –81 to +87 kms^{-1}, peak velocity of –65 kms^{-1} and peak flux density 57 Jy. *357.965–0.164* is the weaker 6.7-GHz methanol maser of the two with the smaller velocity range and most of its emission around the systemic velocity (–6.0 to 0.0 kms^{-1}) and no OH counterpart. It's water maser is also the weaker of the two and has a velocity range of –61.1 to 37.3 kms^{-1}, but most of the strong emission is within a couple of kms^{-1} of the peak (–5.2 kms^{-1}), close to the systemic velocity of the region. The higher velocity features are very weak in comparison ($<$ 0.5 Jy).

359.615–0.243. A strong methanol maser identified to be variable by Caswell et al. (1995) and monitored by Goedhart et al. (2004), and no periodicities in the variability were observed. The associated water maser emission is also quite variable, in 2003 it had a peak flux density of 7 Jy, in 2004 it was 14 Jy (Breen et al. 2010a) and in our 2011 observations 80.2 Jy.

0.546–0.852. The water maser has velocity range of 218.7 kms^{-1}. Water maser emission was previously detected by Forster & Caswell (1999) who found the velocities of the maser site to range from –12.95 to 56.90 kms^{-1}, these were some of the features in the middle of the total velocity range we observed in our observations (see Figure 3.3). Breen et al. (2010a) found an even greater velocity range of –60 to 110 kms^{-1} in 2003, and in our observations we found weaker high-velocity features out to –95.0 and +123.7 kms^{-1}.

5.885–0.393. This source has been studied extensively in water, OH and methanol and the latest water information from Motogi et al. (2011) gives an astrometric distance of $1.28^{+0.09}_{-0.08}$ kpc, and confirms the very large angular extent of more than 4 arcseconds, which is not surprising at this quite small distance. Some of the Motogi et al. (2011) water features are within 2 arcseconds of MMB methanol maser, so even though we find the angular offset to be 3.8 arcseconds we can establish that this water maser emission is associated with the target methanol maser.

6.795–0.257 and 10.342–0.142. These sources are separated from their nearest methanol targets by 3.4 and 3.2 arcseconds respectively. The Breen et al. (2010a) positions for these two masers are a little closer to the methanol masers than the positions obtained in these observations; inspection of the *Spitzer* Galactic Legacy Infrared Midplane Survey Extraor-

dinaire (GLIMPSE) three colour images point to the emission coming from the same object and both water masers have emission at similar velocities to that of their target methanol maser, hence we have classified them as associated with their target methanol maser despite being greater than 3 arcseconds away.

10.287–0.125, 10.886+0.123, 12.909–0.260, 15.665–0.499, 19.496+0.115,19.884–0.534, 14.631–0.577, 18.667+0.025, 18.888–0.475, 19.365–0.030. These sources we identified as having extended emission in the GLIMPSE 4.5 μm band that appear similar to the EGOs identified by Chen et al. (2013a,b); Cyganowski et al. (2008) but are not in their catalogues.

6.189–0.358. This source has a strong methanol maser (221.6 Jy) and a weaker water maser (13.1 Jy). Inspection of the GLIMPSE three colour images shows emission in the 4.5 μm band in excess of the other bands around the object the masers are associated with and this object is embedded within an Infrared Dark Cloud.

10.444–0.018. The GLIMPSE three colour image of this source does not show anything at the location of these masers, although it is associated with a 1.1-mm dust clump detected with the Bolocam Galactic Plane Survey. This is a distant source at 11.0 kpc (Green & McClure-Griffiths 2011) so this may account for the lack of mid-infrared emission. Also associated with this source is an OH and 12.2-GHz methanol maser (Breen et al. 2014; Caswell 1998) the presence of which suggests that this is not a particularly young maser region.

10.472+0.027. This water maser has a high velocity feature offset 250 km s^{-1} from the systemic velocity of the region (assuming the 6.7-GHz methanol maser peak velocity to be at the systemic velocity) and covers a total velocity range of 296 km s^{-1}. It is offset 0.9 arcsec from the 6.7-GHz methanol maser and is the highest velocity water maser feature known in any high mass star formation region. This may be because previous studies have not had the velocity coverage of this survey ($>$ 800 km s^{-1}). Further discussion of this source is presented in Titmarsh et al. (2013). This source was also detected in the Breen et al. (2010a) observations, although they did not have sufficient velocity coverage to detect the extreme high velocity features seen in our observations.

14.457–0.143. We note that there is a typographical error in the MMB paper Green et al. (2010). The declination given is –16°27′57″.5, however, the correct declination is –16°26′57″.5.

18.999–0.239. The 6.7-GHz methanol maser has one narrow feature with a peak velocity of 69.4 km s^{-1}, yet the associated water maser peaks at -11.86 km s^{-1} with no emission anywhere near the velocity of the methanol. Caswell & Phillips (2008) suggested that the water masers dominated by blueshifted emission such as this one generally occur at an early stage in the evolution of a YSO as they generally do not have an associated OH maser (this source does not have an OH maser detected above 0.2 Jy; Caswell et al. 2013). This source was previously unknown, and inspection of the GLIMPSE three colour images shows an EGO associated with this YSO, suggesting that this water maser may be powered by an outflow or shock from this source.

Chapter 4

Discussion of maser properties

This chapter combines the analysis of water and methanol maser luminosities, velocities and variability done in both survey areas, $l = 341° - 6°$ (through 0°) and $l = 6° - 20°$, that were originally published separately. The comparison with the HOPS data is an exception to this however, and has only been done for the $l = 341° - 6°$ (through 0°) as the HOPS high-resolution follow-up data was not available at the time of publication of the other survey region.

There have been a number of previous studies which have compared relative detection rates and properties of water and methanol masers based on various sample selection criteria (Beuther et al. 2002; Szymczak et al. 2005; Xu et al. 2008; Breen et al. 2010a). Beuther et al. (2002) made arcsecond resolution observations of water and 6.7-GHz methanol maser emission towards a sample of 24 star formation regions selected on the basis of infrared (*IRAS*) colours. They found approximately 60 % of the sources with 6.7-GHz methanol masers had an associated water maser (within 1.5 arcseconds) and approximately 65 % of the sources with a water maser had an associated 6.7-GHz methanol maser.

Xu et al. (2008) made a sensitive (rms noise ∼0.1 - 0.2 Jy) though lower resolution search (half-power beam width of ∼2 arcminutes) for 6.7-GHz methanol masers towards a sample of 89 water masers thought to be associated with star formation regions, selected from the Arcetri catalogue (Comoretto et al. 1990; Brand et al. 1994). 81 of the target sources had infrared luminosities which suggest that they are high-mass star formation regions. Xu et al. (2008) detected 10 new 6.7-GHz methanol masers. The Xu et al. (2008) selection criteria initially selected 178 sources, (161 thought to be high-mass star formation regions) of which 47 sources were already known to have an associated 6.7-GHz methanol maser and so were not targeted. Thus the combined detection rate of 6.7-GHz methanol masers towards their sample of 22-GHz water masers associated with high-mass star formation was at least 57 out of 161 (35 %).

Of all the previous investigations in the literature, the two which have the greatest similarity to the current study are those undertaken by Breen et al. (2010a) and Szymczak et al. (2005). Szymczak et al. (2005) used the Effelsberg 100m telescope to search for water masers towards a flux-limited (peak intensity greater than 1.6 Jy), but statistically complete sample of 6.7-GHz methanol masers. They detected 41 water masers towards their sample of 79 sources, a detection rate of 52 ± 8 % for a single epoch search (with an rms noise of 0.45 Jy).

Differences between our observations and those undertaken by Szymczak et al. (2005) are the significantly higher sensitivity and angular resolution and somewhat larger size of our target sample. The first two of these enable us to unambiguously determine when the two maser species are associated, to determine their association with infrared and other sources and also to better investigate if the detection rate for water masers changes with properties such as the 6.7-GHz maser luminosity.

Breen et al. (2010a) used the ATCA to make a sensitive search (5-σ detection limit in a 1 km s^{-1} channel typically less than 0.2 Jy) for water masers towards a large sample of OH and 6.7-GHz methanol masers. In total, 270 6.7-GHz methanol masers were observed, resulting in water maser detections towards 198 sources, a rate of 73 $\pm$ 5 % for a two epoch search. Here and below we use $\sqrt{N_{det}}$, where N_{det} is the number of detections, as an estimate of the uncertainty in the detection rate (this method assumes that the non-detections are due to purely stochastic effects, and considering source evolution there is not a more appropriate method to estimate the errors). The chief differences between our observations and those undertaken by Breen et al. (2010a) is that we have a statistically complete target sample and a similar sensitivity but with a factor of two better velocity resolution. The 6.7-GHz methanol masers observed by Breen et al. (2010a) were primarily those with associated OH maser emission, or those without OH maser emission which had an accurate position determined by Caswell (2009). The Caswell (2009) sample in particular is biased towards sources with a higher 6.7-GHz peak flux density. Breen et al. (2010b) found evidence that 6.7-GHz methanol masers increase in luminosity as they evolve. Also, 6.7-GHz methanol masers associated with OH masers are known to be more evolved than those without. Due to both these factors, the Breen et al. (2010a) is biased towards more evolved sources than our targets from the MMB.

The detection rate we have achieved towards a statistically complete sample of 6.7-GHz methanol masers (48 $\pm$ 3 %) is for a single epoch search. It is slightly lower than that obtained by either Szymczak et al. (2005) in a single epoch search or Breen et al. (2010a) in a two epoch search. Comparing our results with those of Szymczak et al. (2005), we can see that to within the uncertainty of the two studies the detection rates are the same. Furthermore, the Szymczak et al. (2005) study had significantly lower positional accuracy (telescope half power beam width of 40 arcseconds at 22-GHz) and had a less sensitive limit for their target sample (approximately a factor of 2 higher than for the MMB). Both of these factors may influence the detection rate and when we restrict our MMB sample to only sources with a peak flux density greater than 1.6 Jy and relax our association criteria to 40 arcseconds we find a detection rate for water masers towards these sources of 52 percent, the same as Szymczak et al. (2005).

4.1 Luminosities

Work by Szymczak et al. (2005) found no statistically significant difference between the luminosities of 6.7-GHz methanol masers with and without associated water masers. Comparing the 6.7-GHz methanol maser luminosities may be a useful probe of the relative evolutionary timeline of objects with and without water masers as Breen et al. (2010b, 2011) found that methanol masers increase in luminosity as they evolve.

Table 4.1: Luminosities of the 6.7-GHz methanol masers with and without associated water masers.

	Mean int. luminosity	Median int. luminosity	Std. dev.
	(Jy km s^{-1} kpc^2)		
Methanol with water	2468.	191.	9362.
Methanol only	529.	94.	1187.

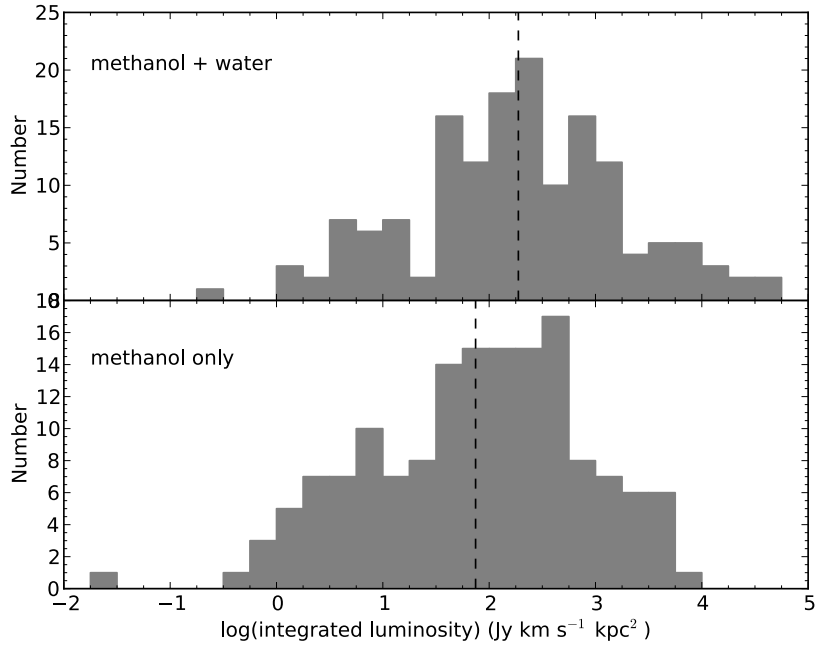

Figure 4.1: Log 6.7-GHz methanol maser integrated luminosities of the methanol masers with and without associated water masers. The dashed line indicate the means.

We compared the mean and median integrated luminosities of the methanol masers with and without associated water masers in our sample (given in Table 4.1). These luminosities were calculated using the distances given in the previous chapter. Using a t-test we find a statistically significant difference between the mean 6.7-GHz methanol maser integrated luminosity between those with and without water (p-value of 0.01). Figure 4.1 shows the distribution of these integrated luminosities, and while the mean is higher for methanol masers with an associated water maser, there is a lot of overlap between the two distributions.

Breen et al. (2010a), in their primarily OH-targeted sample of water masers, investigated the flux densities of solitary water masers and those associated with other masers species and continuum emission. They found the water maser flux densities increased through the association categories of solitary, to sources associated with 6.7-GHz methanol masers, to sources associated with OH masers and 22-GHz continuum. They suggested that this may be evidence that water maser flux densities increase with age, however, they caution that some solitary water masers maybe associated with low-mass stars.

If water masers do increase in luminosity with age, then since there is evidence that the methanol maser luminosities increase with age (Breen et al. 2010b), we might expect the

Table 4.2: Correlation coefficients between the methanol and water luminosities and with distance used to account for bias due to distance.

	peak luminosity	integrated luminosity
methanol - water (R_{mw})	0.68	0.61
methanol - distance (R_{md})	0.60	0.54
water - distance (R_{wd})	0.62	0.57

water and methanol maser luminosities to be correlated. Figures 4.2 and 4.3 show the water maser versus the methanol maser integrated and peak luminosities respectively. We find the integrated luminosity is correlated (Pearson's correlation coefficient of 0.61) and a linear least squares fit to this data gives a statistically significant slope of 0.64 (p-value of 2e-16). The peak luminosities show a tighter correlation (Pearson's correlation coefficient of 0.67) and a linear least squares fit gives a statistically significant slope of 0.69 (p-value of 2e-19). We note that the peak and integrated flux densities of water and methanol masers are also correlated, though the correlations are better for luminosities.

These correlations may be reduced in some individual sources as maser beaming means that the emission is not isotropic and the methanol and water masers may be beamed in different directions. However, over the whole sample this effect should average out. Also, we have used the emission integrated over the whole velocity range of the masers, rather than the peak, and this should average out the effects of beaming in an individual source.

Since for a flux density-limited search the maser luminosities will be correlated with distance, we expect there to be a partial correlation between the luminosities due to this alone. Hence, we have used the procedure outlined in Darling & Giovanelli (2002) to account for this. We found the correlation coefficients between the water and methanol maser peak and integrated luminosities and with distance (see Table 4.2) and calculated the partial correlation coefficients using Equation 4.1. Accounting for the partial correlation, we find the maser luminosities to still be loosely correlated. The water versus methanol maser peak and integrated luminosities have partial correlation coefficients of 0.49 and 0.44 respectively.

$$R_c = \frac{R_{wm} - R_{wd}R_{md}}{\sqrt{(1 - R_{wd}^2)(1 - R_{md}^2)}} \tag{4.1}$$

Since there is evidence that 6.7-GHz methanol masers increase in luminosity as they age this may indicate that there is a trend for water masers to increase in luminosity as they age, although this may be over a long time scale as water masers are well known for their variability. This is consistent with Breen & Ellingsen (2011) who found, based on the 1.2-mm data from dust clumps associated with water masers, some evidence that water masers increase in luminosity as they evolve.

We also fitted a general linear model to the methanol maser luminosity, with the distance and water maser luminosity as the independent variables (we used the logarithms of each of these quantities in the modelling). This modelling showed that while there is a significant dependence of the methanol maser luminosity on distance, after taking that into account a significant dependence on the water maser luminosity is still present. This is consistent

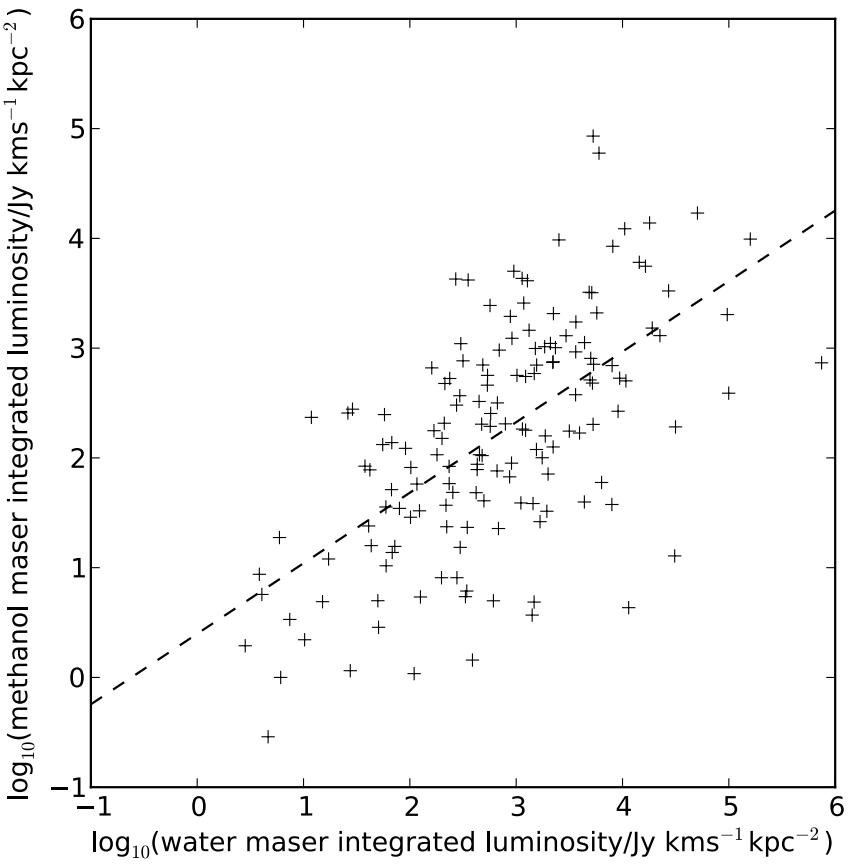

Figure 4.2: Log 6.7-GHz methanol maser integrated luminosity vs. log water maser integrated luminosity. The dashed line is the linear least squares fit to the data.

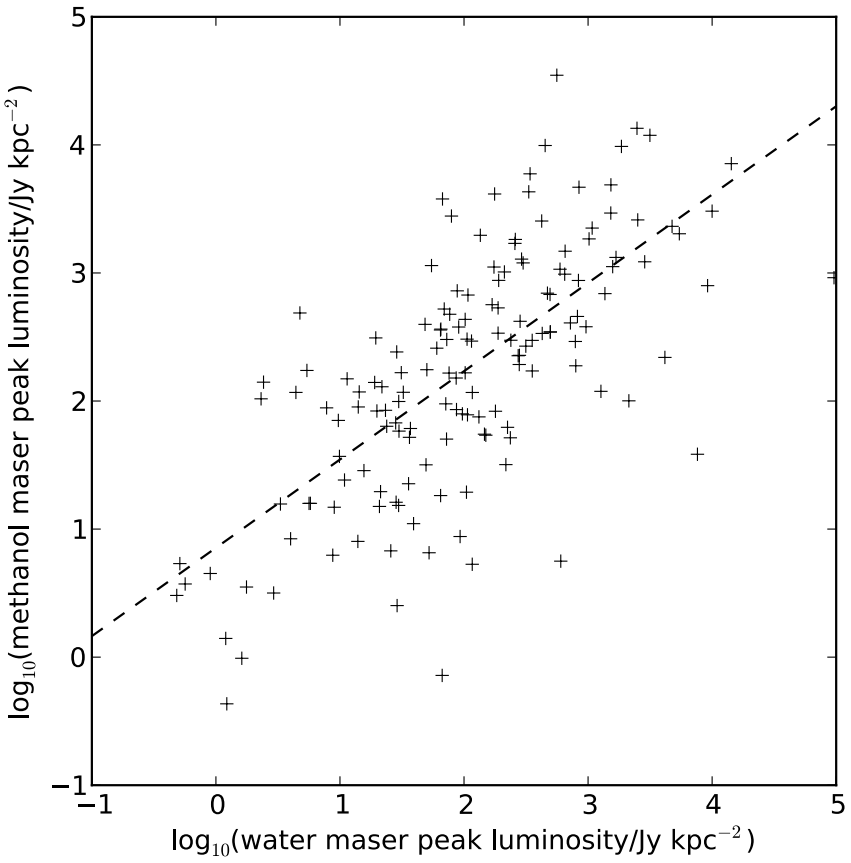

Figure 4.3: Log 6.7-GHz methanol maser peak luminosity vs. log water maser peak luminosity. The dashed line is the linear least squares fit to the data.

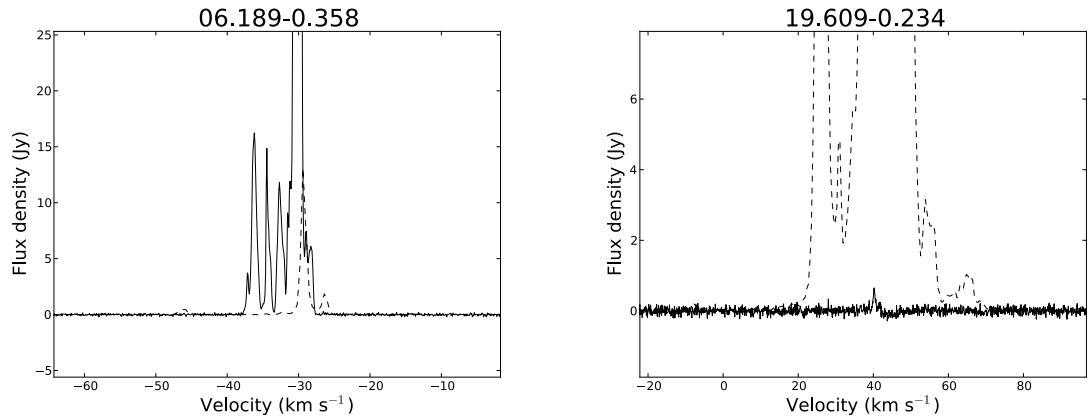

Figure 4.4: Spectra of associated 22-GHz water masers taken with the ATCA (shown with dashed lines) and 6.7-GHz methanol masers from the MMB survey (shown with solid lines).

with the value calculated for the corrected Pearsons correlation coefficient which considers the partial correlation.

The correlation between the peak/integrated luminosities of the two maser species is a general trend and some individual maser sources do not show this. Examples of some of the sources in this sample with extreme differences between the 6.7-GHz methanol and 22-GHz water maser intensities are shown in Figure 4.4. The source 6.189-0.358 has 6.7-GHz methanol maser emission with a peak flux density of 221.6 Jy, while the water maser emission has a peak of only 13.1 Jy. In contrast 19.609-0.234 has a water maser peak flux density of 69.7 Jy associated with a weak methanol maser with a peak of 1 Jy.

4.2 Velocities of water maser emission

Water masers are well known for having velocity features offset from the systemic velocity of the region. The most extreme known water maser in a high-mass star forming region is 10.472+0.027 and has features redshifted up to 250 km s^{-1} from the systemic velocity of the region and covers a total velocity range of nearly 300 km s^{-1} (Titmarsh et al. 2013). Methanol masers at 6.7-GHz typically show emission over a much smaller range of velocities (usually less than 16 km s^{-1}; Caswell 2009) and the central velocities are typically within ± 3 km s^{-1} of the systemic velocity of the region (Szymczak et al. 2007; Caswell 2009; Pandian et al. 2009; Green & McClure-Griffiths 2011). In the investigations below we have used the velocities at the peak flux densities rather than the central velocities, but this will make negligible difference to our results.

Figure 4.5 shows the velocities of the peak emission of the methanol versus the water masers. Our sample shows water and methanol velocities lie within 10 km s^{-1} of each other for 136 of our 156 detections i.e. 87± 8 %, taking the uncertainty as $\sqrt{N_{samp}}$ (the notable outlier in Figure 4.5 is 18.999-0.239 which is discussed in Section 3.2.1). The slightly smaller fraction, 78 %, that was found by Breen et al. (2010a) in their similar study, is consistent with our result to within the uncertainties of both studies. We note that the Breen et al. (2010a) sample is biased more towards sources with OH masers. Szymczak et al. (2005) found an

even smaller fraction, 61 %, displaying velocities differences less than 10 km s^{-1}. This might be because the Szymczak et al. water masers were observed with a larger beam size, and so not all the water masers may be associated with the same powering object as the methanol masers.

In Figure 4.6 we show the distribution of the water maser velocity ranges in our survey. The total velocity range is less than $\sim$ 50 km s^{-1} for the majority of the sample, the median velocity range is 17 km s^{-1} and the average is 31 km s^{-1}. This is close to previous work by Breen et al. (2010a) who found a median velocity range of 15 km s^{-1} in their sample of 379 masers. Szymczak et al. (2005) found that 33 % of their water masers had velocity ranges greater than 20 km s^{-1} and 22 % greater than 40 km s^{-1}. We find 40 and 19 % $\pm$ 5 % greater than 20 km s^{-1} and 40 km s^{-1} respectively which is consistent within the uncertainties with the Szymczak et al. study.

Comparing our velocities with the Caswell & Breen (2010) sample of 32 water masers from their unbiased survey, we find the water masers in our sample typically have smaller velocity ranges. Caswell & Breen (2010) looked at the fraction of water masers with emission spread greater than 30 km s^{-1} from the systemic velocity. They found that 34 % of water masers associated with both methanol and OH masers displayed emission over such a wide range, and 31 % for water masers with only methanol masers associated. In contrast, in our sample we found only 3 % of the water masers had velocity ranges greater than 30 km s^{-1} from the systemic velocity.

Since high velocity emission in water masers is an indicator of outflow activity in the powering source, we wish to see if water maser velocity ranges increase with age. Breen et al. (2010b) found evidence that 6.7-GHz methanol masers increase in luminosity with age, so we have compared the methanol maser luminosity to the water maser velocity range. If more outflow activity occurs with age, then the water maser total velocity range may be correlated with the methanol maser luminosity. However, no correlation was found, so we can not draw any conclusions about different evolutionary phases playing any role in the difference between the sample of Caswell & Breen (2010) and ours.

In Figure 4.7 we investigate the total velocity ranges versus Galactic longitude. The four sources with the largest velocity ranges are 357.967–0.163, 359.138+0.031, 0.546–0.852 and 10.472+0.027. Three of them are close to the Galactic Centre, but otherwise there is no trend in velocity range across the longitudes surveyed.

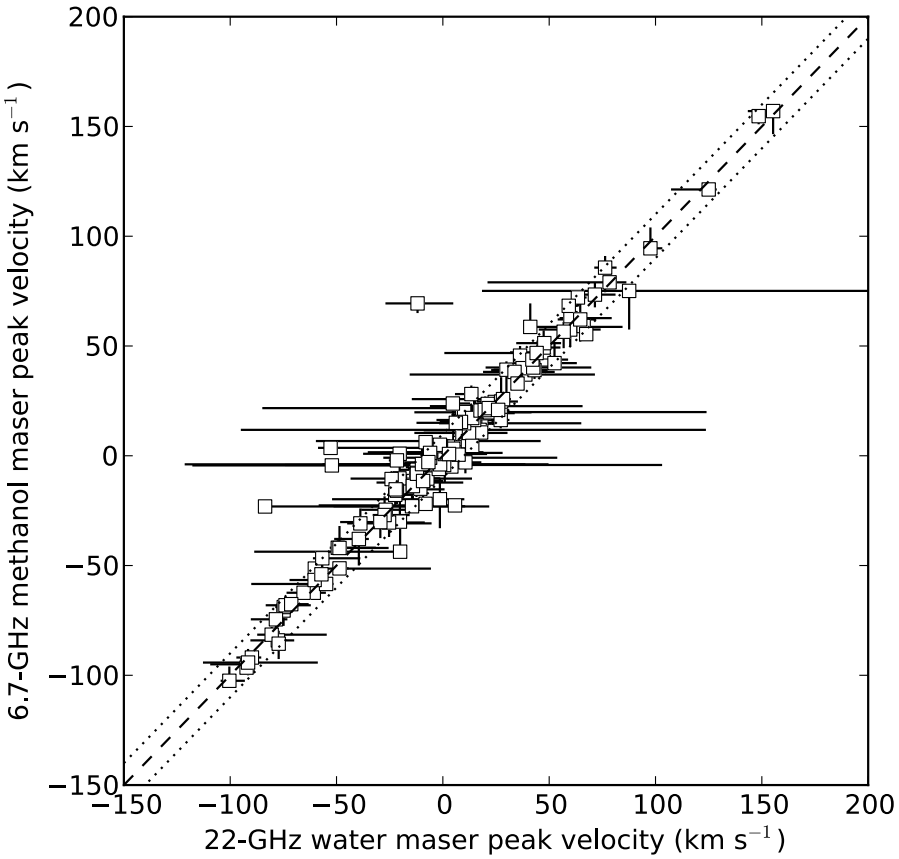

Figure 4.5: Water maser peak velocities vs. associated 6.7-GHz methanol maser peak velocities are shown with squares. The horizontal and vertical bars represent the total velocity ranges of the water and methanol masers respectively. Also plotted is a dashed line with a slope of 1 and two dotted lines showing a deviation of ± 10 km s^{-1} from the dashed line.

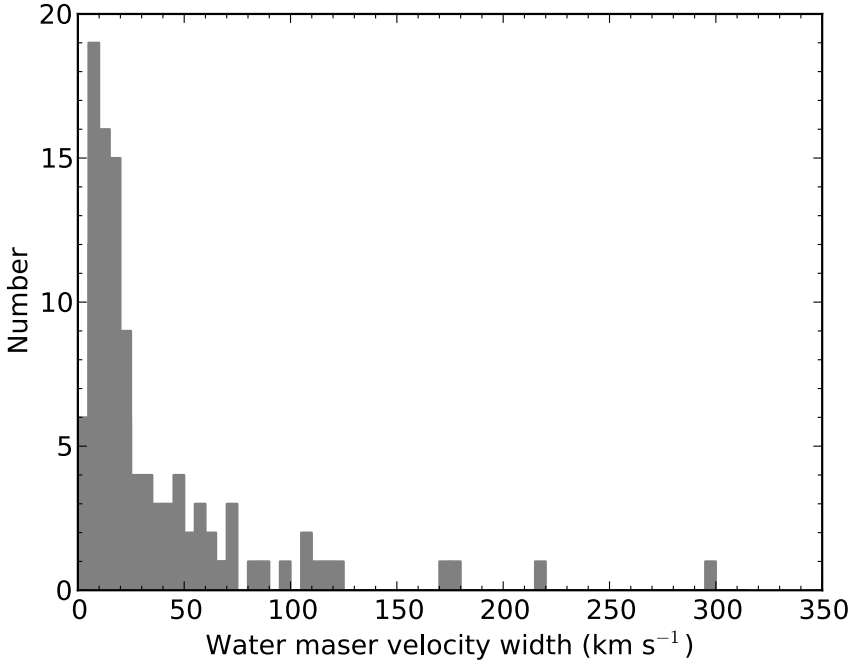

Figure 4.6: Velocity ranges of the water masers associated with a methanol maser.

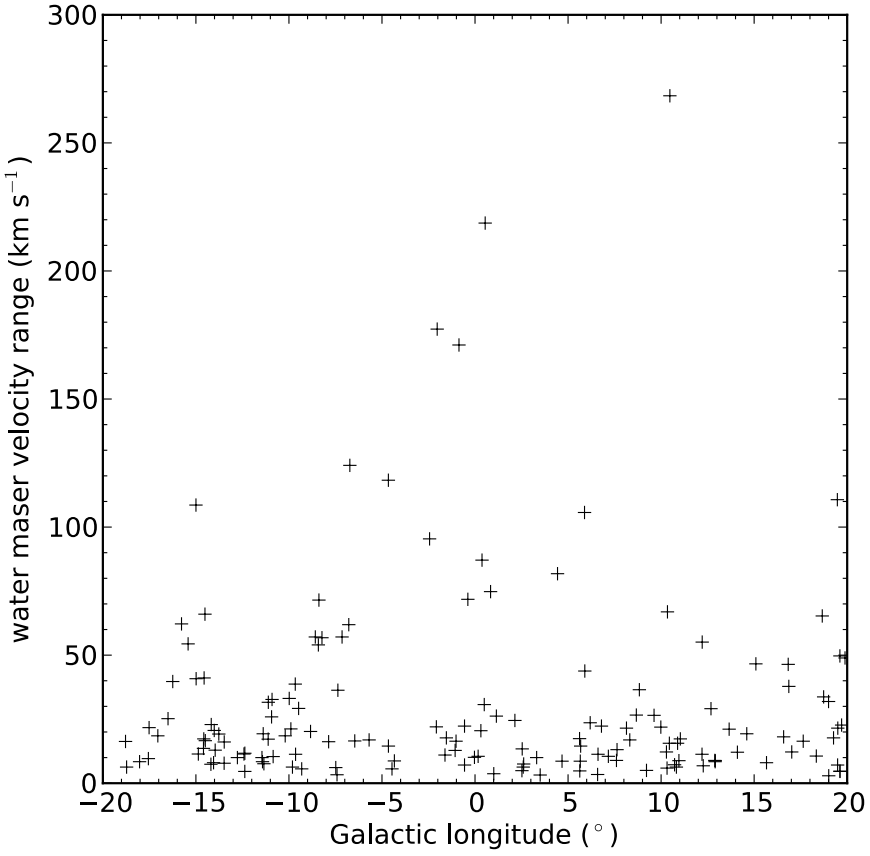

Figure 4.7: Velocity ranges of the water masers vs. Galactic longitude.

4.3 Water maser variability

It is common for water masers to show variability in their flux densities, with studies such as the Arcetri project (Brand et al. 2003; Felli et al. 2007) covering a wide range of timescales and luminosities of the powering YSO. The Arcetri project continued for several decades, but with a fairly small sample size (43 in Felli et al. (2007), and a subset of 14, with more detailed analysis, in Brand et al. (2003)).

For comparison with our sample, we have focused on larger surveys. Two such surveys are Breen et al. (2010a) and Walsh et al. (2011, 2014) which have observed the same water maser sites at more than one epoch. In the Breen et al. (2010a) survey, they observed 253 waters in both 2003 and 2004 and 17 % of these were only detected in one epoch. These masers typically had simpler spectra with only a few velocity features and two-thirds had peak flux densities of less than 2 Jy when they were detected. About a quarter of these were not associated with other maser emission. They also found no statistically significant difference between the proportions of variable water masers associated with methanol and OH masers than from their entire sample.

Some of our sample (observed in 2010 and 2011) overlap with the water masers observed by Breen et al. (2010a) in 2003 and 2004, with many having very different spectra. Figure 4.8 compares (on a log-log scale) the peak flux densities of the water masers from the current sample which were also observed in 2003/2004 by Breen et al. (2010a). All of them show some variation in peak flux density, although some of these may be due different spectral features changing their relative intensities causing features at different velocities to be the peak. There was no overall trend for the masers to increase or decrease in peak flux density with time. Also, masers with both simple and complex spectra were seen to vary. The most extreme case of variability is 11.497–1.485. This maser was 112 Jy in the 2004 observations by Breen et al. (2010a) and not detected (5σ detection limit of 75 mJy) when we observed it in 2010.

Walsh et al. (2011) detected 540 water masers between 2008 - 2010 in an unbiased search for water masers in the Galactic Plane with the Mopra telescope. In 2011/2012 they followed up these detections with high resolution observations from the ATCA (Walsh et al. 2014). 31 sites of water maser emission were not detectable in the second epoch, and like Breen et al. (2010a), they found the most variable sources tended to be weaker with simpler spectra. Unlike Breen et al. (2010a) they found a smaller fraction of the masers not detected in one epoch ($\sim$ 6 %). This is likely to be because the Breen et al. (2010a) survey was much more sensitive than the initial HOPS search (which is estimated to be 98 % complete down to 8.4 Jy) since there is a well established tendency for less luminous water masers to exhibit greater fractional variability.

Only the water masers in the MMB follow-up between $l = 341^\circ - 6^\circ$ (through 0°) have been compared with HOPS data, as the HOPS high-resolution follow-up data was not available at the time of publication of the $l = 6^\circ - 20^\circ$ water maser follow-up. Figure 4.9 plots (on a log-log scale) the peak flux densities of our water maser observations in 2011 against those in 2011/2012 from Walsh et al. (2014). Even though the masers in Breen et al. (2010a) were observed 7 - 8 years apart from our observations, they showed no more scatter in Figure 4.8

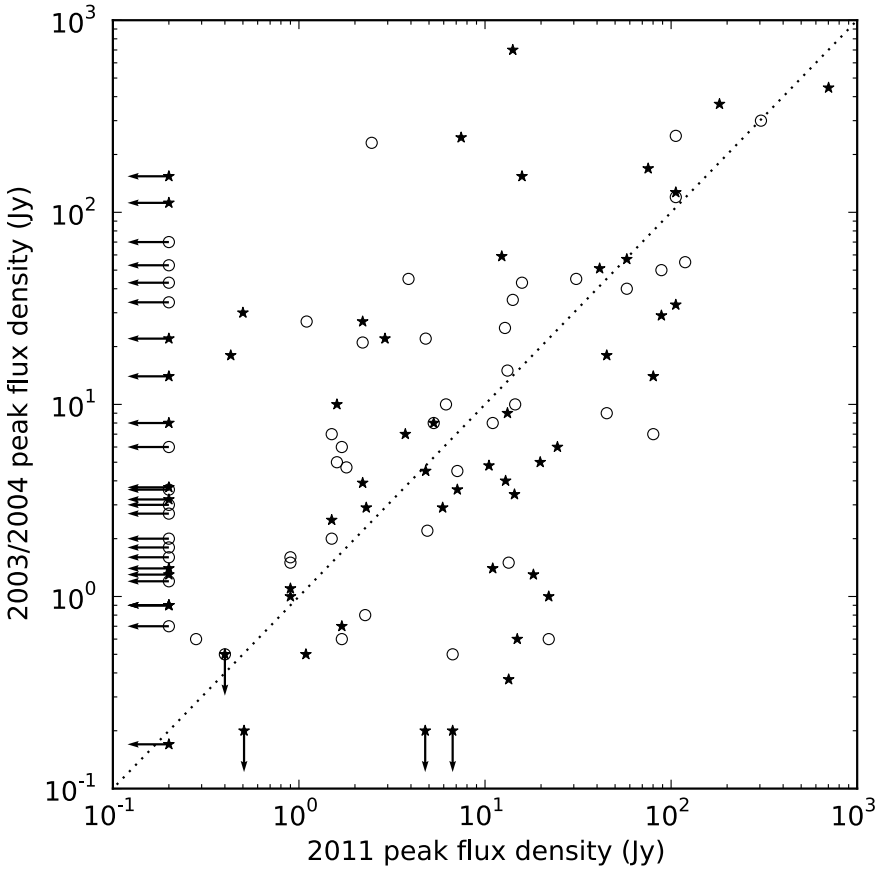

Figure 4.8: Comparison of peak flux densities of the water masers that were observed in both the MMB follow-up (observed in 2010/2011) and the Breen et al., (2010a) sample. The Breen et al. (2010a) observations that were made in 2003 are marked with open circles and those from 2004 are stars. Where masers were detected in one epoch and not the other, 3 σ upper limits on the flux densities are shown with arrows. Also plotted is a dotted line with a slope of 1.

than the HOPS masers that were observed with less than a 12 month separation from our observations.

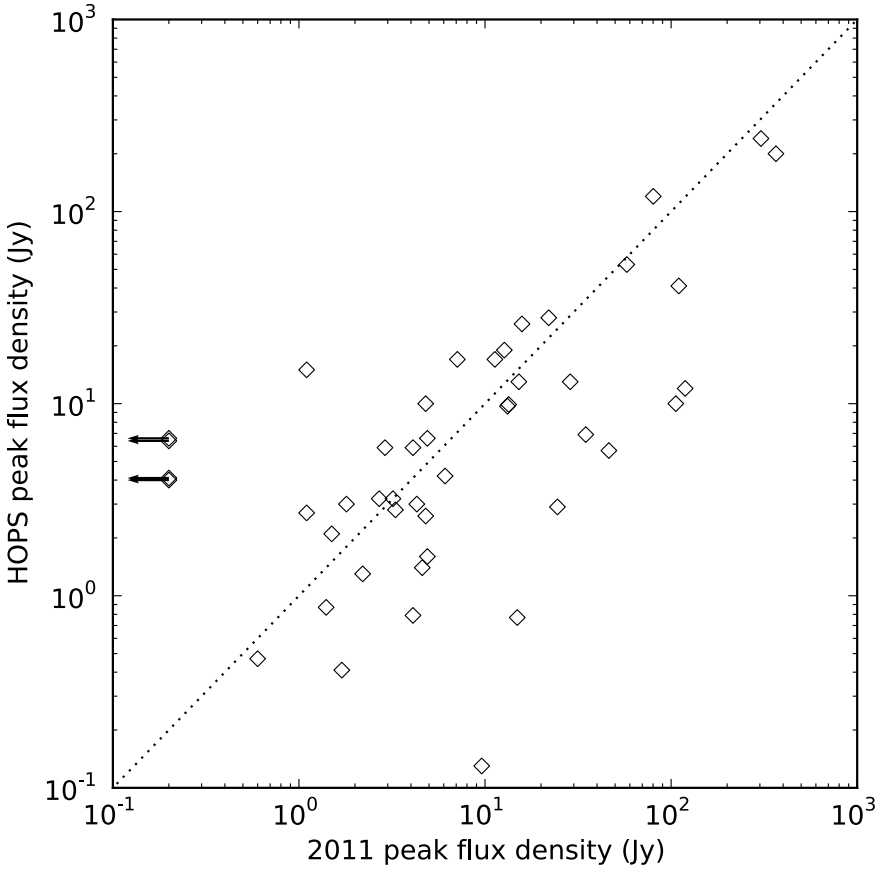

Figure 4.9: Peak flux densities of water masers detected in the MMB follow-up (observed in 2010/2011) and the HOPS high resolution follow-up (observed in 2011 and 2012). There were many sources detected in our observations that were not reported in HOPS. We have not included these as we do not know if they were not found because the initial HOPS search was much less sensitive than ours, or because of variability. Where masers were detected in HOPS and not the MMB follow-up observations, 3 σ upper limits on the flux densities are shown with arrows. Also plotted are dotted lines with slope of 1.

Chapter 5

Infrared and submillimeter comparisons

In this chapter the 6.7-GHz methanol masers with and without associated water masers are compared with infrared and submillimeter emission. Since the MMB water maser follow-up has been published in two separate publications for the $l = 341^\circ - 6^\circ$ (through the Galactic Centre) and $l = 6^\circ - 20^\circ$ ranges, different comparisons have been done with the two samples. The $l = 6^\circ - 20^\circ$ range, has been searched for star formation tracers in the extended infrared emission and compared with the dust emission at 1.1 mm. The masers between $l = 341^\circ - 6^\circ$ (through the Galactic Centre), have been compared with infrared point sources and with dust emission at 870 μm.

5.1 Associations with extended emission in GLIMPSE

The *Spitzer* Galactic Legacy Infrared Midplane Survey Extraordinaire (Benjamin et al. 2003, GLIMPSE) images have been used to examine the mid-infrared environments of the regions where the masers occur (images used are in Appendix .1). 115 of the 119 6.7-GHz methanol masers in the $l = 6^\circ - 20^\circ$ range are within the range covered by the GLIMPSE I and II data sets.

Cyganowski et al. (2008) have identified many Extended Green Objects (EGOs) from the GLIMPSE I survey region and Chen et al. (2013a) have recently identified 98 new EGO sources from the GLIMPSE II region. Chen et al. (2013a) investigated both the infrared and 3-mm molecular line properties of these sources and found them to be consistent with the EGOs being associated with high-mass protostellar objects undergoing active accretion, but at a stage prior to the formation of a UCHII region (Chen et al. 2013a,b). An earlier study has explored associations of EGOs with solitary water masers (no methanol or OH), and water masers accompanied by methanol and/or OH (Breen et al. 2010a). We are now able to expand these results with the statistics of association with methanol masers without water masers.

We first assemble an extensive sample of EGOs for this comparison. The Cyganowski et al. (2008) sample overlaps with our survey in the $l = 10^\circ - 20^\circ$ range and only two of our masers have an EGO match within 30 arcseconds of any EGO in their catalogue (12.904-

0.031 and 19.009-0.029). 30 arcseconds was chosen because it is approximately the largest angular extent of the EGOs in that sample and visual inspection of three colour images of these maser sites confirms that they are associated with the Cyganowski et al. (2008) EGOs. Classification of EGOs is a somewhat subjective process and other authors have defined their own samples of EGOs (e.g. Chen et al. 2013a; Chambers et al. 2009). The sample that has the most matches with ours is Chen et al. (2013a) which has seven matches with our masers in the $l = 6^\circ - 10^\circ$ range. So for this range we used the Chen et al. (2013a) sample and for the rest we decided to search our sample for EGO candidates rather than match with an existing catalogue. Three colour images for each maser site were made using the standard three colour scheme, 3.6 μm - blue, 4.5 μm - green, 8.0 μm - red and visual inspection of the three colour images reveals several other sources that are EGO candidates (see Tables 3.1 and 3.2). There are more EGOs associated with both water and methanol masers than there are with methanol maser only regions (the difference is statistically significant using a Pearson's chi-squared test, p-value of 0.03, see Table 5.1). This may be because water masers are more dependent on the physical conditions of the surrounding environment interacting with the protostar (e.g. outflows interacting with gas the protostar is embedded in) than class II methanol masers. It could also be that since EGOs may be preferentially associated with the later stages of the methanol maser phase, that the water masers switch on later than the methanol masers. Breen et al. (2010a) studied associations of EGOs with solitary water masers, water with associated methanol, water with OH and water with both methanol and OH masers. They found water masers with associated methanol and OH masers were most likely to have an EGO present. They suggest that EGOs occur late enough in the evolution of a protostar for an OH maser to have formed, but not so late that it has developed an UCHII region causing the methanol maser emission to cease.

Another indicator of the early stages of star formation that can be found in GLIMPSE images are Infrared Dark Clouds (IRDCs). IRDCs are regions of cold and dense gas and dust which are seen in absorption against the diffuse mid-infrared background from PAH emission, particularly in the 8 μm band (e.g. Rathborne et al. 2006; Pillai et al. 2006a). Although IRDCs do not trace a specific evolutionary phase of the high-mass star formation process, it is well established that very young protostellar objects, and perhaps even some prestellar cores are embedded within some IRDCs (e.g. Ellingsen 2006).

The IRDC catalogue of Peretto & Fuller (2009) covers our $l = 10^\circ - 20^\circ$ range and cross matching with them gives 19 matches over our whole sample within 1 arcminute and no matches within 3 arcseconds. Thus we decided to inspect our infrared images for IRDCs (see Table 5.1). The classification of objects associated with IRDCs is also somewhat subjective, as IRDCs can only be observed where there is sufficient background diffuse emission and not too much diffuse foreground emission between us and the cold dense gas. The sources we have classified as being associated with an IRDC include both sources which are infrared dark at 8 μm, as well as those associated with infrared bright objects which are surrounded by some infrared darkening. We found no statistically significant difference in the number of IRDCs associated with sources with both methanol and water masers and those with only methanol masers.

Gallaway et al. (2013) investigated the GLIMPSE images of the MMB sources in the

Table 5.1: Numbers of Extended Green Objects and Infrared Dark Clouds found in GLIMPSE associated with 6.7-GHz methanol masers with and without associated water masers in the $l = 6^\circ - 20^\circ$ range. (There are 63 methanol only sources and 52 with water as well.)

	Methanol only sources	Methanol with water sources
EGO	5	10
IRDC	11	10

longitudes $186^\circ \leq l \leq 20^\circ$ and found 26 % were associated with IRDCs and 12 % were IR-dark and do not have an IRDC. In this study we only found the number of IRDCs to be consistent with their study, however, we found only one source to be IR-dark (< 1 %).

5.2 Associations with GLIMPSE point sources

There have been a number of previous studies comparing the GLIMPSE colours of the mid-infrared objects associated with masers (Ellingsen 2006; Breen et al. 2010b; Gallaway et al. 2013). More details can be found in Section 2.6.

We used the Gallaway et al. (2013) Adaptive Non-Circluar Aperture Photometry flux densities to compare the MMB sources between $l = 341^\circ - 5^\circ$ through the Galactic Centre with and without associated water masers in colour-colour and colour-magnitude diagrams. Any difference in the infrared colours could point to differences in evolutionary phase (like those with and without OH masers in Ellingsen (2006)). However, we found no statistically significant difference in the mid-infrared colours between the infrared sources associated with both methanol and water masers and those with only methanol.

5.3 Associations with 1.1-mm emission from dust clumps

The Bolocam Galactic Plane Survey (BGPS; Rosolowsky et al. 2010) used the Bolocam instrument on the Caltech Submillimeter Observatory to undertake a continuum survey of the Milky Way at 1.1-mm. This wavelength is a good tracer of thermal dust emission from the coldest, densest gas and dust cores, the locations believed to be the sites of the earliest stages of high-mass star formation. We have used the second data release of the BGPS (Ginsburg et al. 2013) to compare with our maser sample in the $l = 6^\circ - 20^\circ$ range. The BGPS covered the longitude range of our water maser observations with a latitude coverage of $\pm 1.5^\circ$ (which covers the range of the vast majority of 6.7-GHz methanol maser detections, all but three are in this latitude range). 92 of the 116 6.7-GHz methanol masers in this region had a BGPS counterpart within 33 arcseconds (the effective resolution of the BGPS), and of these 49 had a water maser also. The resolution of the BGPS is much coarser than the size of a star forming core associated with a maser which means that the BGPS flux densities will potentially include emission from many other surrounding sources from the clustered environments where high mass stars are formed.

Previous work by Chen et al. (2012) used BGPS dust clumps as targets for a search for class I methanol masers. They compared the BGPS flux densities, gas masses and beam

averaged column densities of the clumps with and without masers associated (the column density is the molecular hydrogen column inferred from the observed dust emission, an assumed dust-to-gas ratio and assuming that the dust emission is optically thin). They found that BGPS sources with a class I methanol maser had higher BGPS flux densities and beam averaged column densities than those without a maser. Details of how the gas mass and beam averaged column density were derived are given in Equations 2.1, 2.2 and 2.3 in Section 2.7.

Similar to Chen et al. (2012) we found BGPS sources with either class II methanol or water masers had higher BGPS integrated flux densities and beam averaged column densities than the general population (see Figures 5.1 and 5.2). The beam averaged column density is only dependent on the 40 arcsecond flux density as in our calculations we assumed a temperature of 20 K for all sources. No comparison of the gas masses was made due to the lack of distance estimates for the sources without masers. No statistically significant differences in integrated flux density and beam-averaged column density were found between BGPS sources with both and methanol and water masers and the methanol only sources.

Chen et al. (2012) found that intensity of the class I methanol maser emission is correlated with the mass and beam averaged column densities of the BGPS sources. Similar to Chen et al. (2012), we found a correlation between the water maser integrated flux density and the beam averaged column density (see Figure 5.3). However, no correlations were apparent when doing similar comparisons with the 6.7-GHz methanol maser sample. It is not surprising that these water masers show similar correlations to the class I methanol masers as they are also collisionally pumped. Sources with higher integrated column densities tend to be more massive and so this trend is likely a result of there being a larger volume of gas where the conditions are conducive to masing in these sources.

In Figure 5.4 we have plotted the BGPS integrated flux densities against the BGPS 40 arcsecond flux densities. BGPS sources with associated masers are typically the brighter sources, implying that they are higher mass clumps. BGPS clumps with masers associated tend to be the most compact sources having a greater fraction of their integrated flux densities within the 40 arcsecond beam than the majority of the non-maser BGPS sources. It also appears that clumps associated with both water and methanol masers are more compact than those associated with methanol only, although there is a large degree of overlap in these two samples. We have done a linear least squares fit to all the dust clumps in Figure 5.4 that have any maser emission and the differences in the residuals between the maser association categories are shown in Figure 5.5. The mean of the residuals of the clumps that have only methanol masers associated is greater than that of the clumps with both water and methanol masers. This difference is statistically significant; a t-test gives a p-value of 0.01. Dust is accreted onto the protostar as it evolves which implies that the more compact dust clumps may be older. Hence, the dust clumps with both water and methanol masers may be older than the methanol only clumps. This suggests that both class II methanol and water maser emission occurs during the phase of high-mass star formation where large-scale infall is still in progress, consistent with recent observations of molecular gas (Peretto et al. 2013).

While protostars with both 6.7-GHz methanol and water masers may generally be older than those with just 6.7-GHz methanol masers, we suggest that the evolutionary phase traced by water masers is less well-defined than that traced by 6.7-GHz methanol. Our findings

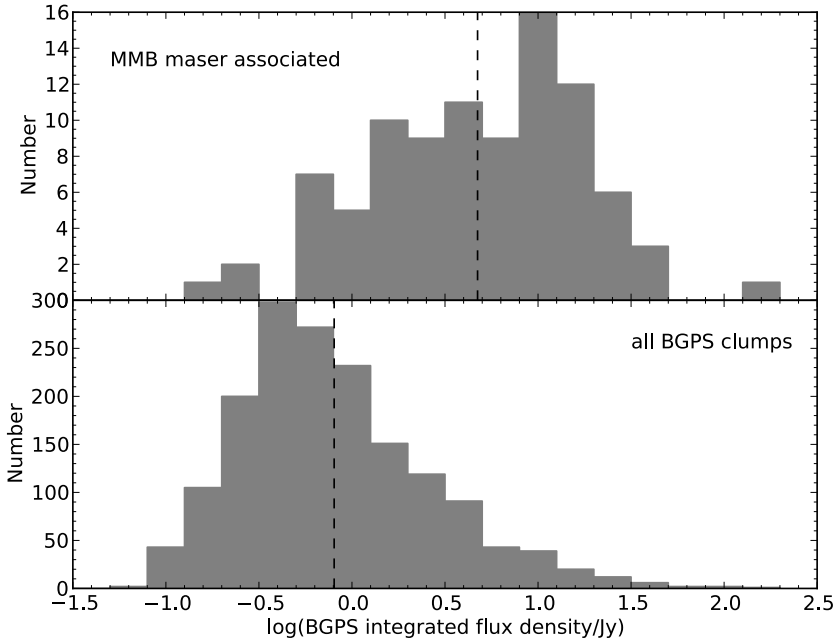

Figure 5.1: Number of sources as a function of BGPS integrated flux density. The top panel shows the dust clumps with associated 6.7-GHz methanol masers and the bottom panel are all the BGPS dust clumps in the $l = 6 - 20°$ region. The dashed lines represent the means.

support the argument of Breen et al. (2014) that class II methanol maser transitions are better tied to the evolutionary phase of the protostar as they are radiatively pumped, existing close to the protostar and so are more closely linked to the protostar's properties. In contrast, water masers, being collisionally pumped and occurring at the interaction of outflows and the surrounding environment could exist over a longer time scale and a wider variety of conditions and so are not well tied to a specific evolutionary phase of the protostar.

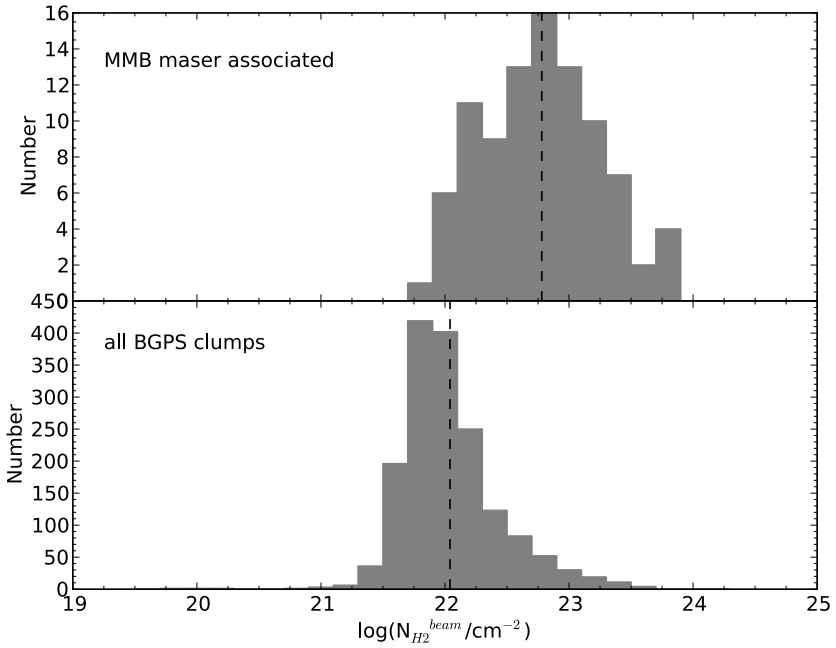

Figure 5.2: Number of sources as a function of beam averaged column density. The top panel shows the dust clumps with associated 6.7-GHz methanol masers and the bottom panel are all the BGPS dust clumps in the $l = 6 - 20°$ region. The dashed lines represent the means.

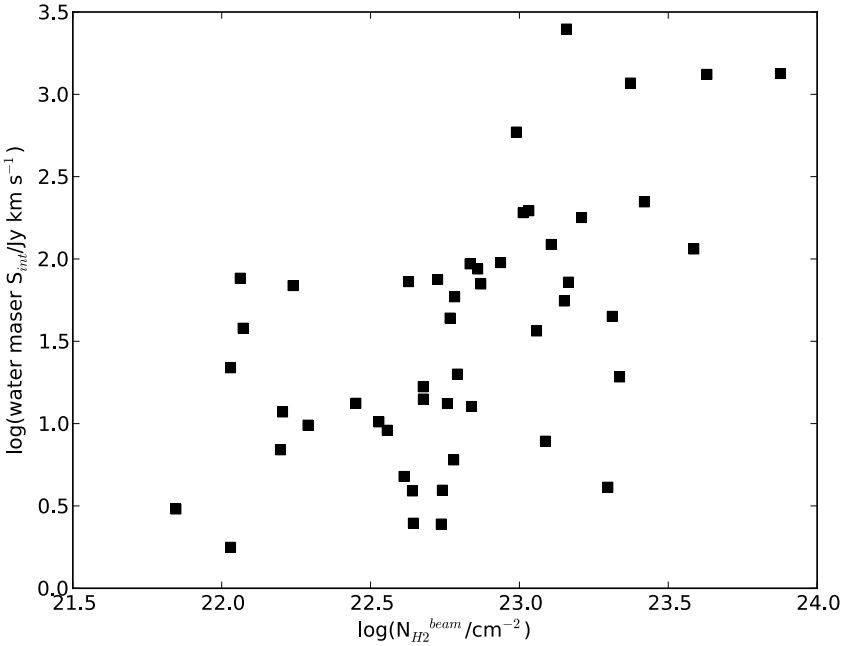

Figure 5.3: Water maser integrated flux density vs. beam averaged column density.

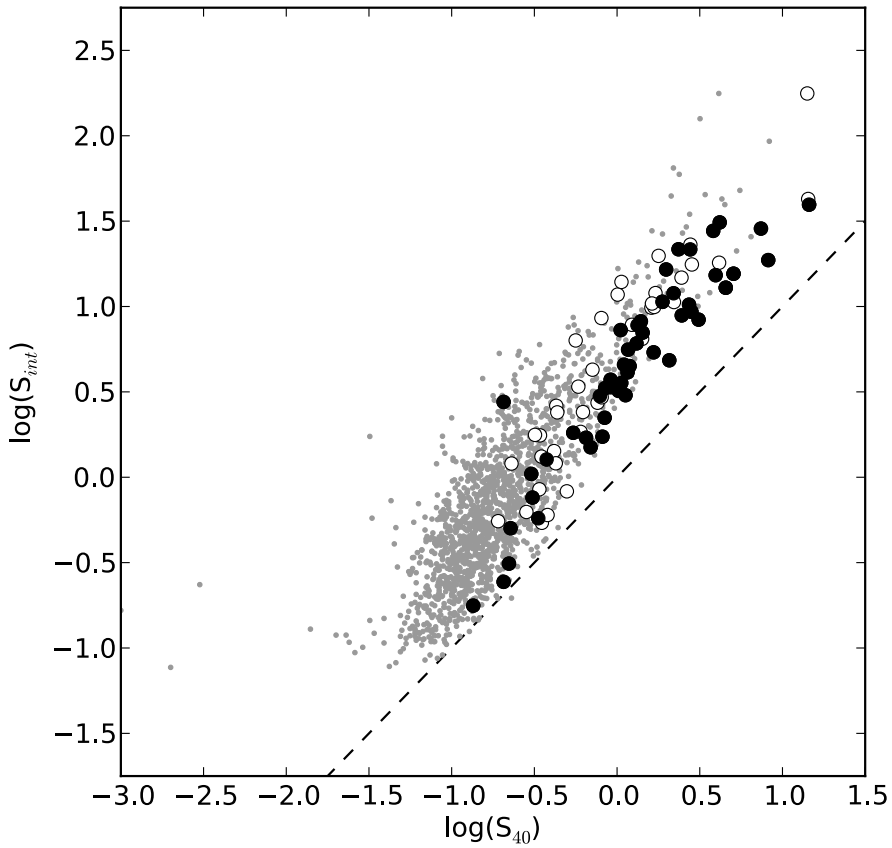

Figure 5.4: BGPS integrated flux density vs. BGPS 40 arcsecond flux density. All the BGPS dust clumps in the l = 6 – 20° region are plotted with grey dots, clumps with only 6.7-GHz methanol masers associated are open circles and clumps with both water and methanol masers associated are black dots. The dashed line has a slope of 1.

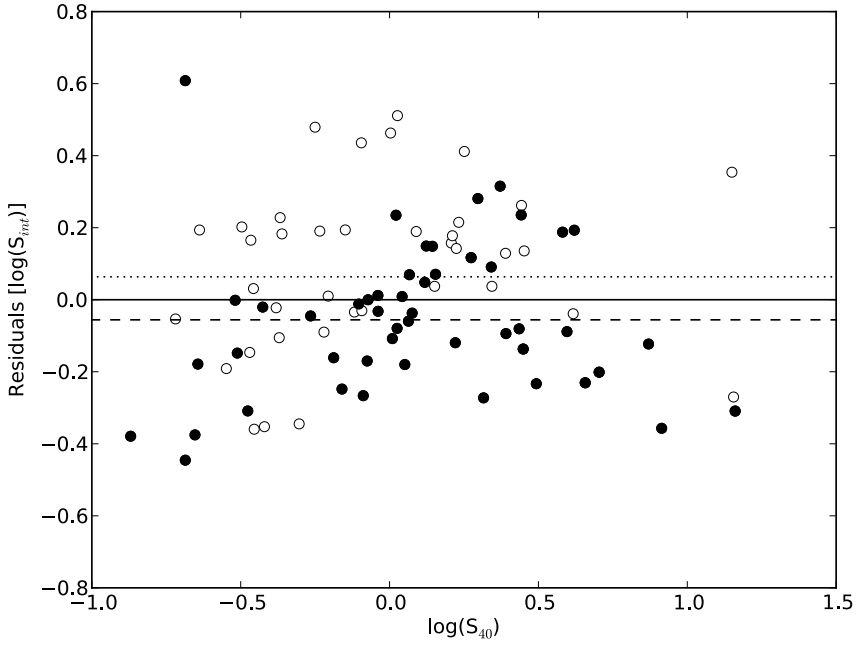

Figure 5.5: Residuals from a linear fit to all the BGPS clumps with an associated methanol maser in the previous figure. Clumps with 6.7-GHz methanol masers associated are open circles and clumps which also have water associated are black dots. The fit to all the clumps with masers is the solid line, the mean of the residuals for methanol-only clumps is the top dashed line and the mean of the water and methanol associated residuals is the lower dashed line.

5.4 Associations with 870-μm emission from dust clumps

Another large survey of continuum dust emission is the APEX Telescope Large Area Survey of the GALaxy (ATLASGAL; Schuller et al. 2009), an unbiased survey of the Galactic Plane at 870 μm with the APEX telescope in Chile.

About 95 % of the MMB masers between $l = 341^\circ - 5^\circ$ (through the Galactic Centre) lie within the region surveyed by ATLASGAL. Urquhart et al. (2013) used the ATLASGAL source catalogues of Contreras et al. (2013) and Csengeri et al. (2014) to match the methanol masers with an associated dust clump. They used a criteria of being within 120 arcseconds of a peak in the 870 μm emission to define an association as this was the largest clump radius (Contreras et al. 2013). If more than one clump was within that radius, they chose the clump with it's peak emission closest. They then inspected the ATLASGAL images to determine if its associations were genuine. Approximately 94 % of MMB masers within the ATLASGAL survey range were found to have an associated 870-μm dust clump.

We used the ATLASGAL-MMB associations identified in Urquhart et al. (2013) to compare the dust emission of the 6.7-GHz methanol masers with and without associated water masers and also to compare the 870-μm emission with the results from Section 5.3 using the 1.1 mm emission from the BGPS. In Section 5.3 we found BGPS sources with an associated MMB maser to have higher integrated flux densities and higher column densities than the general population. However, we found no differences in these properties between the clumps associated with an MMB maser with and without a water maser present. Like class I methanol masers, water masers are also pumped by collisions, and like Chen et al. (2012) we found a weak correlation between the water maser integrated flux density and the beam averaged column density.

To make our ATLASGAL comparisons, we recalculated the masses and column densities of the dust clumps, as we have distance estimates for all the MMB sources in our survey (Urquhart et al. (2013) did not have distances for many of the sources around the Galactic Centre) and we used $\mu = 2.3$ for the mean molecular weight of the ISM to be consistent with Chen et al. (2012). Column densities and clump masses were calculated according to equations 1 and 2 in Chen et al. (2012).

Unlike comparisons with the BGPS in Section 5.3, we found no correlation between the integrated flux density of the water masers and the ATLASGAL column densities of their associated dust clumps. The correlation at 1.1 mm was weak, however, we expected to observe similar results at 870 μm as sources with higher integrated column densities tend to be more massive and there may be a larger volume of gas where the conditions are appropriate for maser emission in these clumps. The reason for the absence of correlation here is not clear, although it may be that the weak correlation observed for the $l = 6^\circ - 20^\circ$ maser sample occurred by chance and is not present in larger source samples. Similar to our comparisons with the BGPS we also found no correlations between the water maser luminosities and the clump masses or between the methanol maser intensities and the column densities and masses. We also found no differences in the distributions of the ATLASGAL column densities and masses of the clumps with both methanol and water masers and those with only methanol.

Figure 5.6 shows the column densities of the clumps with an associated MMB maser

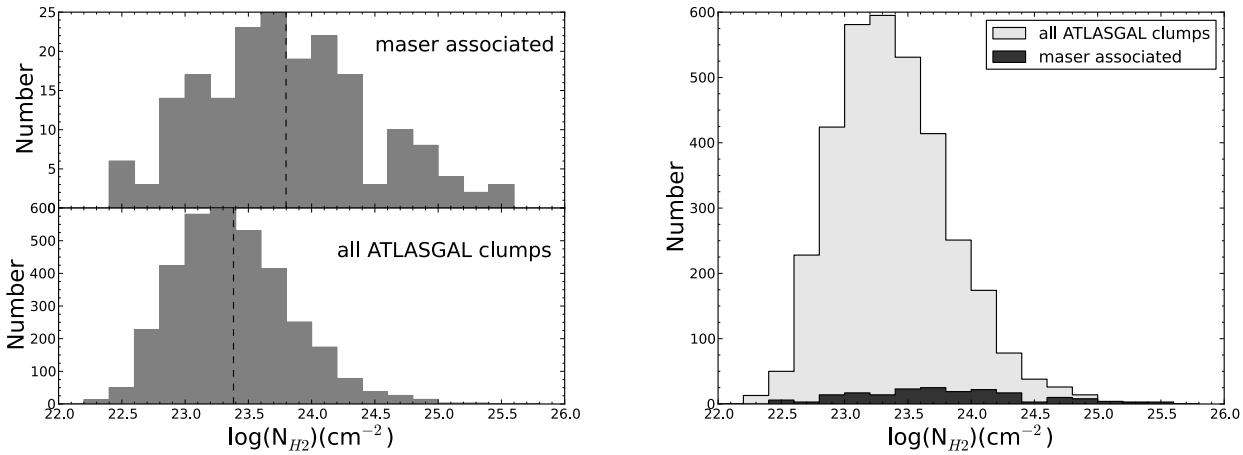

Figure 5.6: Number of sources as a function of column density. In the left figure, the top panel shows the dust clumps detected in ATLASGAL associated with 6.7-GHz methanol masers and the bottom panel are all the clumps detected in the longitude range covered in this paper. The dashed lines represent the means of each sample. The figure on the right has both populations overlaid, showing that at the highest column densities (over $\sim 10^{25}$ cm^{-2}) almost all the dust clumps have an associated methanol maser.

compared to those of all the ATLASGAL clumps within our survey region. The left panel shows the distribution of the clumps with associated masers compared to all the clumps within our survey region on separate scales to clearly show the two distributions, and the right panel shows that the fraction of maser-associated dust clumps increases with increasing column density. At the very highest column densities (over $\sim 10^{25}$ cm^{-2}), almost 100 % of clumps have an associated methanol maser. Like our comparisons with the BGPS, the maser associated clumps are skewed toward the higher mass clumps, unlike our BGPS comparisons, the dust clumps with an associated maser appear to cover the whole range of column densities of the general population. However, this may be a sensitivity issue as the 5 σ sensitivity of ATLASGAL is 0.25 Jy beam^{-1}, corresponding to a hydrogen column density of order 10^{22} cm^{-2} (Schuller et al. 2010) whereas the BGPS was sensitive to column densities greater than 10^{21} cm^{-2}.

Chapter 6

Conclusions

In this thesis, all the 323 known 6.7-GHz methanol masers in the Galactic Plane between $l = 341^\circ$ and $l = 20^\circ$ (through the Galactic centre) have been observed with the ATCA for water maser emission. Of these, 156 had associated water masers within ∼3 arcseconds of their 6.7-GHz methanol maser targets (∼ 48 %). This is consistent with previous studies when the angular resolution and flux density limitations of those studies is taken into consideration.

I have found that 6.7-GHz methanol masers with associated water masers have greater integrated luminosities. Since 6.7-GHz methanol masers get brighter with age, this may be evidence that water masers are often associated with older methanol masers. Also, the methanol and water maser peak and integrated luminosities are correlated, even after taking into account the partial correlation due to distance and I interpret this to be evidence that water maser generally increase in brightness as they age.

The peak velocities of the water and methanol masers are very well correlated in this sample, with 87 % having peak velocities within ± 10 km s^{-1}. I found the median velocity range of the water masers to be 17 km s^{-1} and the average to be 31 km s^{-1}. This is consistent with other methanol-selected samples of water masers, but is smaller than that found in an unbiased survey of water masers by Caswell et al. (2010). The velocity ranges observed in this sample of water masers is consistent with the methanol-targeted search by Szymczak et al. (2005). However, the velocity ranges are generally smaller than those observed by Caswell & Breen (2010) that are associated with both methanol and OH masers.

From the GLIMPSE mid-infrared images, I found that there was no statistically significant difference in the number of IRDCs associated with sources that had both water and methanol masers and the methanol-only sources. But I did find that there are more EGOs associated with water and methanol maser sources than with the methanol-only sources.

Using the GLIMPSE sources and their flux densities in the four *Spitzer* bands extracted by Gallaway et al. (2013), I found no difference in the colours of the mid-infrared sources associated with both methanol and water masers and those with methanol only.

The 1.1-mm data from the BGPS was used to study the properties of the dust emission at these maser sites. I found that dust clumps with associated masers had higher BGPS integrated flux densities than the general population of dust clumps in our survey region. The maser-associated clumps also had a greater fraction of their flux densities within the 40 arcsecond beam of BGPS, implying that they are the more compact sources. The sources with

both water and methanol masers are generally more compact than those with only associated with methanol masers associated. If these dust clumps collapse to form a protostar as they age, then this suggests that 6.7-GHz methanol masers with associated water masers are older than those without water masers.

I investigated the ATLASGAL sources identified to have associated MMB masers in Urquhart et al. (2013), and found that in the submillimetre emission there were no differences between the column densities and masses of clumps associated with both water and methanol masers and those with just methanol. I did find that the clumps associated with methanol masers are skewed towards the higher column densities compared to the general population. This is consistent with my findings for 1.1-mm thermal dust continuum emission from the BGPS.

Like Breen et al. (2014), I conclude that water masers are unlikely to trace such a well defined evolutionary phase in the formation of a protostar as the 6.7-GHz methanol maser transition, which are radiatively pumped and exist close to the protostar and hence are very dependant on its evolutionary phase. Water masers are collisionally pumped, occurring at locations where the protostar is interacting with the surrounding environment (e.g. outflows) which may not exist alongside a specific evolutionary stage of the protostar. Since the methanol maser luminosities, associations with EGOs and dust clump data suggest that water masers often occur later in the 6.7-GHz methanol maser phase, it is likely that the interactions required to produce a water maser increase as the protostar evolves, and therefore the presence of water maser emission alone does not provide a good evolutionary diagnostic. Nevertheless, water maser observations can still provide us with valuable information the physical conditions of the YSO.

6.1 Future work

There are a number of questions which arise from the investigations undertaken as part of this thesis and some additional data available from the observations which was not analysed due to time limitations. I have outlined possible future investigations relating to these below.

There is still work to be done analysing the ammonia and continuum data taken at the same time as the water maser observations during this survey. This will provide valuable information about the temperatures and the presence (or absence) of UCHII regions. These data, combined with the maser, (sub)millimetre continuum and mid-infrared observations will enable further testing and/or refinement of the maser-based evolutionary scheme.

Now that more reliable distance estimates are available for the MMB masers, further investigation of the projected linear separations of the water and methanol masers is necessary. Future investigations can study if water masers closer to their associated 6.7-GHz methanol masers are better correlated with YSO age indicators, implying they are more closely tied to the evolution of their YSO compared to water masers at larger physical separations associated with outflows etc.

A number of the results obtained in this thesis were unexpected and while the results appear to be robust, they require further investigation to understand why they have occurred. These questions include:

- why are the methanol and water maser peak luminosities better correlated than the integrated luminosities?
- why are the water maser integrated flux densities correlated with the column densities derived from the 1.1-mm emission but not the 870-μm emission?
- why are the total velocity ranges of the water maser associated with methanol masers much smaller than those from the Caswell et al. (2010)? Their sample was of 32 water masers from an unbiased survey. To investigate this further, it is necessary to have a larger, sensitive unbiased sample of water masers to compare with.

How water masers without associated methanol masers fit into the maser evolutionary timeline of high-mass star formation still remains unanswered. A large, sensitive, high-resolution, unbiased sample of water masers would allow this population of water masers to be investigated in the future.

Bibliography

Aguirre J. E. et al., 2011, ApJS, 192, 4

Argon A. L., Reid M. J., Menten K. M., 2003, ApJ, 593, 925

Baan W. A., Wood P. A. D., Haschick A. D., 1982, ApJLett, 260, L49

Barlow M. J. et al., 1996, A&A, 315, L241

Barrett A. H., Schwartz P. R., Waters J. W., 1971, ApJLett, 168, L101

Bartkiewicz A., Szymczak M., Pihlström Y. M., van Langevelde H. J., Brunthaler A., Reid M. J., 2011, A&A, 525, A120

Batrla W., Matthews H. E., Menten K. M., Walmsley C. M., 1987, Nature, 326, 49

Benjamin R. A. et al., 2003, PASP, 115, 953

Beuther H., Walsh A., Schilke P., Sridharan T. K., Menten K. M., Wyrowski F., 2002, A&A, 390, 289

Bonnell I. A., Bate M. R., 2006, MNRAS, 370, 488

Brand J. et al., 1994, A&AS, 103, 541

Brand J., Cesaroni R., Comoretto G., Felli M., Palagi F., Palla F., Valdettaro R., 2003, A&A, 407, 573

Breen S. L., Caswell J. L., Ellingsen S. P., Phillips C. J., 2010a, MNRAS, 406, 1487

Breen S. L., Ellingsen S. P., 2011, MNRAS, 416, 178

Breen S. L., Ellingsen S. P., Caswell J. L., Green J. A., Fuller G. A., Voronkov M. A., Quinn L. J., Avison A., 2011, ApJ, 733, 80

Breen S. L. et al., 2014, MNRAS, 438, 3368

Breen S. L., Ellingsen S. P., Caswell J. L., Green J. A., Voronkov M. A., Fuller G. A., Quinn L. J., Avison A., 2012a, MNRAS, 426, 2189

Breen S. L., Ellingsen S. P., Caswell J. L., Green J. A., Voronkov M. A., Fuller G. A., Quinn L. J., Avison A., 2012b, MNRAS, 421, 1703

Breen S. L., Ellingsen S. P., Caswell J. L., Lewis B. E., 2010b, MNRAS, 401, 2219

Breen S. L., Ellingsen S. P., Contreras Y., Green J. A., Caswell J. L., Stevens J. B., Dawson J. R., Voronkov M. A., 2013, MNRAS, 435, 524

Breen S. L. et al., 2015, MNRAS, 450, 4109

Burke B. F., Papa D. C., Papadopoulos G. D., Schwartz P. R., Knowles S. H., Sullivan W. T., Meeks M. L., Moran J. M., 1970, ApJLett, 160, L63

Carrasco-González C. et al., 2015, Science, 348, 114

Caswell J. L., 1996, MNRAS, 279, 79

Caswell J. L., 1997, MNRAS, 289, 203

Caswell J. L., 1998, MNRAS, 297, 215

Caswell J. L., 2009, Publ. Aston. Soc. Aust., 26, 454

Caswell J. L., Breen S. L., 2010, MNRAS, 407, 2599

Caswell J. L. et al., 2010, MNRAS, 404, 1029

Caswell J. L. et al., 2011, MNRAS, 417, 1964

Caswell J. L., Green J. A., Phillips C. J., 2013, MNRAS, 431, 1180

Caswell J. L., Haynes R. F., 1987, Australian Journal of Physics, 40, 215

Caswell J. L., Phillips C. J., 2008, MNRAS, 386, 1521

Caswell J. L., Reynolds J. E., 2001, MNRAS, 325, 1346

Caswell J. L., Vaile R. A., Ellingsen S. P., 1995, Publ. Aston. Soc. Aust., 12, 37

Chambers E. T., Jackson J. M., Rathborne J. M., Simon R., 2009, ApJS, 181, 360

Chen X. et al., 2012, ApJS, 200, 5

Chen X., Ellingsen S. P., Shen Z.-Q., Titmarsh A., Gan C.-G., 2011, ApJS, 196, 9

Chen X., Gan C.-G., Ellingsen S. P., He J.-H., Shen Z.-Q., Titmarsh A., 2013a, ApJS, 206, 9

Chen X., Gan C.-G., Ellingsen S. P., He J.-H., Shen Z.-Q., Titmarsh A., 2013b, ApJS, 206, 22

Cheung A. C., Rank D. M., Townes C. H., Thornton D. D., Welch W. J., 1969, Nature, 221, 626

Churchwell E., 2002, in Astronomical Society of the Pacific Conference Series, Vol. 267, Hot Star Workshop III: The Earliest Phases of Massive Star Birth, Crowther P., ed., p. 3

Claussen M. J., Heiligman G. M., Lo K. Y., 1984, Nature, 310, 298

Claussen M. J., Wilking B. A., Benson P. J., Wootten A., Myers P. C., Terebey S., 1996, ApJS, 106, 111

Comoretto G. et al., 1990, A&AS, 84, 179

Contreras Y. et al., 2013, A&A, 549, A45

Cragg D. M., Johns K. P., Godfrey P. D., Brown R. D., 1992, MNRAS, 259, 203

Cragg D. M., Sobolev A. M., Ellingsen S. P., Caswell J. L., Godfrey P. D., Salii S. V., Dodson R. G., 2001, MNRAS, 323, 939

Cragg D. M., Sobolev A. M., Godfrey P. D., 2002, MNRAS, 331, 521

Cragg D. M., Sobolev A. M., Godfrey P. D., 2005, MNRAS, 360, 533

Csengeri T. et al., 2014, A&A, 565, A75

Cudaback D. D., Read R. B., Rougoor G. W., 1966, AJ, 71, 851

Cyganowski C. J., Brogan C. L., Hunter T. R., Churchwell E., 2009, ApJ, 702, 1615

Cyganowski C. J., Koda J., Rosolowsky E., Towers S., Donovan Meyer J., Egusa F., Momose R., Robitaille T. P., 2013, ApJ, 764, 61

Cyganowski C. J. et al., 2008, AJ, 136, 2391

Darling J., Giovanelli R., 2002, AJ, 124, 100

De Buizer J. M., Vacca W. D., 2010, AJ, 140, 196

Dickinson D. F., 1976, ApJS, 30, 259

Dunham M. K. et al., 2010, ApJ, 717, 1157

Egan M. P., Shipman R. F., Price S. D., Carey S. J., Clark F. O., Cohen M., 1998, ApJLett, 494, L199

Elitzur M., Hollenbach D. J., McKee C. F., 1989, ApJ, 346, 983

Ellingsen S. P., 2006, ApJ, 638, 241

Ellingsen S. P., Breen S. L., Voronkov M. A., Dawson J. R., 2013, MNRAS, 429, 3501

Ellingsen S. P., Sobolev A. M., Cragg D. M., Godfrey P. D., 2012, ApJLett, 759, L5

Ellingsen S. P., von Bibra M. L., McCulloch P. M., Norris R. P., Deshpande A. A., Phillips C. J., 1996, MNRAS, 280, 378

Ellingsen S. P., Voronkov M. A., Cragg D. M., Sobolev A. M., Breen S. L., Godfrey P. D., 2007, in IAU Symposium, Vol. 242, IAU Symposium, Chapman J. M., Baan W. A., eds., pp. 213–217

Felli M. et al., 2007, A&A, 476, 373

Fish V. L., Reid M. J., 2007, ApJ, 656, 952

Fish V. L., Reid M. J., Argon A. L., Menten K. M., 2003, ApJ, 596, 328

Forster J. R., Caswell J. L., 1989, A&A, 213, 339

Forster J. R., Caswell J. L., 1999, A&AS, 137, 43

Furuya R. S., Kitamura Y., Wootten A., Claussen M. J., Kawabe R., 2003, ApJS, 144, 71

Gallaway M. et al., 2013, MNRAS, 430, 808

Genzel R., Reid M. J., Moran J. M., Downes D., 1981, ApJ, 244, 884

Ginsburg A. et al., 2013, ApJS, 208, 14

Goedhart S., Gaylard M. J., van der Walt D. J., 2004, MNRAS, 355, 553

Goedhart S., Langa M. C., Gaylard M. J., van der Walt D. J., 2009, MNRAS, 398, 995

Green J. A. et al., 2009, MNRAS, 392, 783

Green J. A. et al., 2010, MNRAS, 409, 913

Green J. A. et al., 2012, MNRAS, 420, 3108

Green J. A., McClure-Griffiths N. M., 2011, MNRAS, 417, 2500

Heiles C., Goodman A. A., McKee C. F., Zweibel E. G., 1993, in Protostars and Planets III, Levy E. H., Lunine J. I., eds., pp. 279–326

Hildebrand R. H., 1983, QJRAS, 24, 267

Hinkle K. H., Barnes T. G., 1979, ApJ, 227, 923

Hofner P., Churchwell E., 1996, A&AS, 120, 283

Jackson J. M. et al., 2013, Publ. Aston. Soc. Aust., 30, 57

Jordan C. H. et al., 2015, MNRAS, 448, 2344

Kalenskii S. V., Johansson L. E. B., Bergman P., Kurtz S., Hofner P., Walmsley C. M., Slysh V. I., 2010, MNRAS, 405, 613

Klessen R. S., Ballesteros-Paredes J., Vázquez-Semadeni E., Durán-Rojas C., 2005, ApJ, 620, 786

Knowles S. H., Mayer C. H., Cheung A. C., Rank D. M., Townes C. H., 1969, Science, 163, 1055

Krishnan V. et al., 2015, ApJ, 805, 129

Krumholz M. R., Klein R. I., McKee C. F., Offner S. S. R., Cunningham A. J., 2009, Science, 323, 754

Kudritzki R. P., 2002, ApJ, 577, 389

Kurtz S., Hofner P., Álvarez C. V., 2004, ApJS, 155, 149

Mac Low M.-M., Klessen R. S., 2004, Reviews of Modern Physics, 76, 125

Menten K., 1991, in Astronomical Society of the Pacific Conference Series, Vol. 16, Atoms, Ions and Molecules: New Results in Spectral Line Astrophysics, Haschick A. D., Ho P. T. P., eds., p. 119

Menten K. M., Batrla W., 1989, ApJ, 341, 839

Minier V., Ellingsen S. P., Norris R. P., Booth R. S., 2003, A&A, 403, 1095

Miranda L. F., Gómez Y., Anglada G., Torrelles J. M., 2001, Nature, 414, 284

Moran J. M., Burke B. F., Barrett A. H., Rogers A. E. E., Ball J. A., Carter J. C., Cudaback D. D., 1968, ApJLett, 152, L97

Moscadelli L., Menten K. M., Walmsley C. M., Reid M. J., 2002, ApJ, 564, 813

Motogi K., Sorai K., Habe A., Honma M., Kobayashi H., Sato K., 2011, PASJ, 63, 31

Müller H. S. P., Menten K. M., Mäder H., 2004, A&A, 428, 1019

Ossenkopf V., Henning T., 1994, A&A, 291, 943

Padoan P., Nordlund Å., 2002, ApJ, 576, 870

Pandian J. D., Menten K. M., Goldsmith P. F., 2009, ApJ, 706, 1609

Perault M. et al., 1996, A&A, 315, L165

Peretto N., Fuller G. A., 2009, A&A, 505, 405

Peretto N. et al., 2013, A&A, 555, A112

Phillips C. J., Norris R. P., Ellingsen S. P., McCulloch P. M., 1998, MNRAS, 300, 1131

Pillai T., Wyrowski F., Carey S. J., Menten K. M., 2006a, A&A, 450, 569

Pillai T., Wyrowski F., Menten K. M., Krügel E., 2006b, A&A, 447, 929

Rathborne J. M., Jackson J. M., Simon R., 2006, ApJ, 641, 389

Reid M. J. et al., 2009, ApJ, 700, 137

Reid M. J., Schneps M. H., Moran J. M., Gwinn C. R., Genzel R., Downes D., Roennaeng B., 1988, ApJ, 330, 809

Richards A. M. S., Elitzur M., Yates J. A., 2011, A&A, 525, A56

Rosolowsky E. et al., 2010, ApJS, 188, 123

Sault R. J., Teuben P. J., Wright M. C. H., 1995, in Astronomical Society of the Pacific Conference Series, Vol. 77, Astronomical Data Analysis Software and Systems IV, Shaw R. A., Payne H. E., Hayes J. J. E., eds., p. 433

Schuller F. et al., 2010, The Messenger, 141, 20

Schuller F. et al., 2009, A&A, 504, 415

Sevenster M. N., Chapman J. M., Habing H. J., Killeen N. E. B., Lindqvist M., 1997, A&AS, 122, 79

Shu F. H., Adams F. C., Lizano S., 1987, ARA&A, 25, 23

Sobolev A. M., Deguchi S., 1994, A&A, 291, 569

Sullivan, III W. T., 1971, ApJ, 166, 321

Sutton E. C., Sobolev A. M., Ellingsen S. P., Cragg D. M., Mehringer D. M., Ostrovskii A. B., Godfrey P. D., 2001, ApJ, 554, 173

Szymczak M., Bartkiewicz A., Richards A. M. S., 2007, A&A, 468, 617

Szymczak M., Pillai T., Menten K. M., 2005, A&A, 434, 613

Szymczak M., Wolak P., Bartkiewicz A., 2015, MNRAS, 448, 2284

Taquet V., Peters P. S., Kahane C., Ceccarelli C., López-Sepulcre A., Toubin C., Duflot D., Wiesenfeld L., 2013, A&A, 550, A127

Titmarsh A. M., Ellingsen S. P., Breen S. L., Caswell J. L., Voronkov M. A., 2013, ApJLett, 775, L12

Torrelles J. M., Gómez J. F., Rodríguez L. F., Curiel S., Anglada G., Ho P. T. P., 1998, ApJ, 505, 756

Urquhart J. S. et al., 2013, MNRAS, 431, 1752

Voronkov M. A., Brooks K. J., Sobolev A. M., Ellingsen S. P., Ostrovskii A. B., Caswell J. L., 2006, MNRAS, 373, 411

Voronkov M. A., Caswell J. L., Britton T. R., Green J. A., Sobolev A. M., Ellingsen S. P., 2010, MNRAS, 408, 133

Voronkov M. A., Caswell J. L., Ellingsen S. P., Green J. A., Breen S. L., 2014, MNRAS, 439, 2584

Voronkov M. A., Sobolev A. M., Ellingsen S. P., Ostrovskii A. B., 2005, MNRAS, 362, 995

Voronkov M. A., Walsh A. J., Caswell J. L., Ellingsen S. P., Breen S. L., Longmore S. N., Purcell C. R., Urquhart J. S., 2011, MNRAS, 413, 2339

Walsh A. J. et al., 2011, MNRAS, 416, 1764

Walsh A. J., Burton M. G., Hyland A. R., Robinson G., 1998, MNRAS, 301, 640

Walsh A. J., Purcell C. R., Longmore S. N., Breen S. L., Green J. A., Harvey-Smith L., Jordan C. H., Macpherson C., 2014, MNRAS, 442, 2240

Wardle M., Yusef-Zadeh F., 2002, Science, 296, 2350

Weaver H., Williams D. R. W., Dieter N. H., Lum W. T., 1965, Nature, 208, 29

Weinreb S., Meeks M. L., Carter J. C., 1965, Nature, 208, 440

Wilson T. L., Walmsley C. M., Jewell P. R., Snyder L. E., 1984, A&A, 134, L7

Wilson T. L., Walmsley C. M., Menten K. M., Hermsen W., 1985, A&A, 147, L19

Wilson W. E. et al., 2011, MNRAS, 416, 832

Xu Y., Li J. J., Hachisuka K., Pandian J. D., Menten K. M., Henkel C., 2008, A&A, 485, 729

Appendices

.1 GLIMPSE three colour images

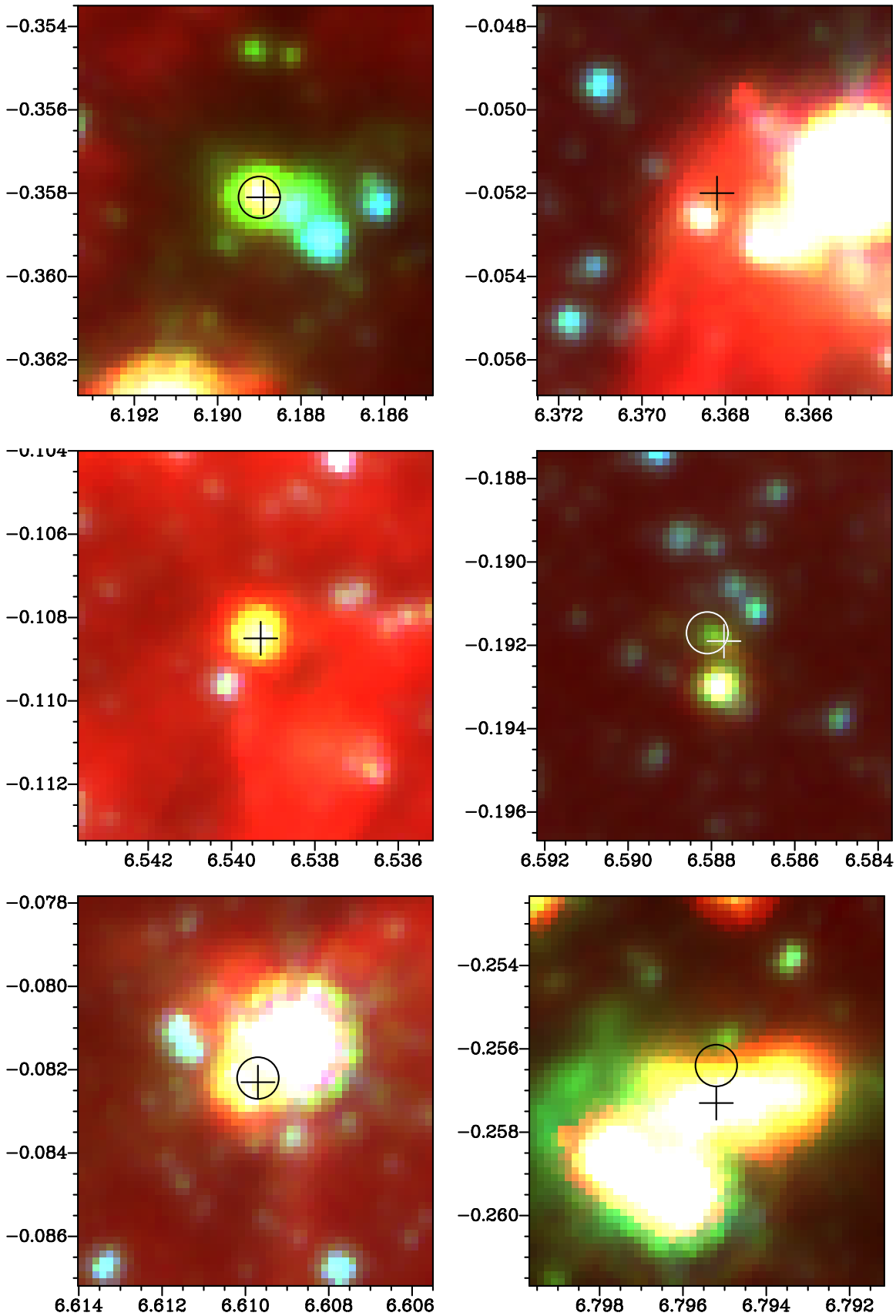

Figure 1: GLIMPSE three colour images: 3.6μm is blue, 4.5μm is green and 8.0μm is red. 6.7-GHz methanol maser positions are marked with crosses and 22-GHz water maser positions are marked with circles. The axes are Galactic Longitude vs. Galactic Latitude.

Figure 1: – *continued*

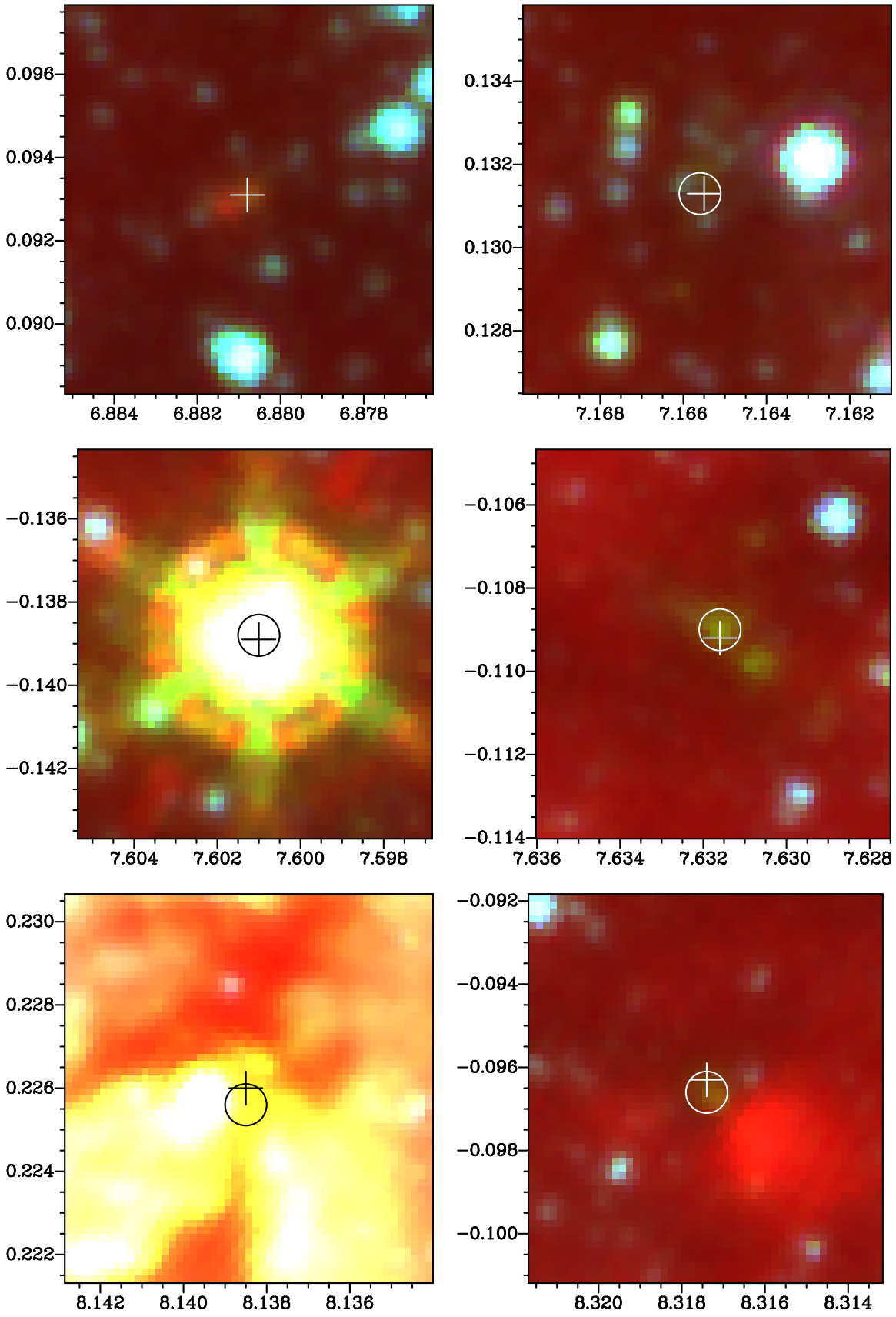

Figure 1: – *continued*

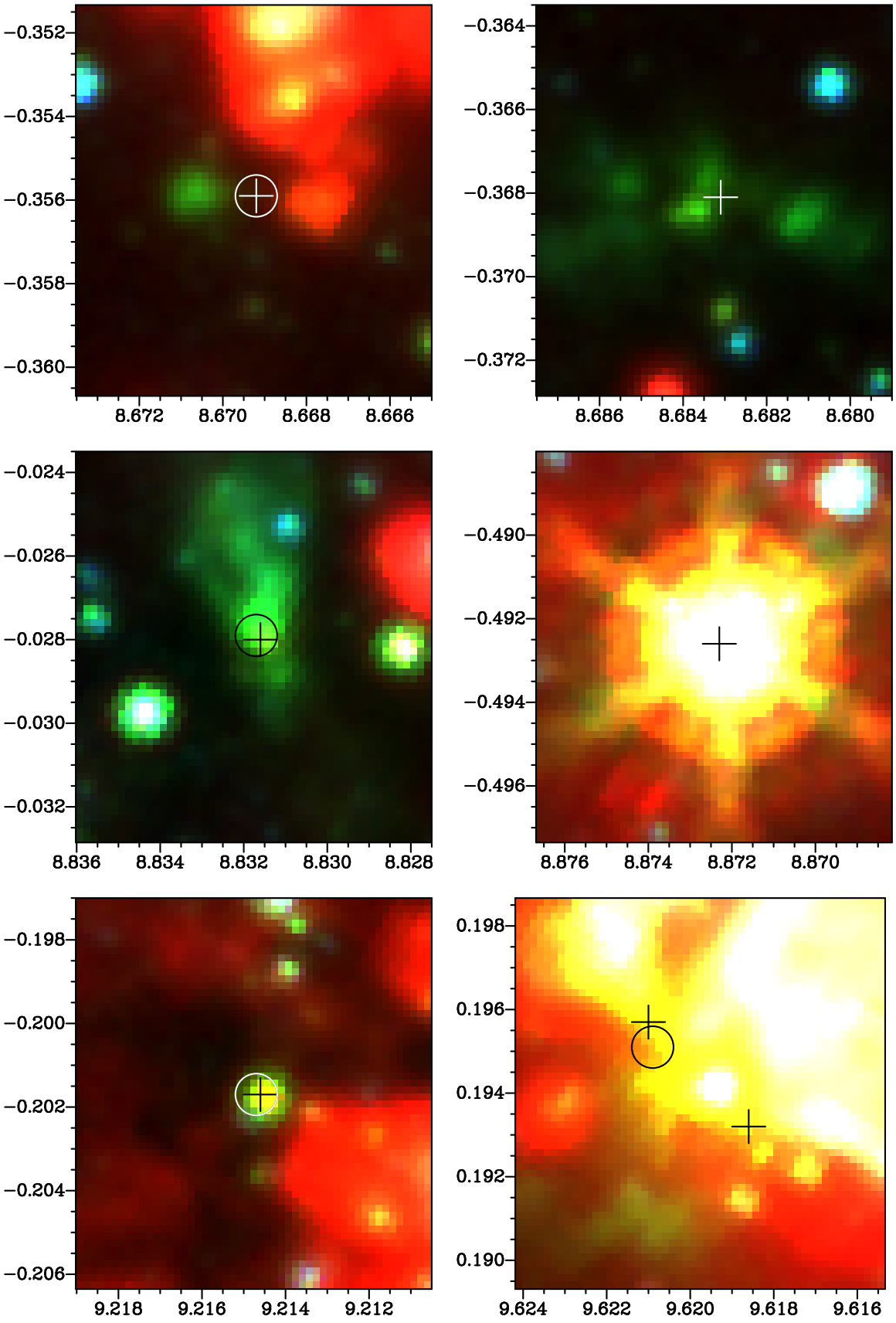

Figure 1: – *continued*

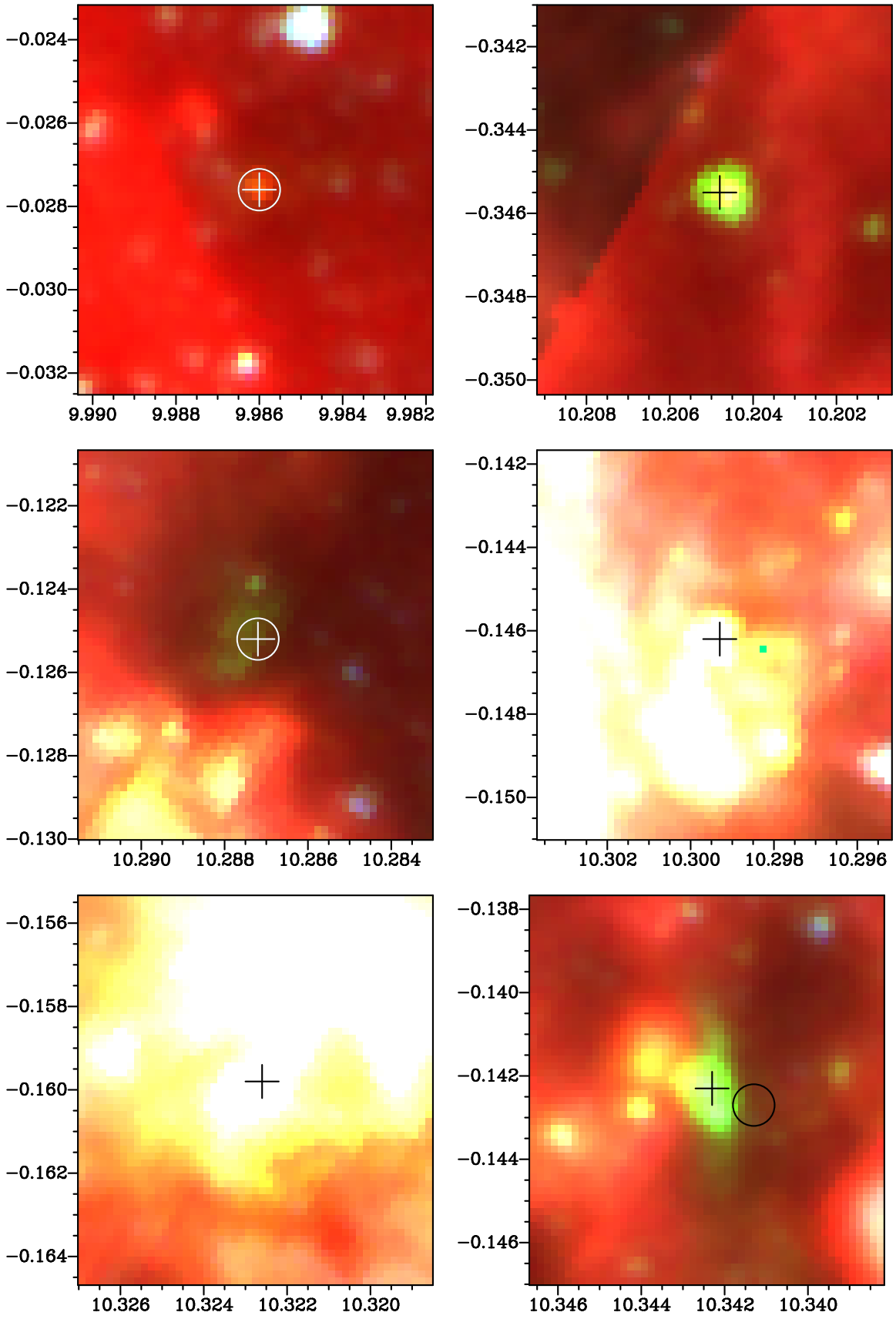

Figure 1: – *continued*

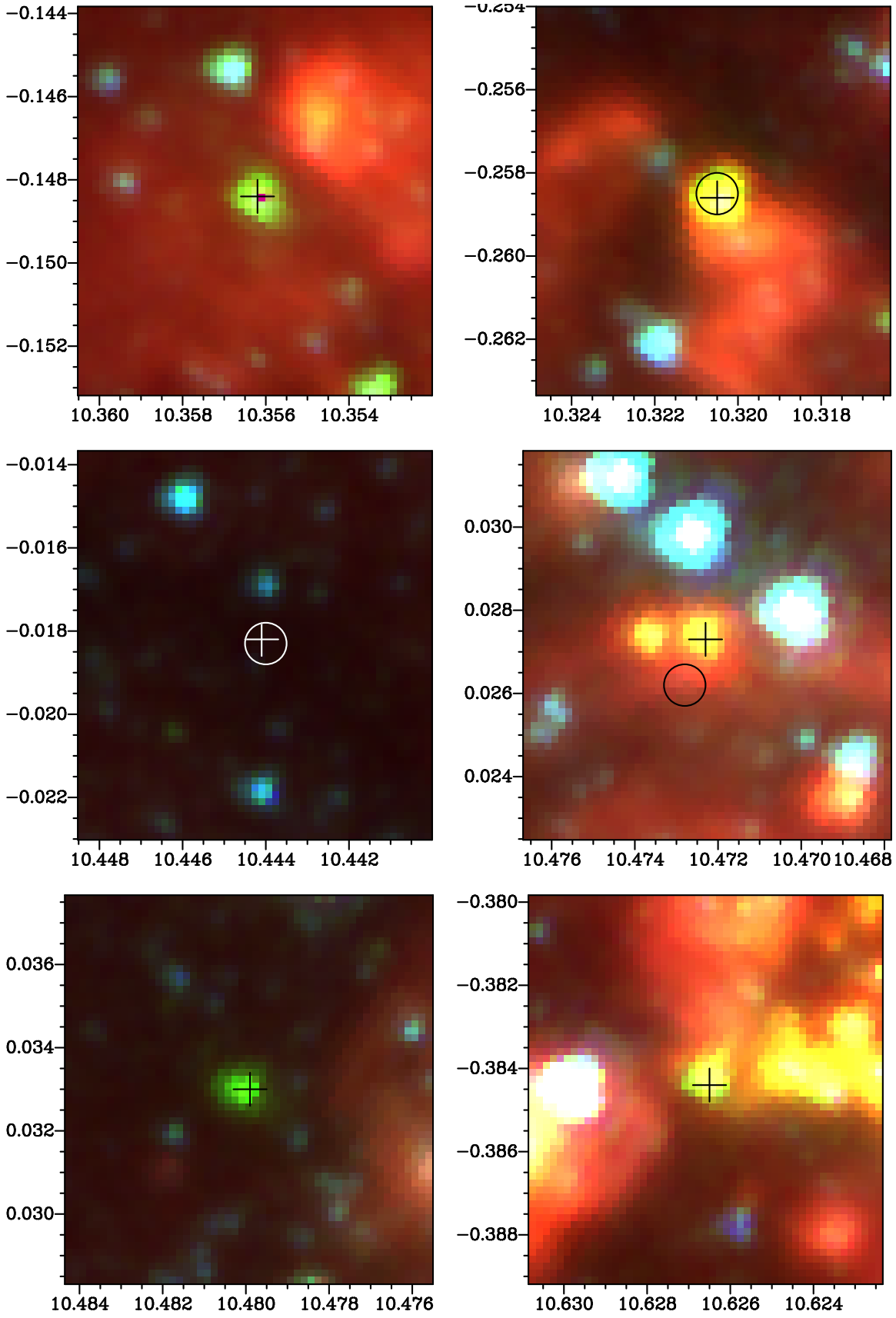

Figure 1: – *continued*

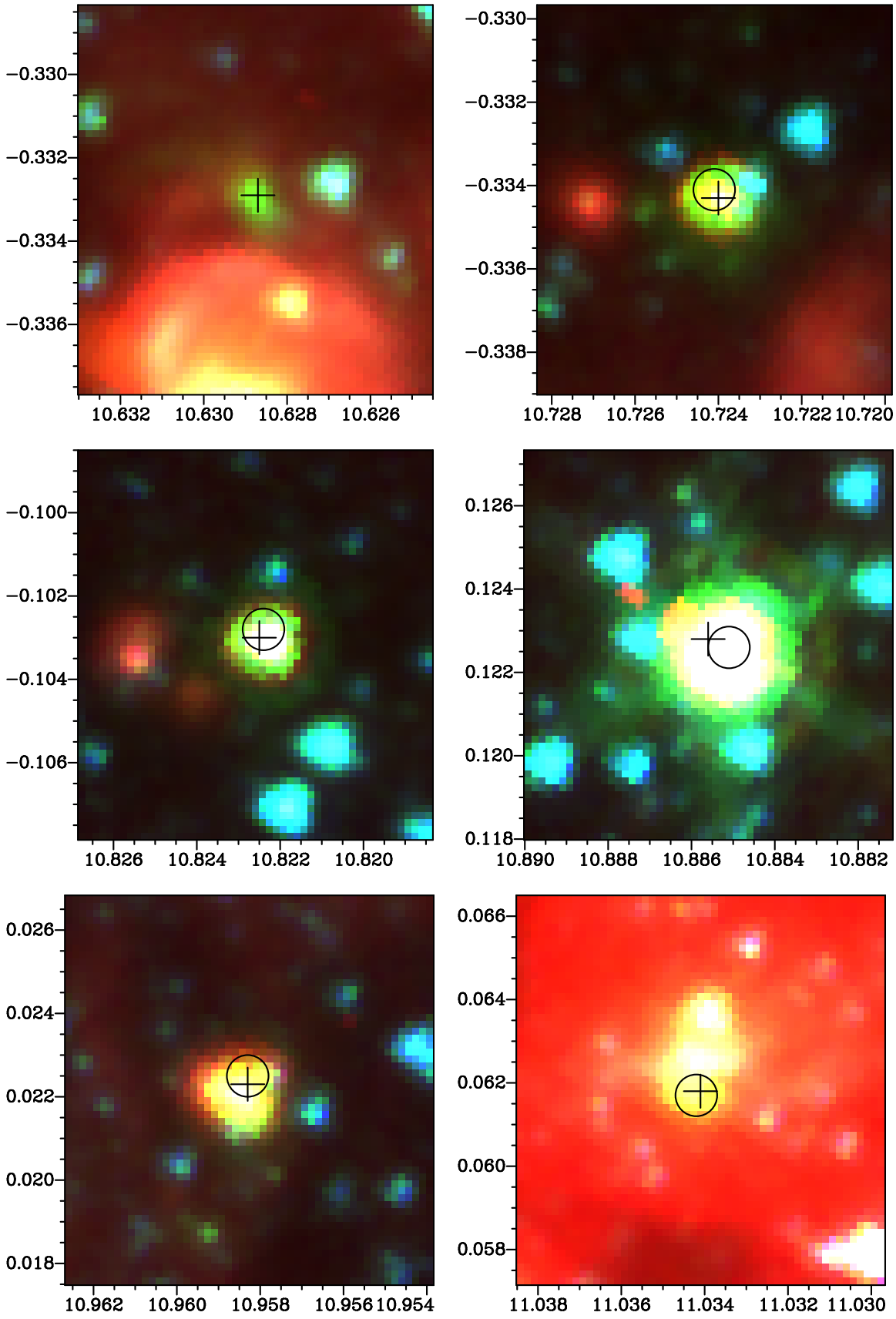

Figure 1: – *continued*

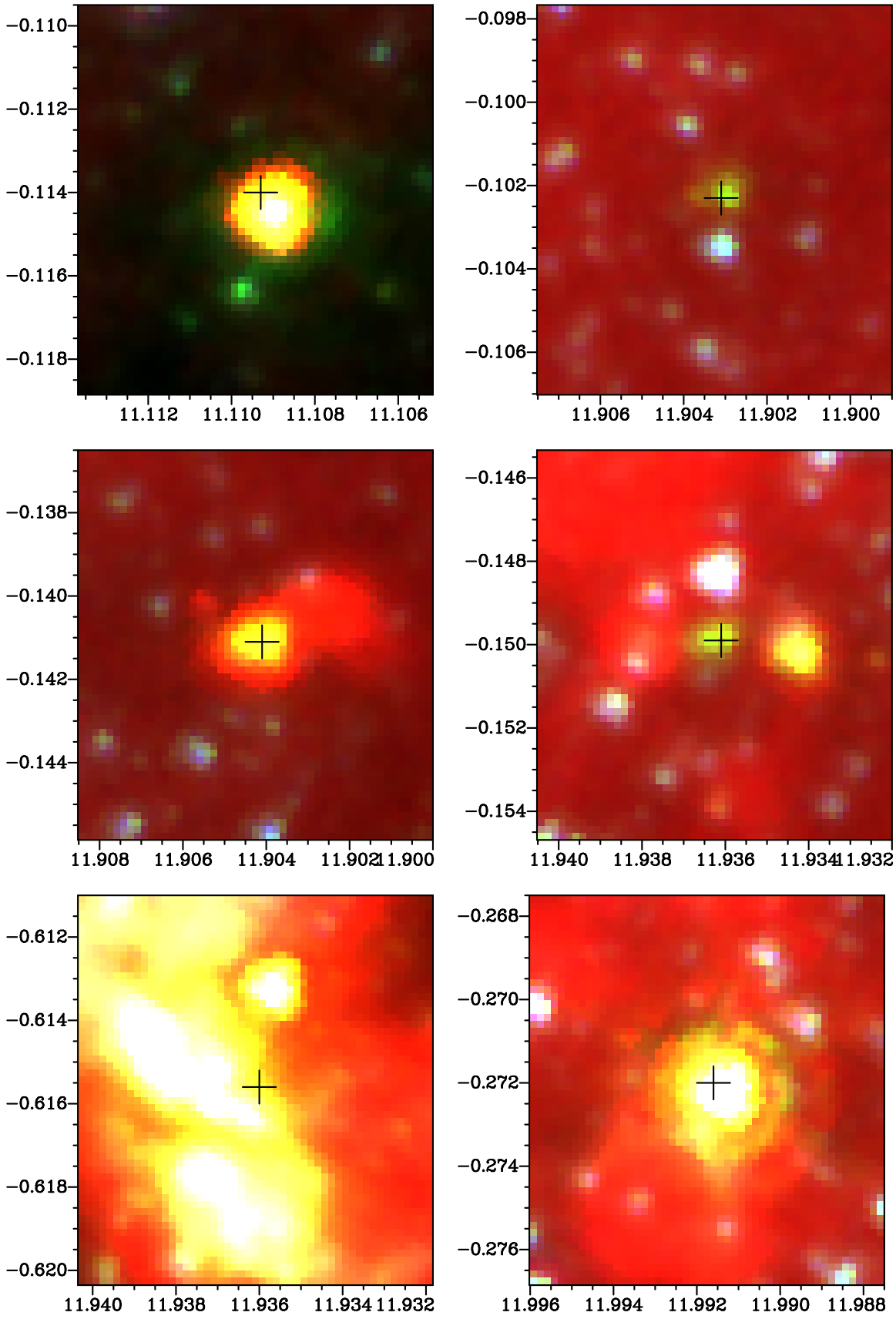

Figure 1: – *continued*

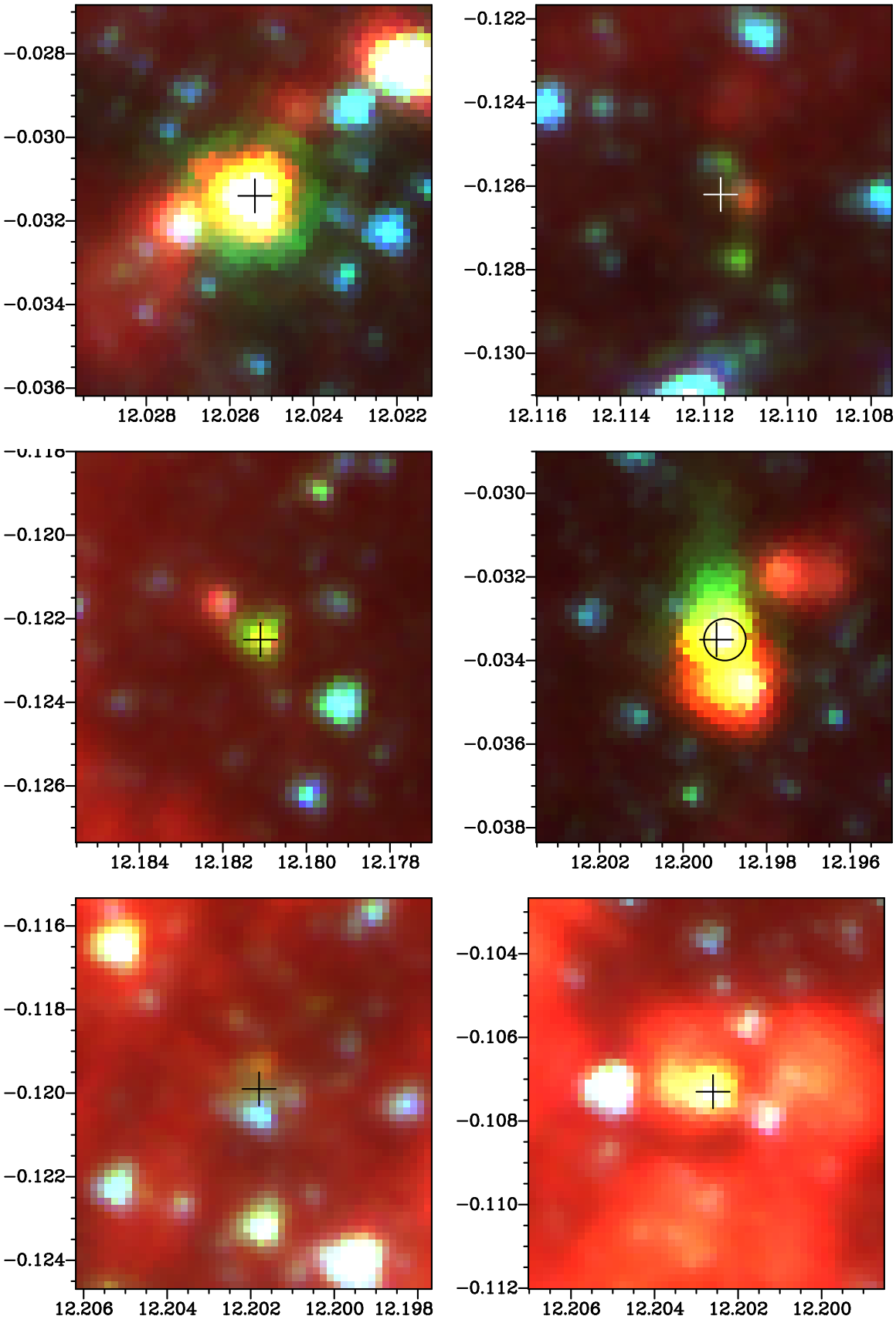

Figure 1: – *continued*

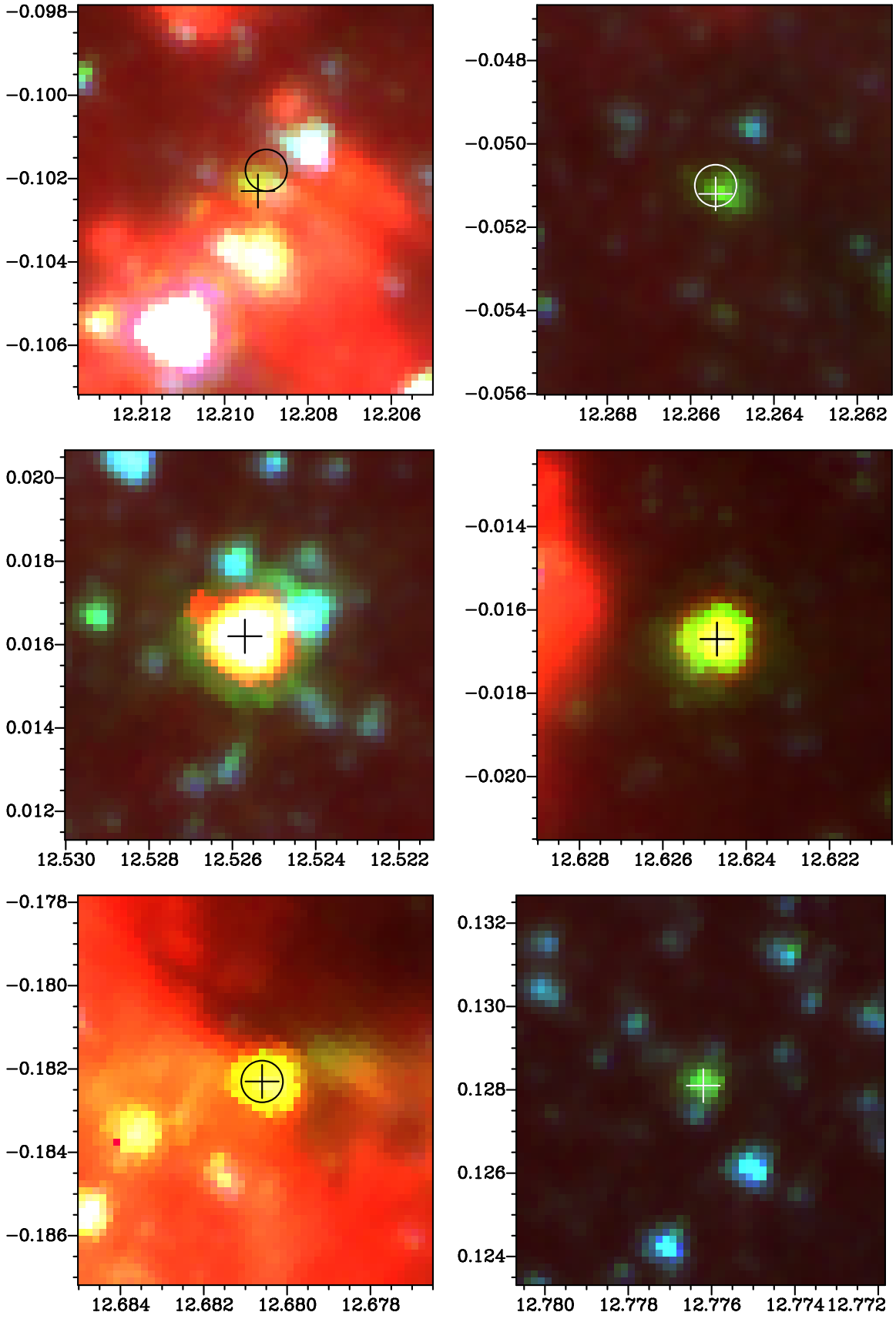

Figure 1: – *continued*

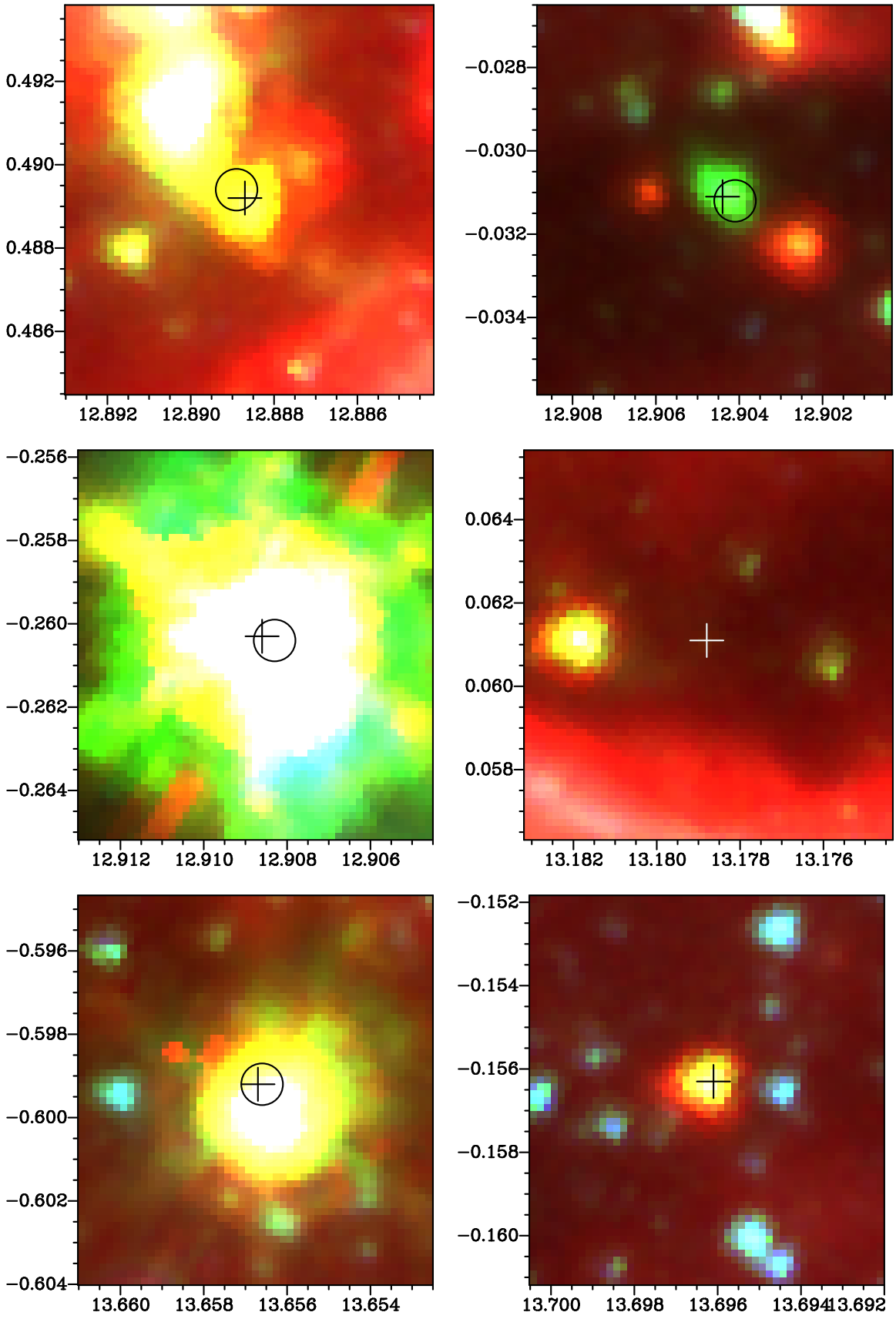

Figure 1: – *continued*

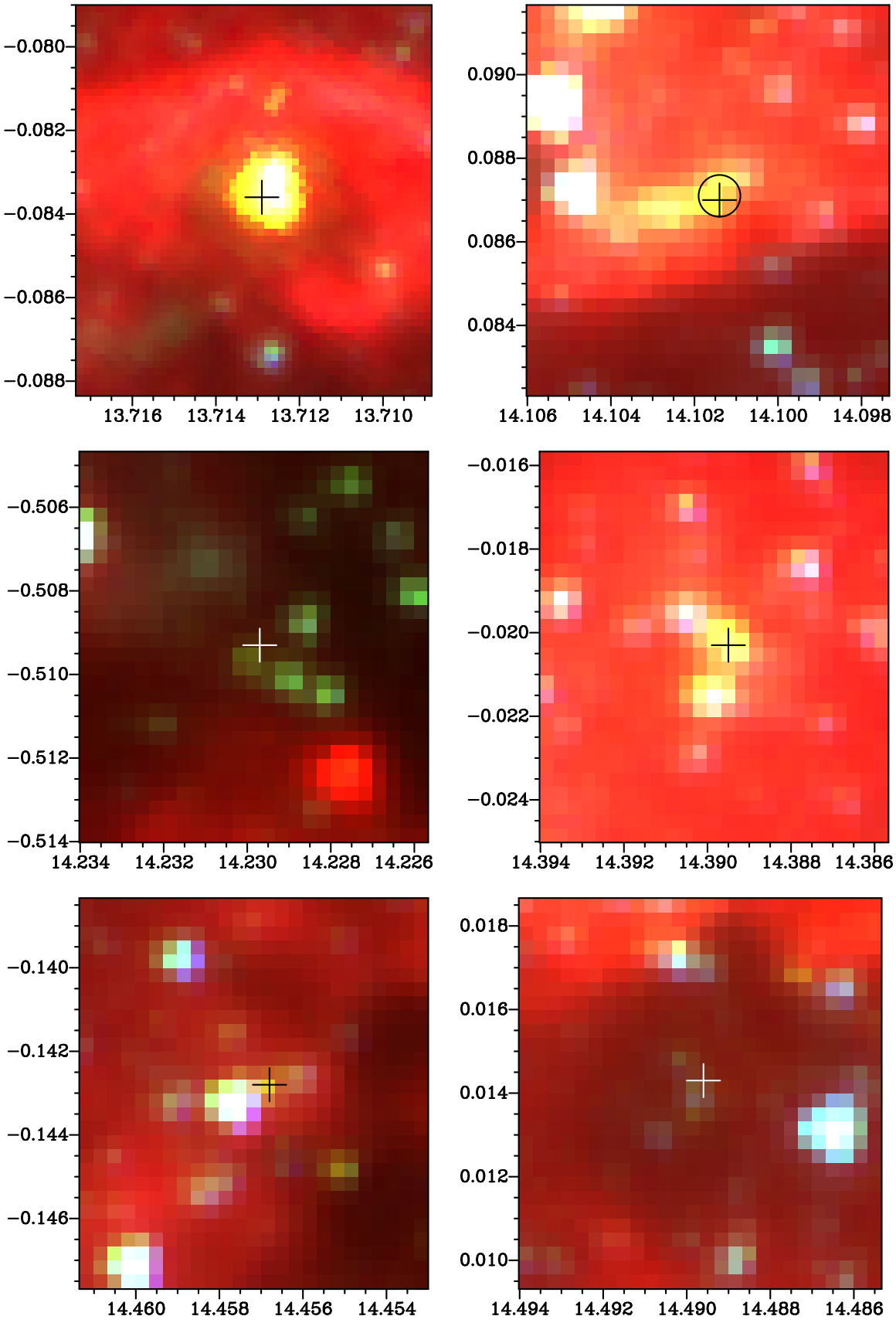

Figure 1: – *continued*

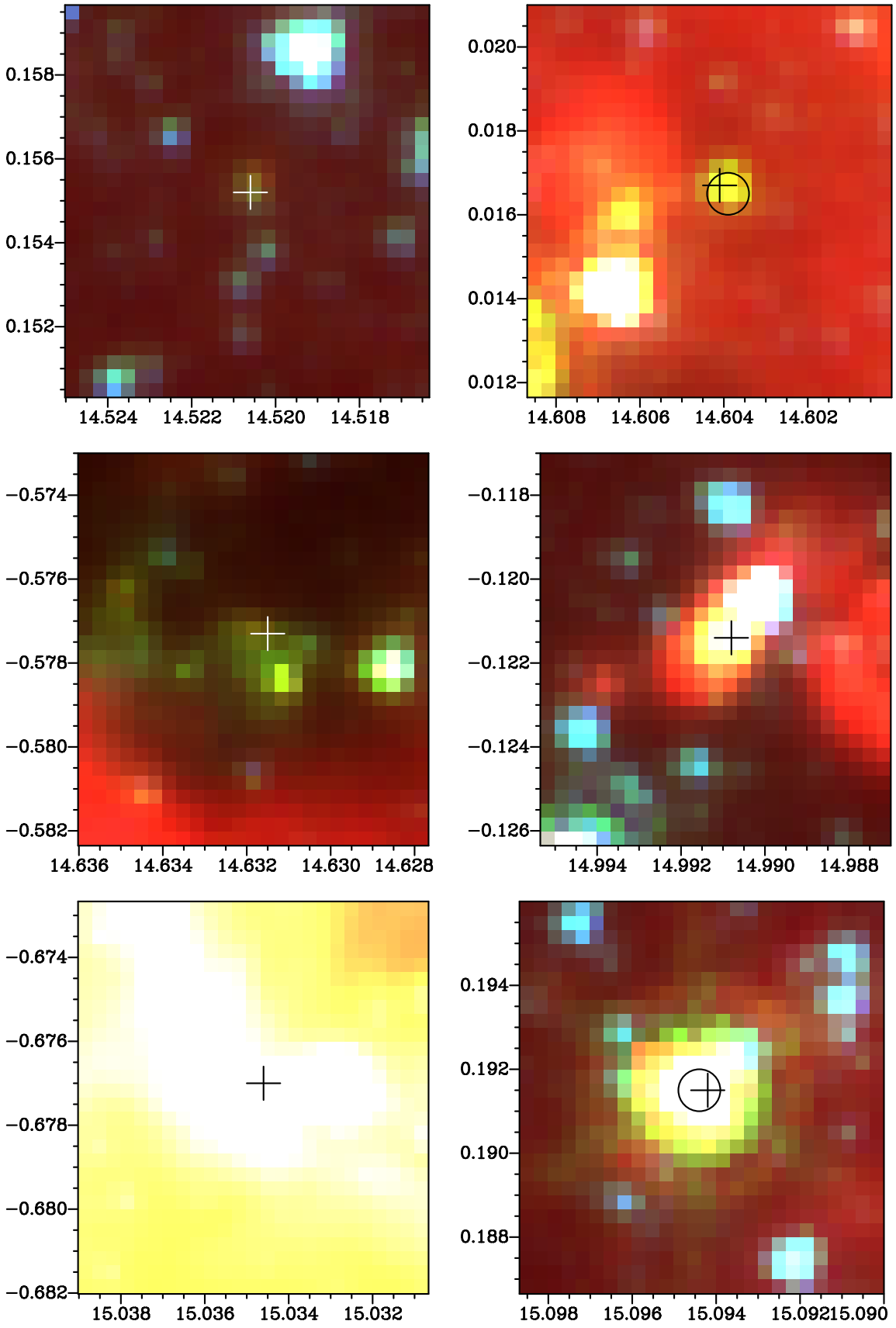

Figure 1: – *continued*

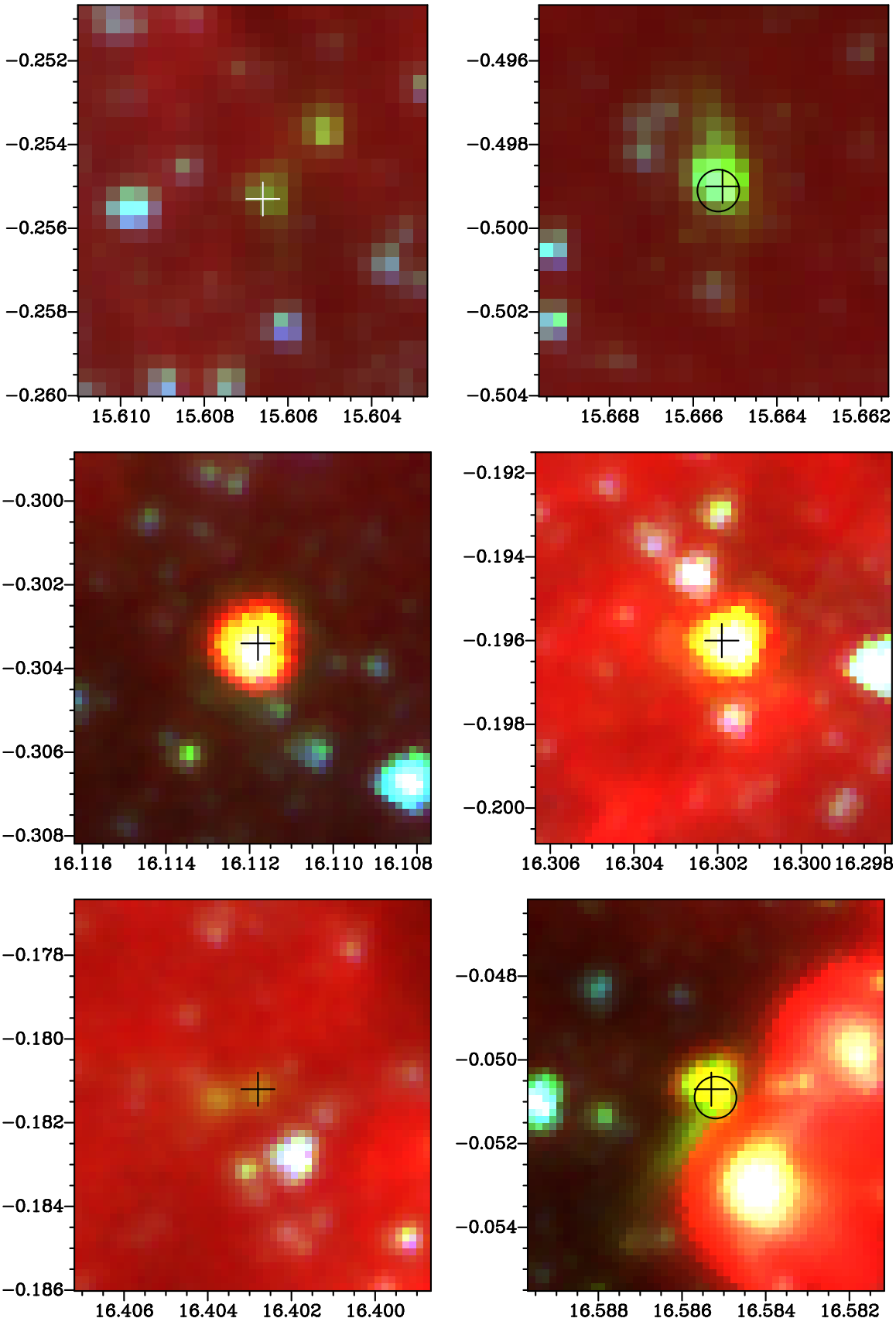

Figure 1: – *continued*

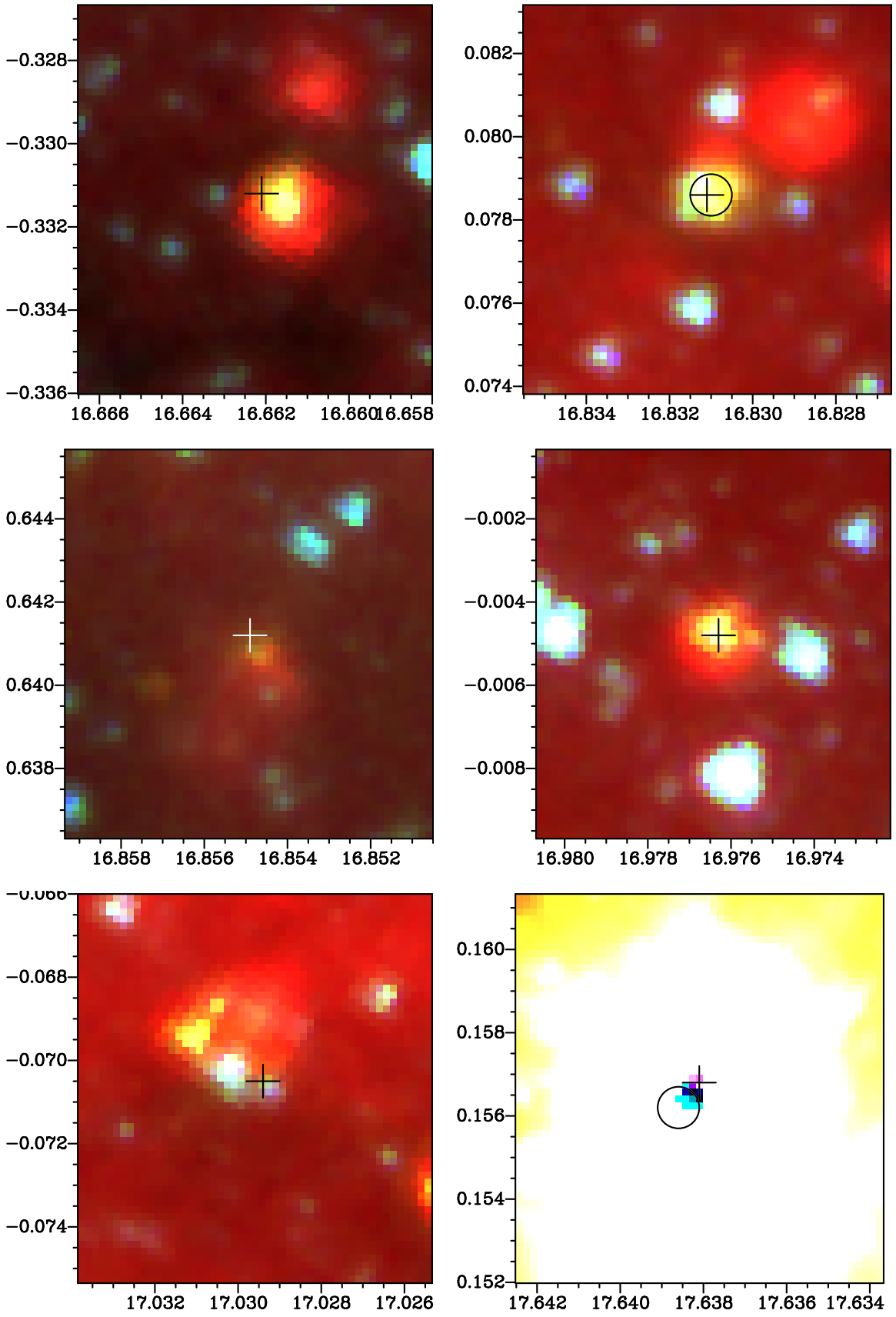

Figure 1: – *continued*

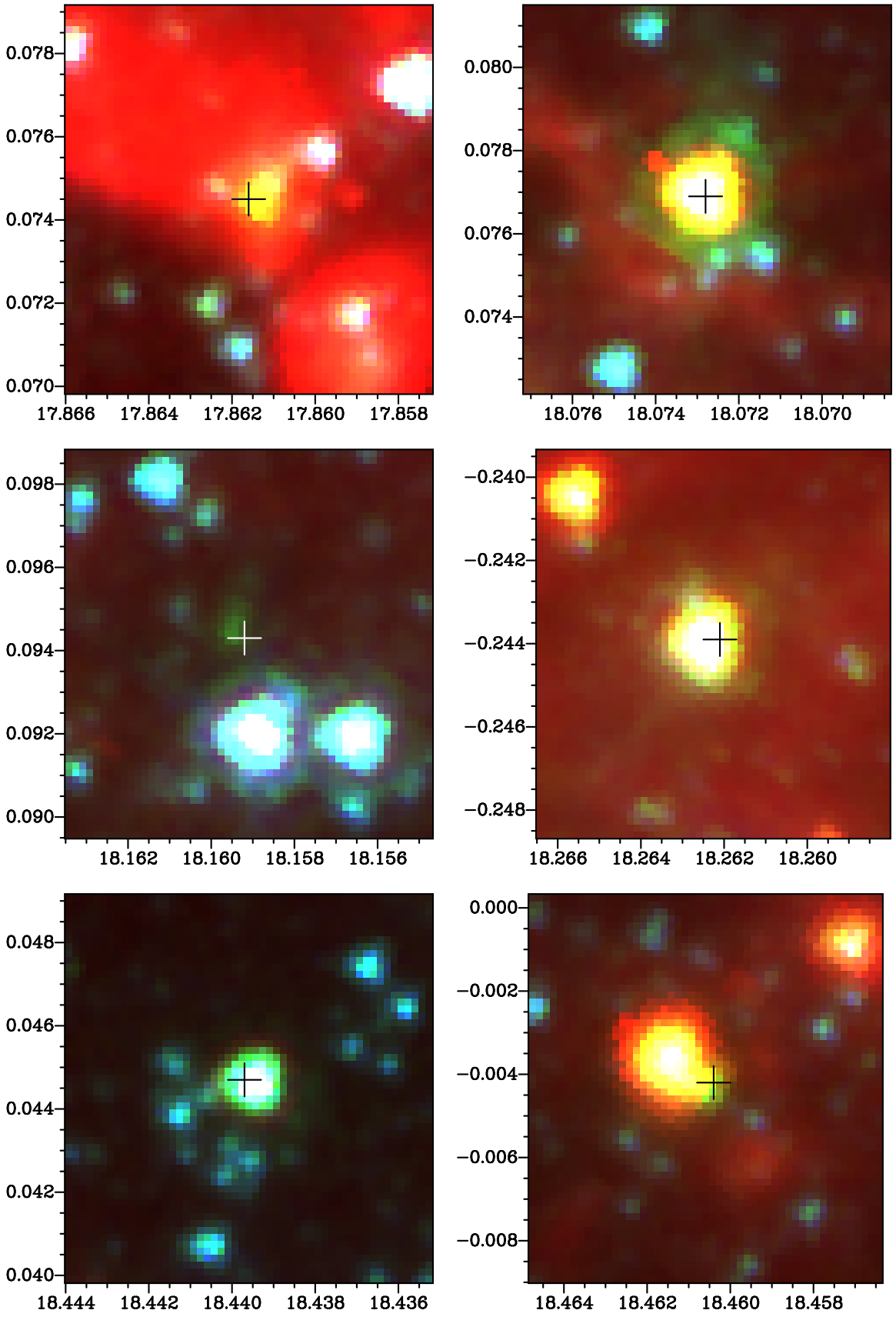

Figure 1: – *continued*

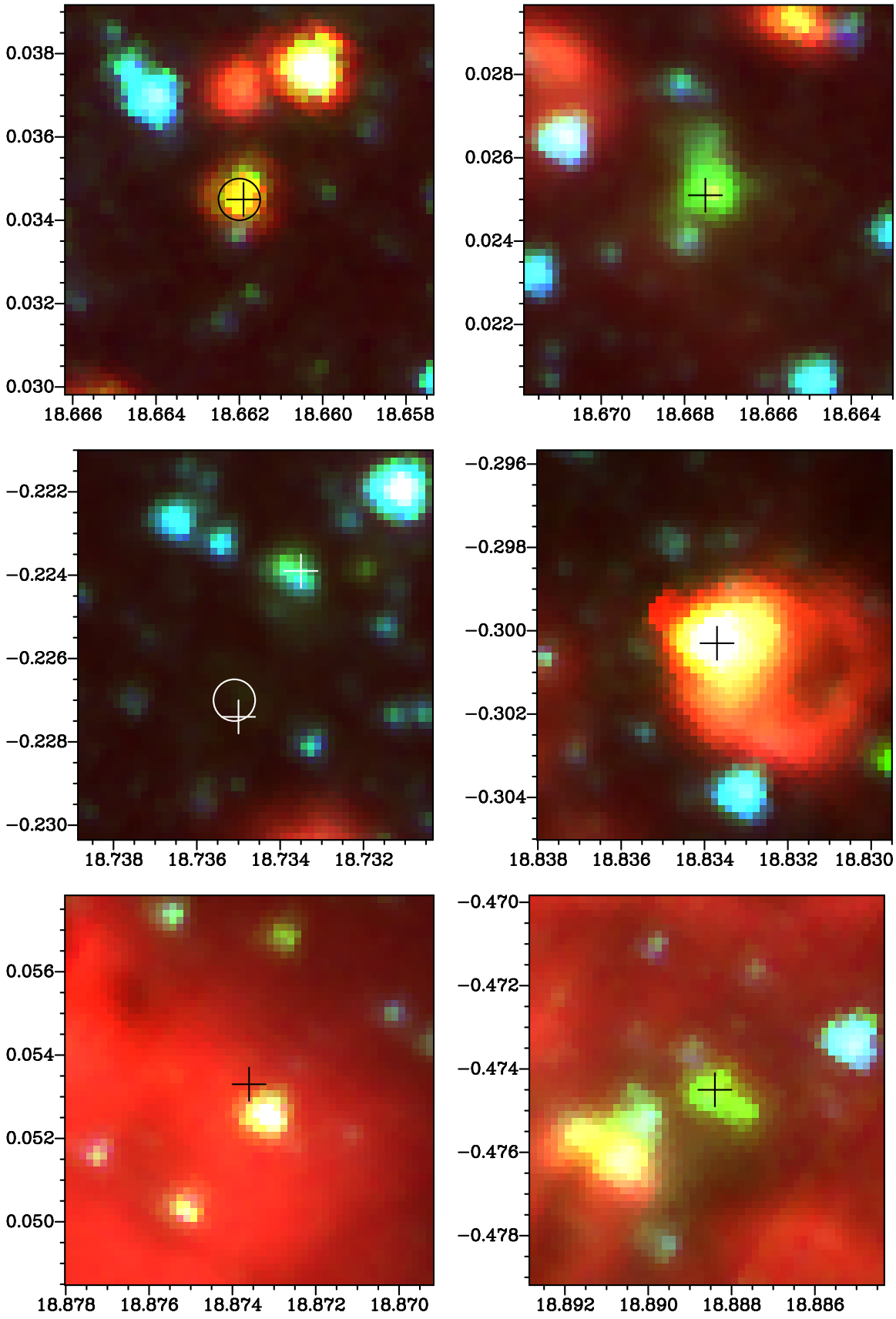

Figure 1: – *continued*

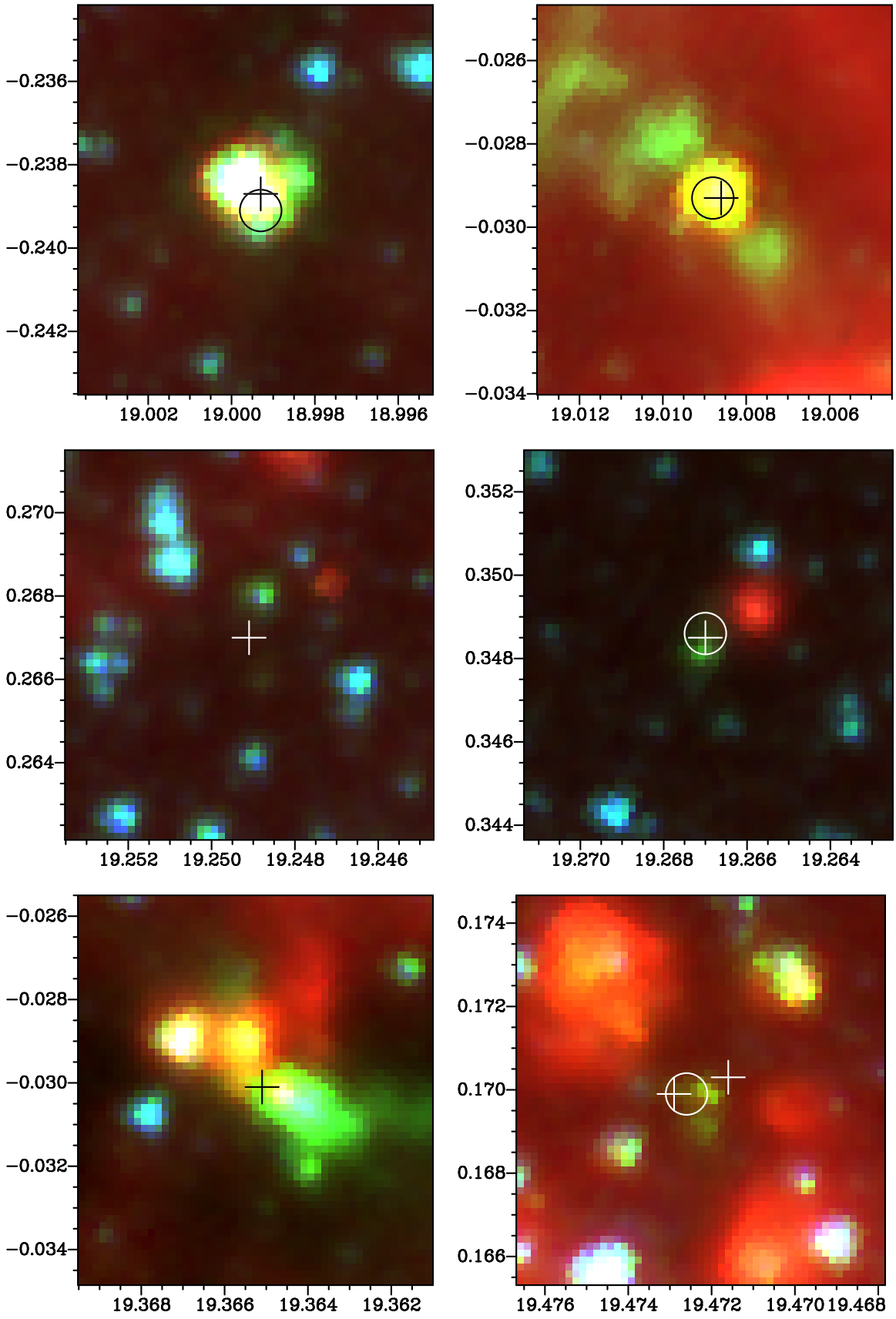

Figure 1: – *continued*

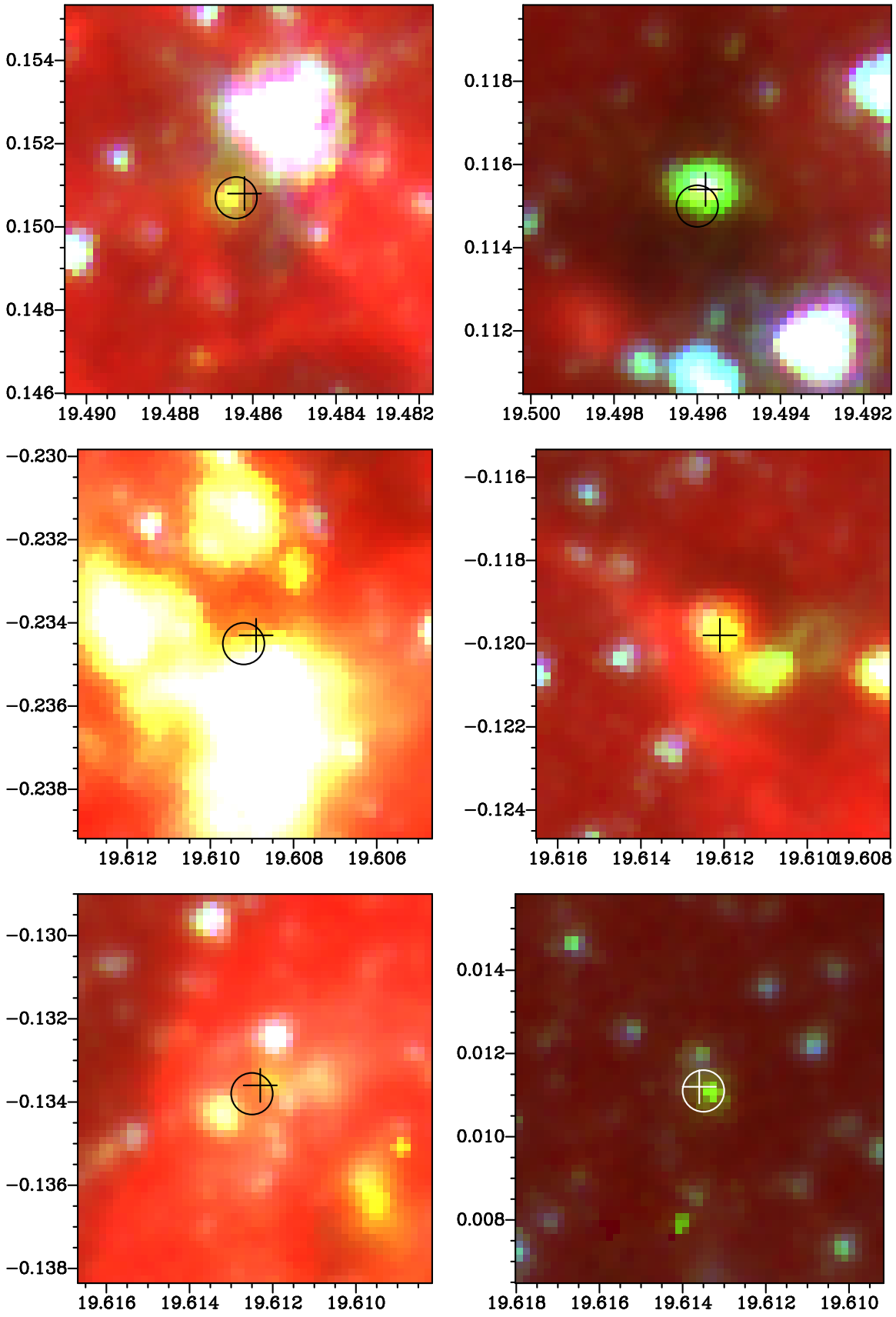

Figure 1: – *continued*